Report No. 6445-T-29

INVESTIGATION OF A YAW DAMPER FOR AIRCRAFT

by

Edward F. Gallagher Robert L. Jungklas
William D. Spiegel

INSTRUMENTATION LABORATORY

MASSACHUSETTS INSTITUTE OF TECHNOLOGY

Cambridge 39, Mass.

INVESTIGATION OF A YAW DAMPER FOR AIRCRAFT

by

Edward F. Gallagher	B.S., U.S. Naval Academy, 1941
Robert L. Jungklas	B.S., U.S. Naval Academy, 1942
William D. Spiegel	B.S., U.S. Naval Academy, 1941

SUBMITTED IN PARTIAL FULFILLMENT OF THE
REQUIREMENTS FOR THE DEGREE OF
MASTER OF SCIENCE
at
MASSACHUSETTS INSTITUTE OF TECHNOLOGY
1950

May 19, 1950

Prof. Joseph S. Newell
Secretary of the Faculty
Massachusetts Institute of Technology
Cambridge 39, Massachusetts

Dear Professor Newell:

In accordance with the regulations of the faculty, we hereby submit a thesis entitled, "Investigation of a Yaw Damper for Aircraft", in partial fulfillment of the requirements for the degree of Master of Science (Aeronautical Engineering).

ACKNOWLEDGMENT

The authors wish to express their deep appreciation to Prof. Otto K. Koppen and to Prof. Robert C. Seamans, Jr. for the interest, encouragement, and assistance given by them in supervising the progress of this work.

The authors also wish to thank Prof. Dominic Amara and Mr. George Coury of the Fire Control Instrument Laboratory for their technical advice and aid in setting up experimental equipment.

Thanks are also extended to Mr. Charles Olson for his assistance in the design of the wind tunnel model.

Valuable advice on wind tunnel testing and techniques was given by Mr. Eugene E. Larabee of the Department of Aeronautical Engineering.

Thanks are given to Mr. L. E. Payne and his associates of Jackson & Moreland for their part in the preparation of the text and illustrations.

The graduate work, for which this thesis is a partial requirement, was performed while the authors were assigned to the Naval Training School, Massachusetts Institute of Technology. This thesis was prepared under the auspices of D.I.C. Project 6445, sponsored by the Office of Air Research and the Armament Laboratory, Engineering Division, Air Materiel Command, through Contract W33-038ac-13969, Project RR3.

ABSTRACT

An investigation was made of a method for improving the lateral stability characteristics of an aircraft by means of a Yaw Damper. The Yaw Damper was a simplified system to the extent that power amplification was obtained as a result of a servo tab which positioned a rudder. The control system consisted of a single degree of freedom gyroscope sensitive to yawing rates, a mechanical linkage to position a tab control surface, and a free rudder whose position was a function of the tab deflection.

Model tests were conducted in the 4 1/2 by 6 foot wind tunnel of the Guggenheim Aeronautical Laboratory located at the Massachusetts Institute of Technology to determine the damping effectiveness of the control system.

The results of the investigation show that a Yaw Damper of this type is very effective in damping large magnitude lateral disturbances. For small amplitudes, the arrangement produces a control system stability problem in that rudder and tab oscillations occur which are only slightly damped. These oscillations are considered to be functions of the time lags associated with unsteady aerodynamic forces and circulation of the air stream as well as the effects of mechanical backlash and coulomb friction.

Further tests with the rudder fixed, which made the gyro and tab a direct damping in yaw control, resulted in the elimination of the control system instability problem for small amplitude lateral disturbances. It was observed, however, that this stability was obtained at the expense of the effectiveness of the original control system in damping in yaw.

The tests indicate that a small airplane of the Piper "Clipper" size could be stabilized laterally by means of a gyroscopically controlled yaw damper to increase the aircraft spiral stability at all airspeeds. At the same time, the damping of the Dutch Roll oscillation would be also improved. High performance aircraft using the same system would be able to replace the tab amplifier with a servo system to provide an irreversible control system to produce the desired response specifications.

TABLE OF CONTENTS

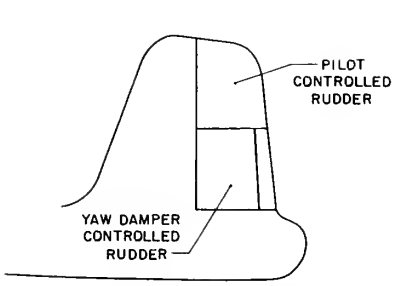

FIG. 1b. SCHEMATIC DIAGRAM
OF DIVIDED RUDDER SYSTEM

FIG. 1a. SCHEMATIC DIAGRAM OF YAW DAMPER

Chapter 1

INTRODUCTION

This paper presents a theoretical investigation into a method of improving the lateral stability characteristics of an aircraft by means of a Yaw Damper. It is a fact well known among aeronautical engineers that increased damping in yaw is not only desirable but may even be a requirement in some airplanes of the future.

A Yaw Damper can be designed so that an airplane that is basically spirally unstable can be made spirally stable to a high degree, and at the same time can achieve a marked reduction in the amplitude and period of the Dutch Roll oscillation. This improvement in lateral stability characteristics results from the action of the Yaw Damper in effectively increasing the value of the airplane stability coefficient, C_{nr}. The result of increasing the value of C_{nr} is illustrated in Appendix A, Table III.

An aircraft would be considered to have high spiral stability if its spiral mode would damp to one-half amplitude in one second. It would also possess above average lateral stability characteristics if its Dutch Roll oscillation would damp to one-half in one quarter of a cycle. Such an airplane would be easy to fly and pleasant to ride in. In addition, an aircraft that could meet these specifications for spiral stability and Dutch Roll, when properly trimmed, could be flown "hands off" even in gusty air. This would be ideal, not only from the viewpoint of pilot and passenger comfort, but even more important, from flight safety considerations. For instance, a pilot inexperienced in instrument flying who might find himself caught in poor visibility conditions would have the comfort of knowing that the plane would not inadvertently wind up in a graveyard spiral if flown "hands off." In fact, such an aircraft could be eased to the ground with wings level, simply by retarding the throttle and maintaining flying speed — without touching the flight controls.

It can be shown that the lateral equations of motion for a conventional type airplane, controls fixed, can be reduced to a quartic and that the four roots will consist of a large roll subsidence, a small spiral divergence, and

a Dutch Roll oscillation. The spiral mode may be positive at and above cruising speeds, but even so the time required to damp to one-half amplitude would be 52 seconds for a B-26C, Medium Bomber. This is practically marginal stability, as shown in the calculations of Appendix A.

Because the spiral instability is generally small and acts slowly, it is usually corrected by the pilot without his knowledge, but the fact remains that it has to be corrected by one means or another, and it remains a potential source of trouble for the pilot. The Dutch Roll oscillation is present to some degree in all aircraft, as it is a function of wing dihedral and vertical tail area. It is desirable both from the viewpoint of pilot control and passenger comfort to keep the amplitude and period of this oscillation as low as possible. From military considerations it means a more stable gun or bombing platform.

In a flight analysis conducted by the Cornell Aeronautical Laboratory, a large group of experienced pilots flew an F4U-5 Chance-Vought Corsair equipped with a yaw damper. The vertical tail surfaces were so modified that automatic damping in yaw was made proportional to a gain control knob setting which the pilot could adjust in flight. It was determined by all the pilots, without exception, that the handling and flying characteristics of the airplane were best for the maximum setting; that is, the optimum setting was that which gave the maximum amount of damping.

In addition, Mr. Roland J. White, Aerodynamicist of the Boeing Airplane Company, has stated[4] after considerable investigation and analysis of flight test data on the XB-47 that some means must be found to improve the damping on all future high-performance airplanes because of the adverse effects of altitude and wing loading on yaw damping.

One method of improving the damping in yaw that is familiar to all aeronautical engineers is to increase the size and length of the vertical tail. However, there is a limit to which this can be carried, because the disturbances of the airplane due to side gusts will likewise be greater. For smooth flying qualities and optimum controllability and riding comfort, other means of increasing the damping in yaw should be utilized. For example, a rate gyro could be installed so as to automatically move a control surface in response to a disturbance of the aircraft about the yaw axis.

The idea for using a rate gyro to increase the damping in yaw is not new. It has been used in the XB-47, and in the F4U-5 mentioned above, and it is known that there have also been other applications of this principle in the field of automatic aircraft control. The important distinction between this Yaw Damper and those previously designed is in its simplification.

This investigation is an attempt to simplify the Yaw Damper to the extent where it will be readily available and usable, not only in the high performance airplanes of tomorrow, but in the large and small aircraft of today as well. Reference 4 describes a yaw damper as designed for use in the XB-47 airplane, and concludes that "other methods should be investigated with the single aim of simplifying the yaw damper." The unique simplification of the Yaw Damper described in this paper is that although the system is fully automatic, and within itself constitutes a closed-loop servomechanism, it operates without the aid of an electronic servo amplifier or servo motor. The "muscle" of the system is the output of a single-degree-of-freedom rate gyroscope, which is mechanically linked to a servo tab — the output of the gyro and the deflection of the tab being proportional to the angular velocity of yaw. A rudder tab with an aerodynamic balance is the power amplifier which positions the rudder. The rudder itself has an aerodynamic balance to reduce the hinge moments of the system. The general arrangement of the yaw damper is shown in Fig. 1a.

The size and configuration of the aircraft in which such a simplified Yaw Damper would be adequate to produce the required or desired increased damping in yaw is presently limited by the size of the gyroscopes available. A preliminary investigation indicated that a small airplane of the Piper Clipper configuration could be adequately stabilized with the gyroscope at hand for experimental purposes. It is estimated that a larger airplane could be handled by a gyro with a larger value of angular momentum (which is a function of the moment of inertia and the angular velocity of the gyro wheel), or a servo amplifier could be inserted in the closed loop which would adequately increase the gain of the Yaw Damper so that it would operate according to desired specifications.

Chapter 2

DEVELOPMENT OF THE YAW DAMPER

The calculations given in Appendix A indicate than an airplane with the desired lateral stability characteristics (the spiral mode to damp to one-half amplitude in one second, and the oscillatory mode to damp to one-half amplitude in one-quarter of a cycle) would be realizable if C_{n_r} were increased four times and if C_{l_β} were increased four times. If C_{n_r} alone were increased sixteen times, the lateral stability characteristics would be even better than that obtained by increasing C_{n_r} four times and C_{l_β} four times; but this is not a practical solution, as it would require a larger than normal rudder surface.

Flight Condition 3 of Appendix A indicates that increasing the value of C_{n_r} by a factor of four improves the spiral stability but does not bring it within the specifications listed above. However, the Dutch Roll oscillation is improved to such a degree that it was decided to sacrifice some of this improvement in the interest of the spiral mode. This was done by increasing the value of C_{l_β} by a factor of four, as in Flight Condition 4, Appendix A. Inasmuch as the value of C_{l_β} is a function of wing dihedral and the Dutch Roll oscillation is also a function of wing dihedral, it is observed that the Dutch Roll oscillation is slightly greater in Flight Condition 4 than it is in Flight Condition 3, but is still within the specifications. It is seen that the spiral stability is now within the desired specification.

One reason that more dihedral has not been used in airplane design is because of its adverse effect on the Dutch Roll oscillation. Dihedral improves the spiral stability but, paradoxically, also increases the amplitude of the Dutch Roll oscillation, the latter effect generally determining the amount of dihedral employed in a given design. Now, with the Yaw Damper to increase the effective value of C_{n_r} and thus the damping, more dihedral can be employed.

The results of the investigation cited in reference 6 support the conclusion that:

> "The maximum tolerable effective dihedral at cruising speed was indicated to be about 22 degrees. An effective dihedral as high as 28.4 degrees did not cause the airplane to exhibit intolerable stability and control characteristics at landing-approach speed, . . . even though the airplane was oscillatory [sic] unstable. The term 'tolerable' describes a condition which would not be dangerous in normal fighter operation, but which is not necessarily 'desirable' or 'pleasant.'
>
> "It was the opinion of the pilots that the optimum values of effective dihedral investigated were 6.2 degrees (normal airplane) for the cruising condition and 14.2 degrees for the landing-approach condition. They thought more than normal amounts of dihedral were desirable in the approach condition because of the good response in roll to rudder control. It is noteworthy that this is the direction of the variation of effective dihedral with lift coefficient for swept-back wings; that is, increasing lift coefficient results in increasing effective dihedral."

As pointed out above and indicated in Appendix A, the Yaw Damper would permit even greater values of effective dihedral. It is a fact known to aeronautical engineers that anything that improves the damping also improves the controllability, particularly at the low speeds of landing and take-off.

No further mention will be made of the increase in C_{l_β}; it is assumed that it can be accomplished by increasing the effective dihedral area or the dihedral angle, or by sweepback. The problem to be solved is how to increase the effective value of C_{n_r} four times so that the desired specifications for lateral stability will be met.

Neglecting the possibility of increasing the vertical tail area by four, or doubling the length of the vertical tail, either of which would solve the immediate problem (but would also introduce additional difficulties resulting from high weathercock stability and increased drag), it is observed that if artificial means of increasing the damping are used, there are at least two designs available which incorporate the use of a rate gyro. The rate gyro improves the lateral stability by automatically moving a control surface in response to an aircraft disturbance. The first is to connect the gyro to a tab which would move the whole rudder surface. The second is to connect the gyro to a tab which would move only part of the rudder surface. The arrangement of connecting the output

of the gyro directly to the rudder (i.e., no tab) might be feasible if it would not require too large a gyro to do the work. This increase in gyro size is due to the loss in power amplification experienced when the tab is not used to operate the rudder.

The first possibility was rejected because, if the damper were to operate the whole rudder surface through the deflection of the tab, the rudder pedals would move as the Yaw Damper operated unless a mechanical differential functioned so as to keep the motion of the rudder surface from feeding back to the rudder pedals. Such an arrangement is possible in airplanes equipped with the control boost systems described in reference 4. The requirement of having to design a mechanical differential was effectively bypassed by resorting to the remaining practical solution; namely, connecting the gyro output to a tab which would move only part of the rudder surface.

Inasmuch as C_{n_r} was to be increased only four times, it was decided to divide the rudder in two, horizontally, and to connect the top half to the pilot's rudder pedals so as to permit this section to be controlled in the conventional manner. Figure 1b illustrates this configuration. The bottom half is to be controlled automatically by a rate gyro without the pilot's assistance or knowledge. The only information manifested to the pilot on the operation of the yaw damper is that which is reflected in the improved flying characteristics and lateral stability of the airplane.

The control surface that the pilot ordinarily would have subject to his control is reduced by half; however, the controllability of the aircraft has not been reduced in the same proportion. This is because the gyro-controlled section aids the pilot, especially in the landing and take-off flight conditions. However, it is estimated that the area of the vertical tail should be increased by approximately 20 percent to give the pilot sufficient controllability to sideslip 15 degrees — a value which is considered to be an adequate controllability criterion for a conventional aircraft. The reasons for this increase are further commented upon in Appendix B.

Although the Yaw Damper is beneficial at the start of a turn, it does act adversely during steady turning flight. Because the Yaw Damper acts to bring the airplane out of a steady turn, the pilot will have to apply more than normal rudder pedal force in order to make a smooth, steady turn. A method

for yaw compensation during steady turning flight may be desirable if the increased pedal forces are considered objectionable from a "feel" viewpoint. The actual increase in pedal force in pounds will not be high. It is mostly a matter of familiarization and the acquisition of a new "feel" through flight experience. Reference 4 describes two methods of accomplishing yaw compensation in steady turns — methods which apply to electro-hydraulic systems. It is considered that yaw compensation, while desirable for a mechanical system such as described herein, is beyond the scope of this thesis. However, one simple expedient is mentioned — that of cutting out the adverse effect of the Yaw Damper in steady turning flight by caging the gyro.

Chapter 3

DESCRIPTION OF THE YAW DAMPER

The Yaw Damper consists essentially of four parts: (1) a gyroscope; (2) the linkage connecting the output motion of the gyroscope to the tab surface; (3) the tab surface whose angular deflection is proportional to the precession of the gyro; (4) the rudder surface whose angular deflection, (within defined limits), is proportional to the tab deflection. It is planned to restrict the tab deflection to a maximum of 15 degrees in order to keep the deflection within the linear range. Figure 1a is a schematic representation of the Yaw Damper.

The gyroscope is a single-degree-of-freedom gyro in which the precession is resisted by an elastic restraint; this places the instrument in the category of rate gyros. In this type of gyro an angular velocity input causes a torque to be applied, as output, to the restraint. In the application under discussion, the elastic restraint is the air load, which creates a moment about the tab hinge line proportional to the deflection of the tab. The gyroscope is mounted in such a manner that its spin axis is directed parallel to the X-axis of the aircraft; its input axis is parallel to the Z-, or Yaw, axis, and its output axis is parallel to the Y-axis of the aircraft. Figure 2 is a schematic diagram of a single-degree-of-freedom gyro, indicating its reference axes and component parts.

The Yaw Damper system works as follows when the airplane is disturbed by a side gust that induces an angular velocity about the vertical axis: The gyro senses this angular velocity and, because of its restraint, produces an output position angle. According to the gyroscopic law,* the gyro precesses

*From page 8-3, ref. 7, "The condensed form of this law relates the applied torque, M, the angular momentum of the rotor, H, and the absolute precessional angular velocity of the spin axis, W, by $\overline{M} = \overline{W} \times \overline{H}$, or $\overline{W} = \frac{\overline{H} \times \overline{M}}{H^2}$. In non-vectorial form, this law may be written W = M/H, plus the rule that 'the spin vector precesses toward the torque vector.' If a torque is applied tending to change the direction of the angular momentum vector, the vector will precess about an axis at right (concluded on following page)

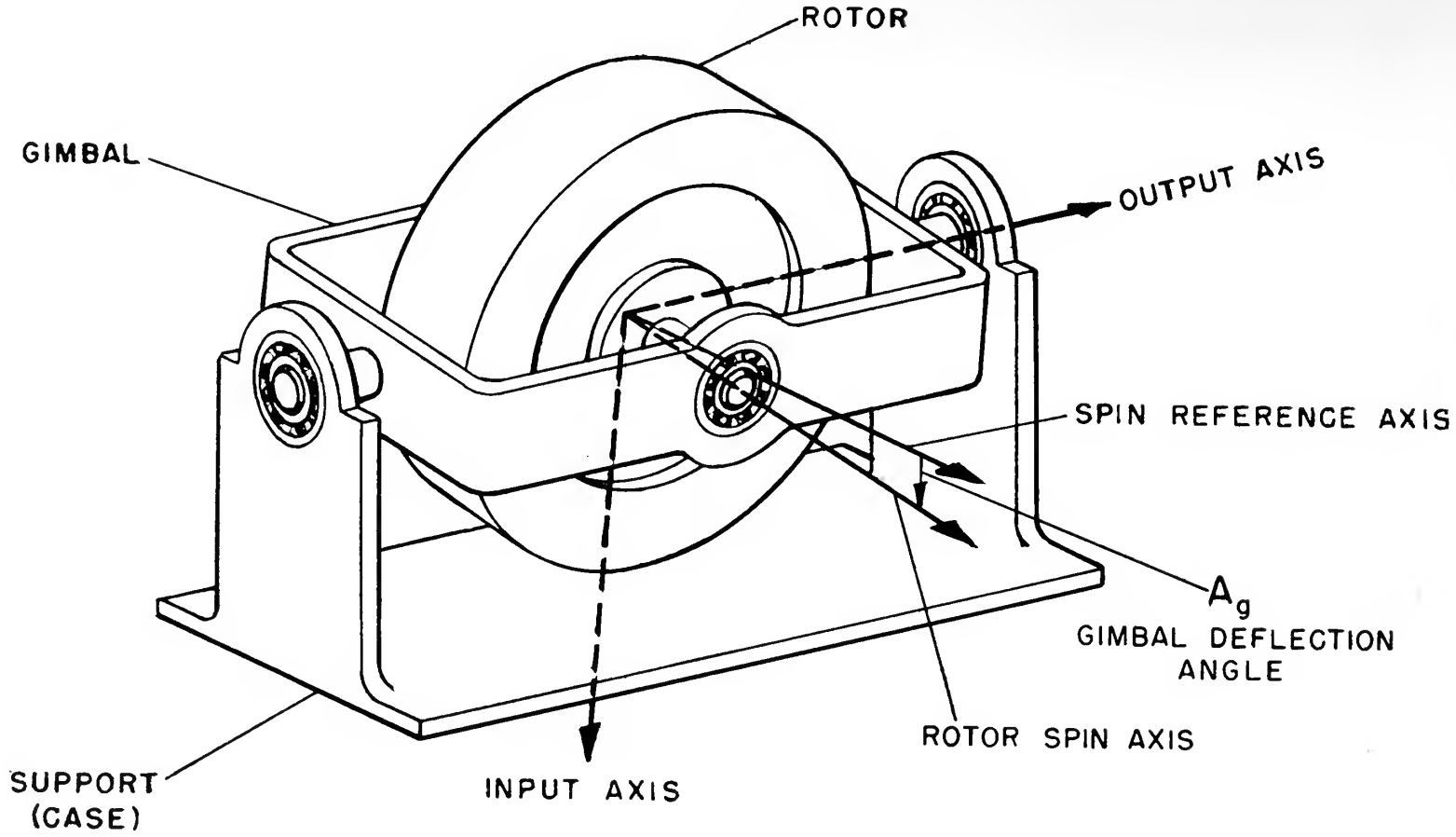

FIG. 2. SINGLE-DEGREE-OF-FREEDOM GYRO

about its output axis, which is perpendicular to both the input axis and the spin axis. The tendency is for the spin axis to precess toward alignment with the input angular velocity vector. This moves the gyro pickoff link, which is attached to the output axis. This motion in turn, is translated to the rudder tab which, by deflecting, causes the rudder to deflect so as to oppose the motion of the airplane. This, of course, reduces the input almost instantaneously, only a small time lag occurring between the deflection of the tab and the response of the rudder to the tab deflection. Figure 3 is a block diagram of the complete Yaw Damper system.

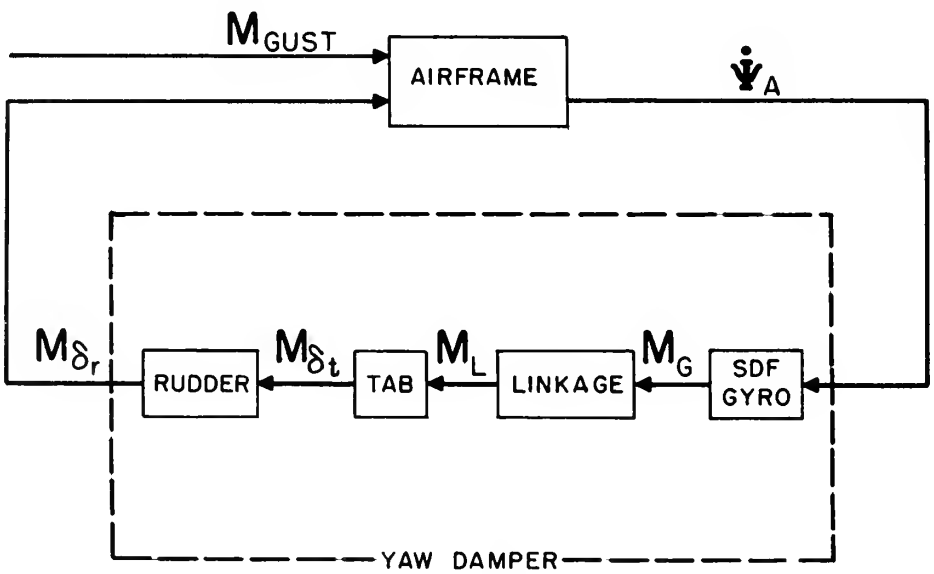

FIG. 3. YAW DAMPER FUNCTIONAL DIAGRAM.

(continued) angles to both itself and the axis of the applied torque at a rate proportional to the applied torque and inversely proportional to the angular momentum. The law of the gyroscope is a reversible one, i.e., a torque input results in an angular velocity output (precession) and an angular velocity input (forced precession) results in a torque output being applied to whatever restraint is provided in the instrument."

Chapter 4

PRELIMINARY DESIGN OF THE YAW DAMPER

The airplane lateral stability criteria as developed in Appendix A, indicated that an increase in the aircraft damping in yaw was desirable. To accomplish this, a method based on the output torque characteristics of a single-degree-of-freedom rate gyroscope was selected.

In this design, the gyroscope is oriented to receive rate of yaw of the aircraft as an input; the gyroscope torque output then acts to produce a rudder position in the proper direction to oppose and dampen the yawing rate of the airplane. The rudder is positioned by means of a tab which is operated directly by the gyroscope output, and is effectively a power amplifier between the gyro and the rudder.

Without adequate information concerning the characteristics of such a power system, it was necessary to make a preliminary investigation into the practicability of the design. A primary factor of interest was the friction level in the system. For a reasonable friction level, the remaining torque from the gyro had to be sufficient to position the rudder tab against the opposing aerodynamic hinge moment of the tab when operating in a moving air stream.

In order to simplify the tests, the tab hinge moment characteristics were assumed to be sufficiently linear to permit simulation by a spring restraint. Since the rate gyro requires a spring restraint, this restriction on the tab hinge moment parameter permitted the tab to perform this function directly.

Further restrictions on the maximum angular displacements of the tab and rudder permitted the additional assumption that rudder motion would not affect tab position during operation. With this assumption, the tab position would be a function of the gyro output only, and a direct calibration could then be made for gyro output moments. For a symmetrical system no angular restrictions are necessary up to the stall region.

In the preliminary tests, an estimate of aerodynamic tab hinge moments was made in order to select the size of the gyroscope required in an actual

aircraft installation. From the law of the gyroscope, as developed in reference 7 and other sources, $\bar{M}_{out} = \bar{H} \times \bar{W} = HW \cos Ag$. By proper selection of the gyro-to-tab linkage ratio, the angular displacement of the gyro was limited to 15 degrees, a value which would introduce a maximum output torque reduction of only 4 percent if the cosine term were to be neglected.

For an estimated tab hinge moment of 1.5 inch-pound, and an angular rate of yaw of 1.5 degrees/sec for full tab angular displacement, application of the gyroscope law shows that a gyro H value of 64.5×10^6 dyne-cm-sec was required. The largest gyro available had a specification of 72×10^6 dyne-cm-sec and was selected on the premise that the friction level and unbalance and uncertainty torques would not prevent the realization of the estimated torque requirements. It was found that the physical size was also practical for possible installation in small aircraft of the Piper "Clipper" type for later testing.

Since the preliminary setup was to be for the full-size system, efforts were made to simulate closely the conditions of operation. A rudder trim tab and a self-aligning bearing for a Navy SNJ type aircraft were obtained and formed, with the gyro, the basic units in the mockup. No attempt was made to reduce hinge moments in the tab; however, the self-aligning bearing was cleaned and lubricated with a light oil, on the predication that such care would be required on the actual installation for best operation of the system. The previous assumption of non-interaction between rudder and tab positions enabled the mockup to be shortened by attaching the gyro linkage directly to the tab, thus bypassing a free-link rudder support. This permitted the entire system to be mounted on a board of convenient length for making turntable tests. Figures 4, 5 and 6 are photographs of the mockup used in the tests.

From initial static tests, the friction torque level measured at the tab was found to be 0.0394×10^6 dyne-cm. A calibration run using balance weights was made at 26.18 mr/sec for the gyro output and the tab input moments. From this data, the friction torque was found to be 0.039×10^6 dyne-cm, or 7 percent of the gyro output torque. With no spring restraint, the system was sensitive to a minimum table rate of 0.4091 milliradian/sec, indicating a Coulomb Friction level of 0.029×10^6 dyne-cm. A slightly higher friction level due to the rudder free-link support is to be expected, but the total is not

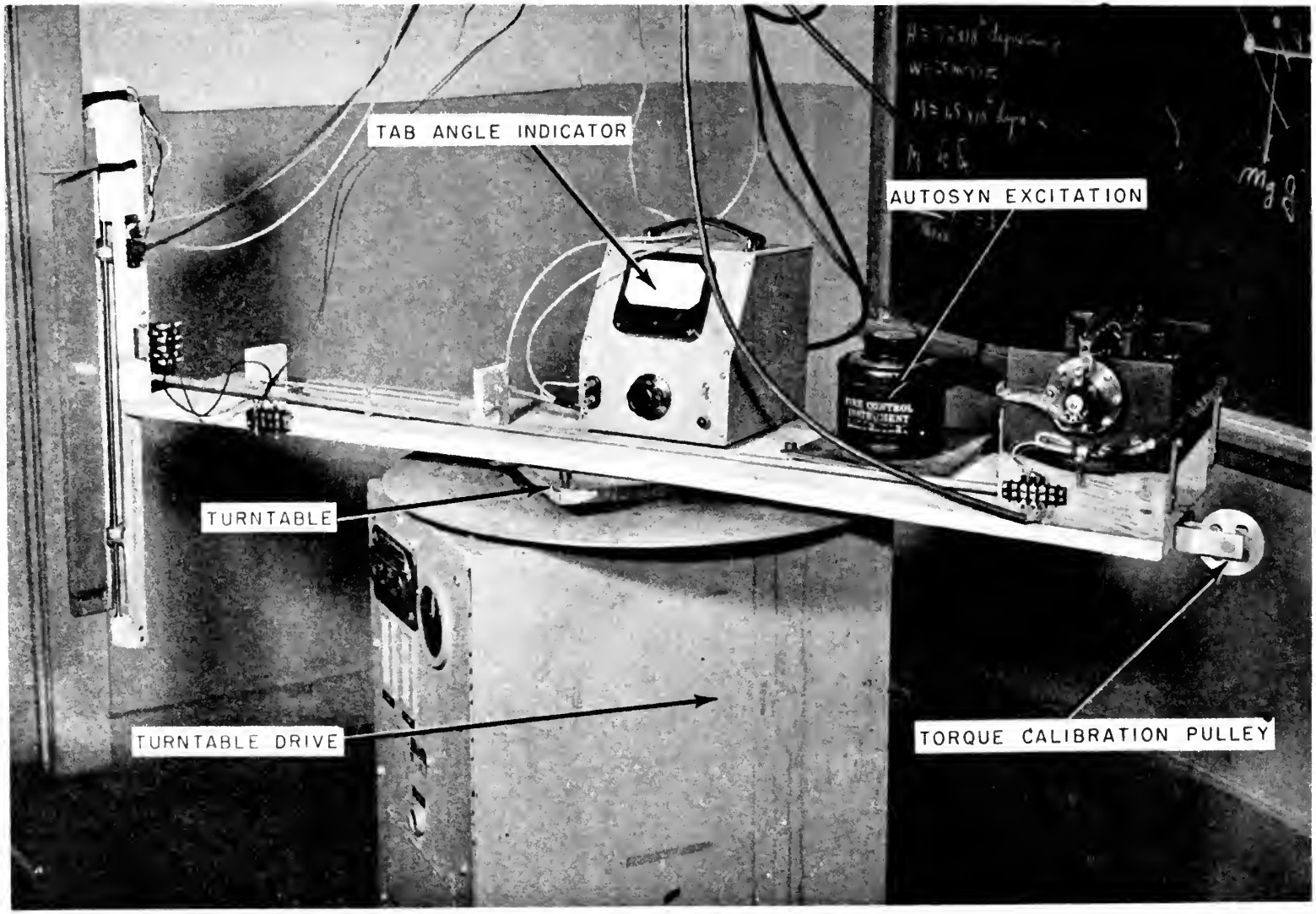

FIG. 4. GENERAL LAYOUT — YAW DAMPER INSTALLED FOR TURNTABLE TESTS

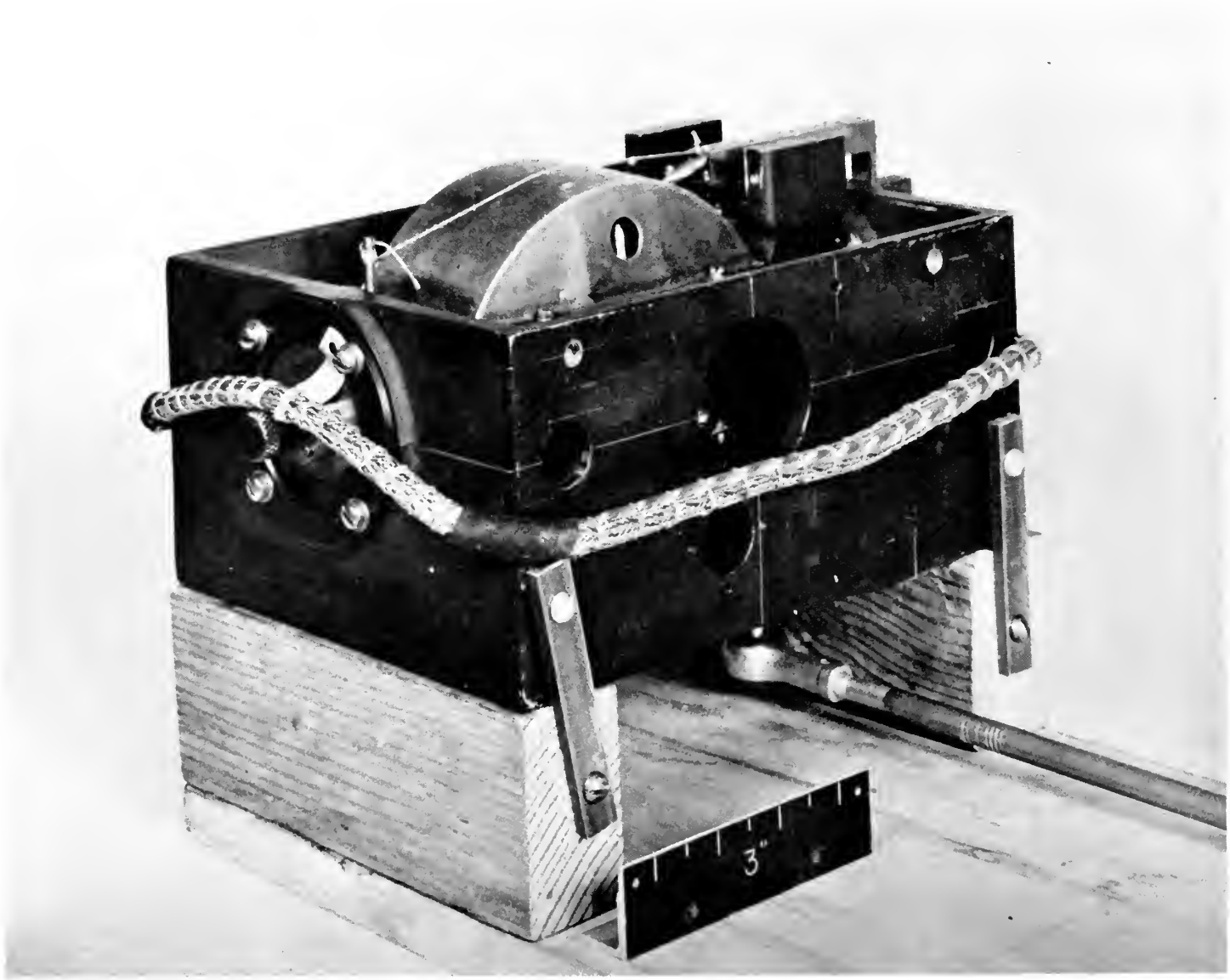

FIG. 5. DETAIL SHOWING GYROSCOPE AND LINKAGE CONNECTION

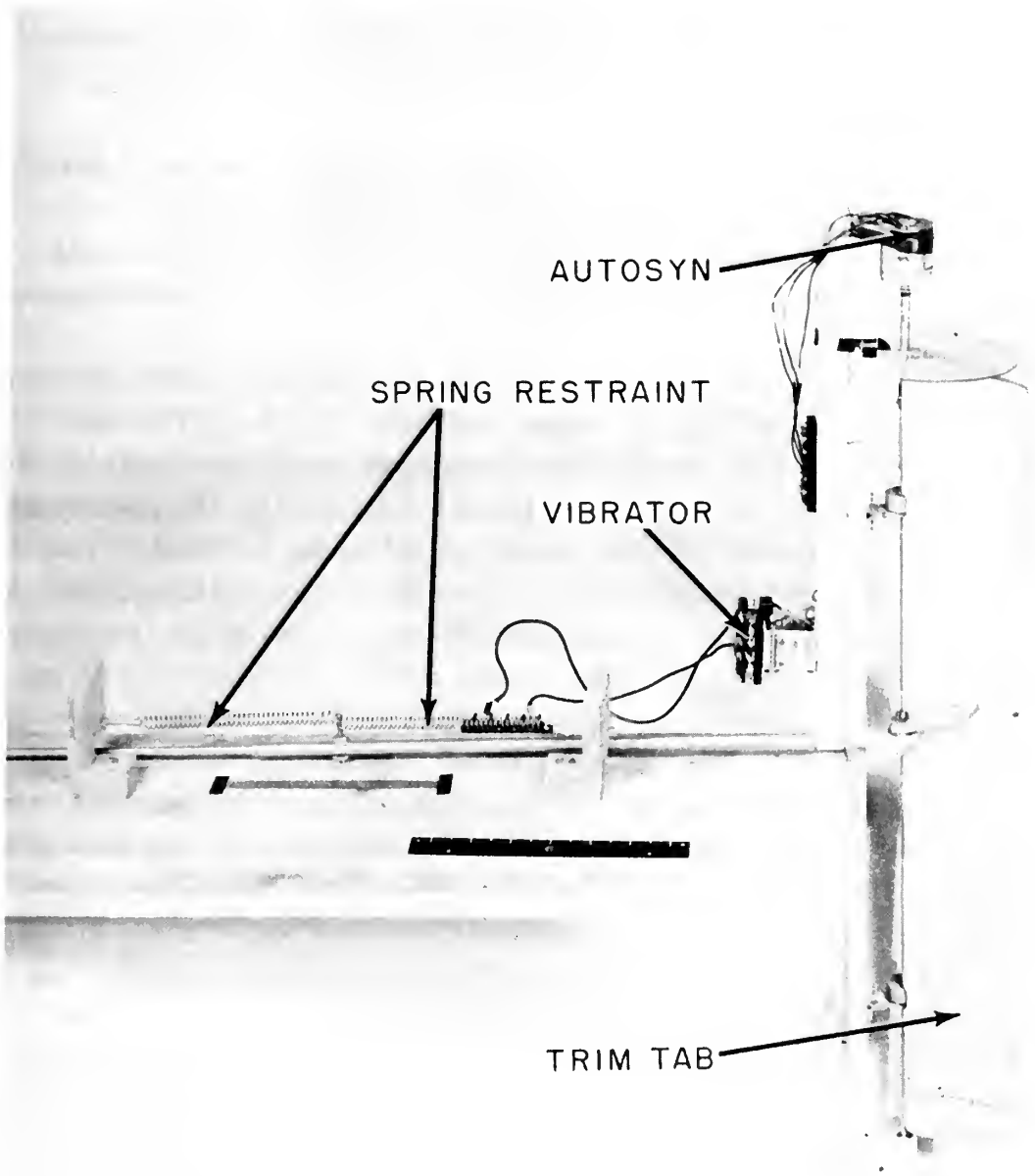

FIG. 6. DETAIL SHOWING TRIM TAB, AUTOSYN AND SPRING RESTRAINT

expected to exceed 15 percent. For this value of friction, the gyro selected appeared to be of a reasonable size to carry out the design specification for the tab positioning function.

The spring constant was calculated to be 0.082×10^6 dyne-cm/degree for the spring used in these tests. No attempt was made to reproduce an aerodynamic spring constant accurately, since a reasonable correlation of the mockup data to wind tunnel test data could be accomplished by applying a constant multiplying factor.

For a final check, the system was placed on a sinusoidal input table and the frequency at which oscillations began was found to be 1.6 cycles/sec. Based on a normal design criteria of 0.5 cycle/sec as an upper limit for aircraft undamped natural frequencies, it is not anticipated that the yaw damper unit natural frequency will create a stability problem due to vibration coupling.

In all the mockup tests a 60-cycle vibrator was exercised to simulate the aircraft airborne vibrations. It thus tended to reduce all friction levels to a minimum, particularly the Coulomb Friction effects.

On the basis of the test information obtained as described above, the feasability of the system mockup was accepted and the construction of a wind tunnel model incorporating this system was begun. The scale model was built to permit wind tunnel testing of the Yaw Damper performance under simulated flight conditions.

Chapter 5

DESIGN OF THE WIND TUNNEL MODEL

Theoretical analysis established the benefits that may be derived by increasing the damping coefficient in yaw, C_{n_r}, by a factor of four. Preliminary design studies indicated that this increase might be achieved through the use of a rate gyro.

Under actual flight conditions the amplitude and phase relationships between the airplane motion and the rudder motion become functions of many variables, such as the amount of inertia of the gyro linkage system (which consists of the moment of inertia of the gyro about its output axis, the moment of inertia of the tab about its hinge line, and the inertia of the linkage system), the moment of inertia of the rudder, the forcing frequencies of the aircraft due to gusts, the aerodynamic configuration of the tab and rudder, the degree of static and dynamic balance of the tab and rudder, size of the air gap between the rudder and the vertical fin and between the tab and the rudder, the slack or lost motion in the linkage system, and friction in the system. It is conceivable that with all of these variables amplification, rather than damping, could result under certain conditions of flight. In an attempt to evaluate and select the variables that would produce an optimum system, the investigation was carried into the wind tunnel.

Two gyros were available for this investigation. The first gyro G(1) had an angular momentum of 72×10^6 dyne-centimeter-seconds. The second gyro G(2) had an angular momentum of 0.88×10^6 dyne-centimeter-seconds. By definition, angular momentum H is equal to the product $I_{spin}\, W_{spin}$. For both gyros, W_{spin} equals 12,000 rpm. Preliminary design studies indicated that the first gyro, G(1), was of sufficient size to produce the desired increase in yaw damping in a light aircraft. Installation and test of G(1) in a typical light airplane suggests an interesting extension to this investigation.

It was decided to install G(2) in the wind tunnel model. Since the two gyros were the controlling scale factor in deciding the model size, and since the aerodynamic moments vary as the cube of the airplane dimensions, the ratio of lengths between the prototype with G(1) installed, and the model with G(2) installed became;

$$\text{Scale Factor} = \frac{72 \times 10^6}{.88 \times 10^6} = \frac{4.35}{1}$$

Assuming the fuselage length of the prototype to be 22 feet, the length of the model became 5.06 feet. An overall length of 5.0 feet was actually used for the model.

The wind tunnel model, mounted in the horizontal plane, was constrained about all axes except the vertical axis. Since the only alteration in the aircraft being considered in increasing the damping was in the vertical tail configuration, the model merely consisted of a fuselage and a vertical tail.

The fuselage was constructed of balsawood (Fig. 7), and proportioned to accomodate the gyro, its associated linkage, and the angle-measuring instruments. In other words, the fuselage was designed as a streamlined box to carry the vertical tail and the necessary measuring instruments. Slab sides with curved edges, and as many straight-line panels as possible, were used to decrease model cost and construction time. The proportions of the fuselage are similar to those of the B-26. The fuselage was dowelled together with pine wood inserts to facilitate the use of wood screws in joining the parts. Hardwood inserts were used at all of the pressure points to add sturdiness to the model.

The fuselage was designed in four parts: the streamlined solid nose; the underbody extending from the nose back to the tail; the forward top section extending half way back from the nose to the tail; and the after top section (Fig. 8) carrying the vertical tail, the gyro, and the associated linkage. This subdivision was made so that access to the inside of the fuselage would be simple, and so that installation and tests of the components could be carried out in the laboratory prior to assembly. The gyro and linkage were secured to the

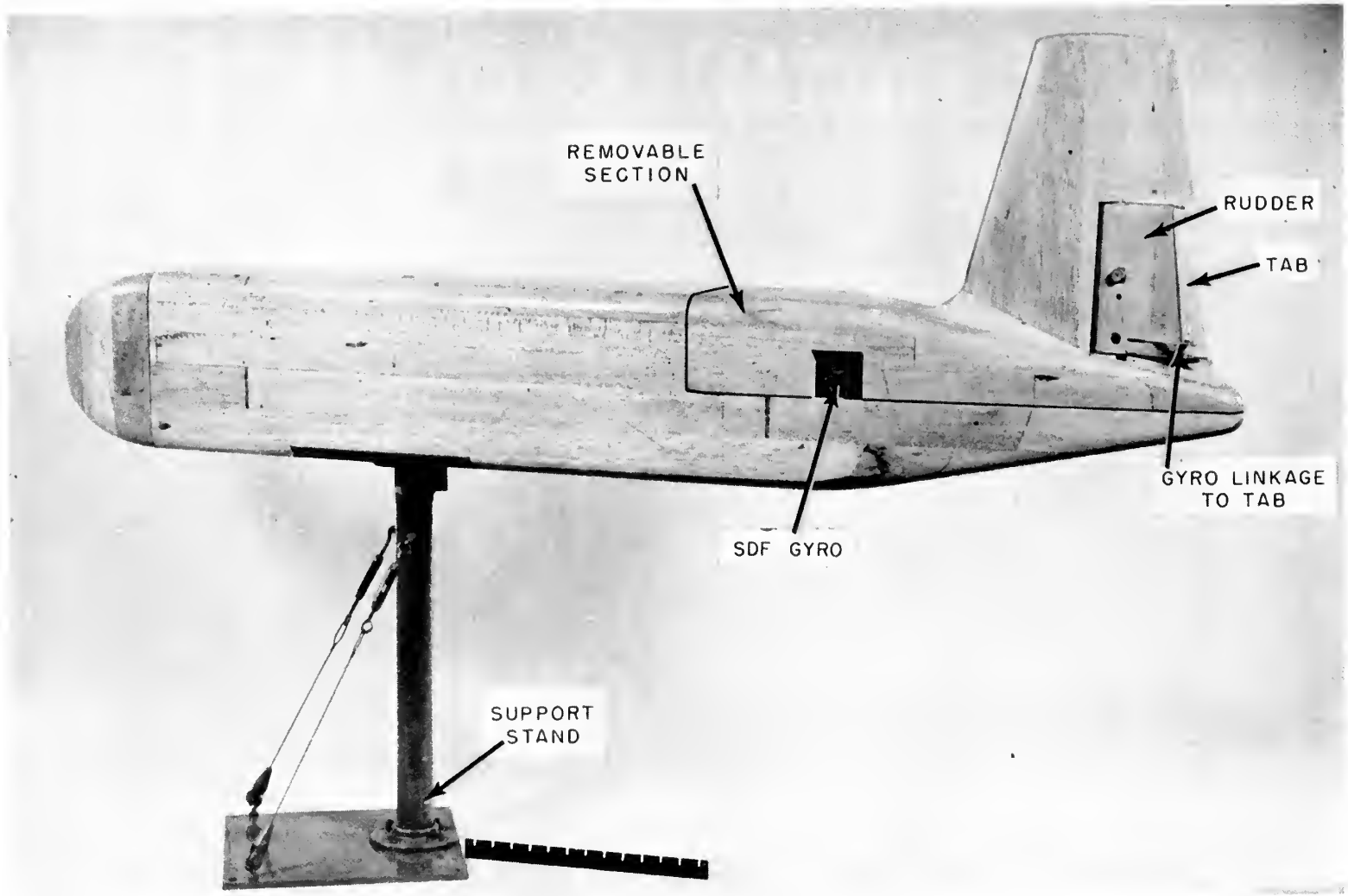

FIG. 7. SCALE MODEL FOR WIND TUNNEL TESTS OF YAW DAMPER

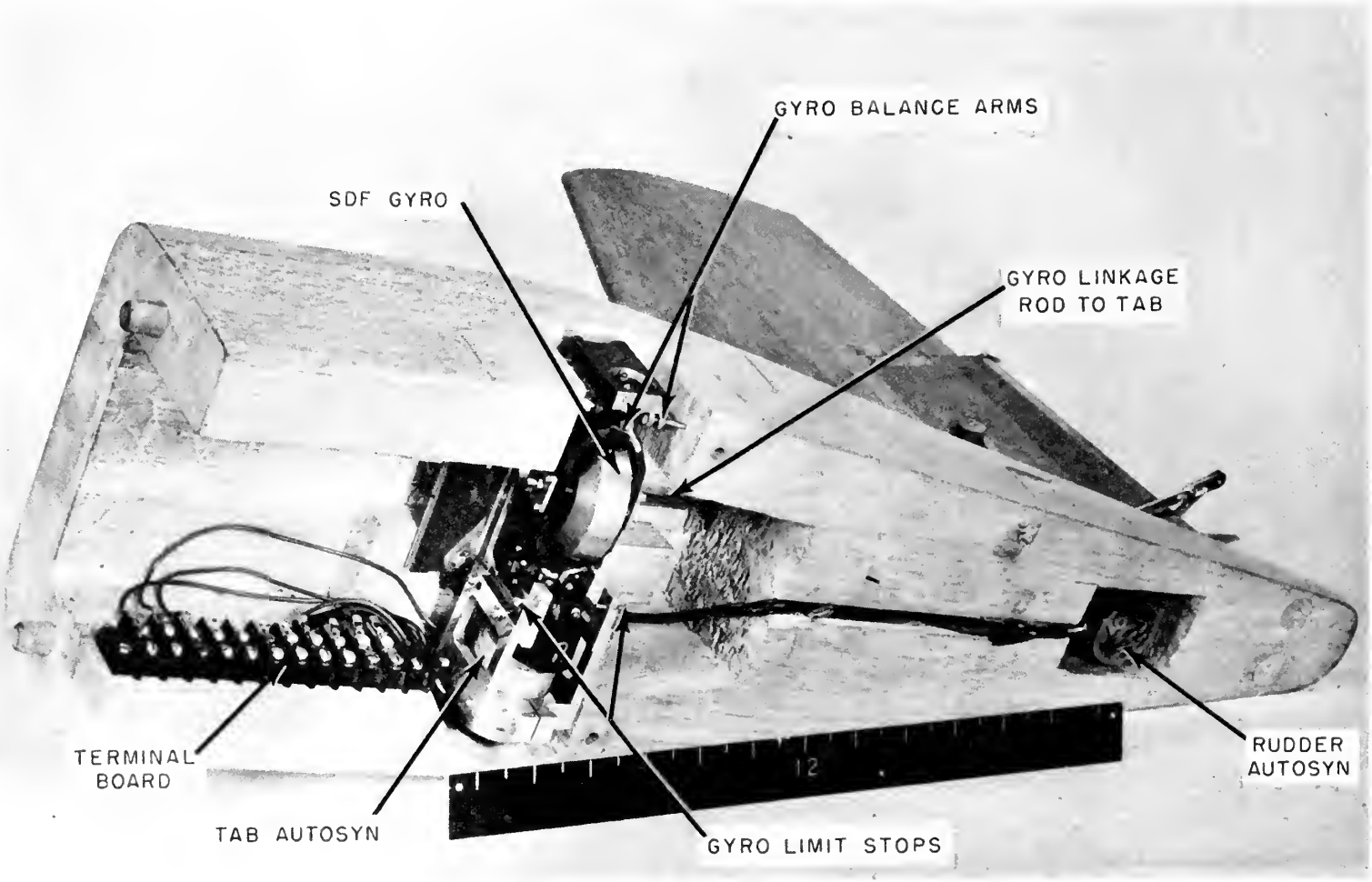

FIG. 8. CLOSE-UP OF REMOVABLE SECTION SHOWING INTERIOR DETAILS

after top section containing the vertical tail, tab, and rudder. With this arrangement the tests for friction, and gyro output versus angular rate, were made comparatively easy.

The fuselage was supported by a two-inch vertical steel pipe fixed to the floor of the tunnel. This support was mounted on an aluminum plate that was bolted to the tunnel floor. Two tension cables helped to steady the support during the actual tunnel tests. The support being hollow, a means was afforded for streaming the leads to the gyro and to the recording instruments. The fuselage was supported at a point one-third of the way back from the nose. This point was considered to be the center of gravity of the airplane. The model was provided with a means for varying the moment of inertia, I_{mod}, by varying the distance of a lead weight from the pivot point.

The vertical tail was made of balsawood having an NACA 0012 cross section. Figure 9 shows the size and important dimensions of the tail. The tail height, h_{vt}, was controlled by the selection of the aspect ratio, $(AR)_{vt}$, and the vertical tail area, S_{vt}. An $(AR)_{vt}$ of 1.8 was chosen for two reasons, the first being that the model differed from the normal geometric configuration in that no horizontal tail, which would act as an end plate and increase the $(AR)_{eff}$, was present on the model. This endplate effect increases the $(AR)_{eff}$ by a factor of 1.55 (Ref. NACA TN 755). The second reason is that there is a tendency in modern aircraft design to increase the $(AR)_{vt}$, within structural limits, thereby increasing the slope of the lift curve of the vertical tail, and the tail effectiveness.

Since the wind tunnel tests are to be run with the idea of determining the increase in yaw damping through the introduction of the gyro-controlled surface, the design of the vertical tail was solid, simulating a stick-fixed flight condition, except for the gyro-controlled portion. As has been previously explained, the tail on an actual plane would consist of a vertical fin and two rudders, one controlled by the pilot and the other controlled by the gyro-tab combination. These two rudders would be of approximately the same size. The pilot-controlled portion should be designed to allow the same pilot control of the aircraft as is required in present-day specifications. It was

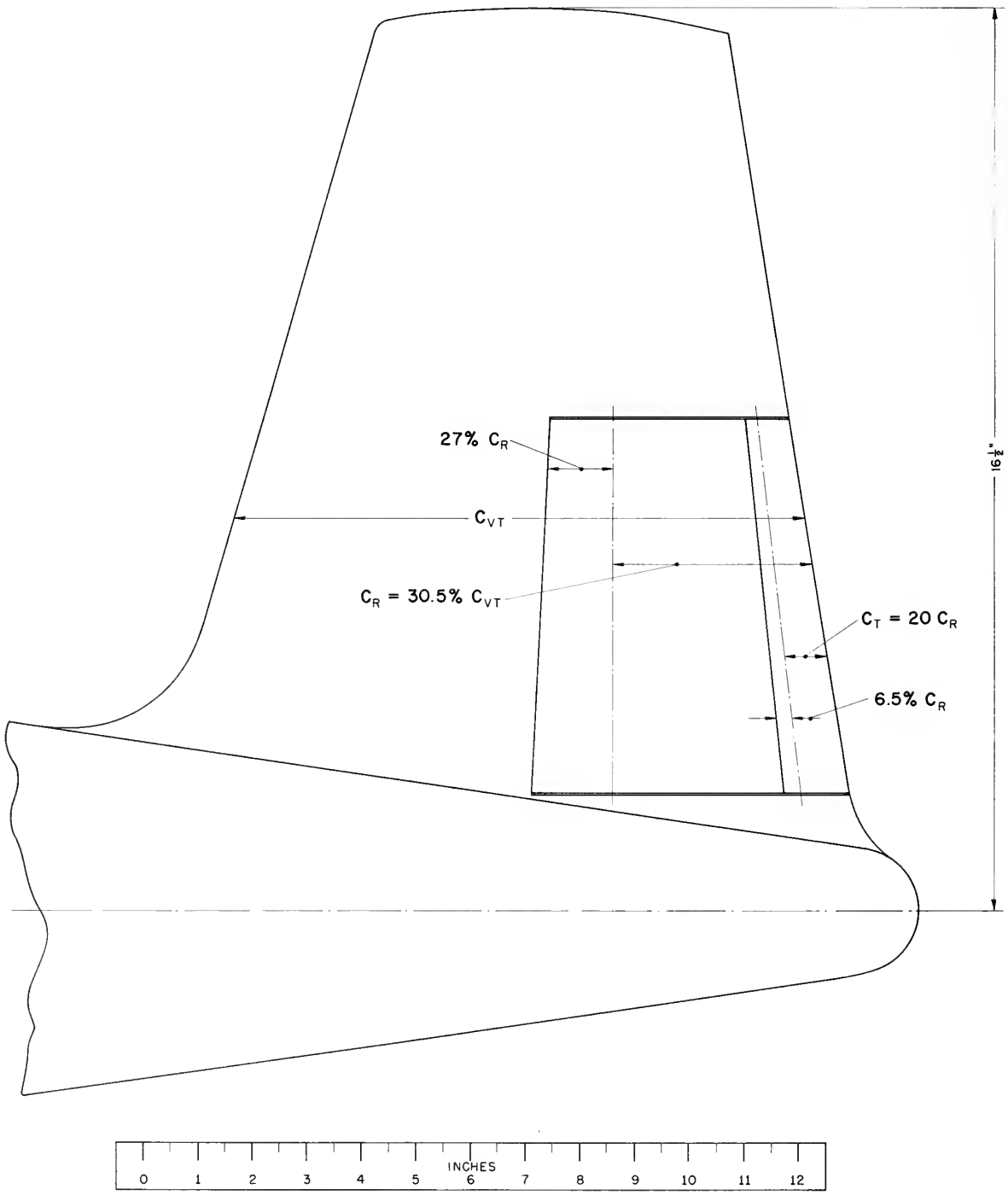

FIG 9 DETAILED DESIGN OF THE VERTICAL TAIL FOR THE WIND TUNNEL MODEL.

estimated that the gyro-controlled portion of the rudder would aid the pilot as much as 20 percent in slow flight while correcting for yaw, such as in a landing or take-off run. The gyro-controlled rudder, being more sensitive to rates than the pilot, should greatly enhance the flight characteristics of the plane. In steady turns the pilot would have to overcome the forces resulting from the controlled-rudder output.

The vertical tail area, S_{vt}, was selected to be 12 percent of the area of the wing of the aircraft. Since the ratio for small planes rarely exceeds 10 percent, this increase in design area was an attempt to insure the pilot-controlled section remaining as effective as is required by lateral control specifications.

The gyro-controlled tab was made of pine because of the small size of the tab and because of the magnitude of forces from the link and hinge that are imposed on the tab. Several tabs were constructed and tests for system stability were made for each tab. The tab was actually supported by ball bearings fitted into aluminum end plates that were carried by the rudder. See Fig. 12 for tab design and table of modifications.

The rudder was made of balsawood and hollowed out to accomodate the linkage system. The actual construction of the rudder can best be understood by studying Fig. 1 a.

The design configuration for the tab and the rudder resulted from a study of systems that would produce small hinge moments per degree of rudder tab effectiveness. See Appendix B. This led to an aerodynamically balanced rudder and an under-balanced tab. The hinge positions, chord lengths and areas are shown in Fig. 9. The leading edge of both the rudder and the tab were made elliptical. It was felt that sharpening the nose might be necessary, but this modification would be comparatively easy to accomplish in a wooden control surface.

The rudder was statically balanced about its hinge line as nearly as possible so that it would be insensitive to inertia effects as a result of angular accelerations of the fuselage about the vertical, Z-axis. Means for statically balancing the rudder were provided by inserting lead weights in the rudder nose in a void provided for the weights. The linkage was constrained in the XZ plane so that its inertia effects could also be neglected.

The angular position of the fuselage with respect to the center line of the tunnel was measured with an autosyn, an instrument whose voltage output is a linear function of angular displacement. The case of the autosyn was fixed relative to the support; the rotor shaft moved with the fuselage as indicated in Fig. 1 a. Rudder angle was measured by an autosyn that acted as the bottom hinge for the rudder. Tab angle, being a function of the gyro gimbal position about the output axis, was measured at the gyro. Voltages were picked off by a three-channel recording instrument that photographed these angular measurements on a permanent trace on the same time scale.

It was an important design consideration to keep the system as symmetrical as possible so that rudder motion would not effect tab deflection. This was accomplished by running the linkage from the gyro along the fuselage axis of symmetry, to the rudder hinge point. The installation of the gyro linkage arrangement can be seen in Fig. 1 a. The gyro output axis was mounted horizontally along the Y-axis of the airplane so that angular rates would result in torque outputs directly proportional to this angular rate. The torque output about the output axis of the gyro was transmitted back to the tab by the linkage arrangement. A discontinuous rudder hinge was necessary so that the linkage could be symmetrical.

The gyro with the links attached was balanced about the gyro output axis to insure that the forces on the tab were functions only of angular rate of yaw and not of angular position of the output gimbal. The linkage was made adjustable so that the tab and gyro could be properly centered. Means were provided whereby the ratio of tab deflection to gyro gimbal rotation could be varied. A linkage ratio was chosen so that a 7.5-degree gyro gimbal angle produced a maximum tab deflection of 15 degrees. In order to reduce weight and friction in the system to the minimum, magnesium and aluminum links and fittings were used with miniature ball bearings at all of the moving joints.

The air gap between rudder and vertical fin, and between rudder and tab was made less than 0.025 inch by filling up the gap with masking tape until the desirable clearance was obtained.

Control strings from either side of the tail to observers on either side of the tunnel test section provided means for introducing yaw angles and for stopping undesirable oscillations during the wind tunnel tests.

Chapter 6

WIND TUNNEL TESTS

In order to measure the effect of a control surface actuated by a rate gyro in increasing the damping in yaw, model tests were conducted in the small wind tunnel located in the Guggenheim Aeronautical Laboratory at the Massachusetts Institute of Technology, Cambridge, Massachusetts. Figure 10 shows the layout and general dimensions of this wind tunnel.

The 4.35:1 scale model was instrumented and mounted on a pedestal which was located on the tunnel center line. Figure 11 illustrates the general arrangement for the test runs. A preliminary test was made to observe the air flow around the model. Small strings were attached to the tail section to indicate any boundary layer separations. No separation was observed at any speed for yaw angles up to 20 degrees, at which point the vertical tail had reached the stalled condition.

It was observed that the tunnel air flow was not smooth and that the model oscillated in response to the turbulence of the tunnel flow. This turbulence or "noise" was a random effect and had high frequency harmonics. A more detailed analysis of noise characteristics is beyond the scope of this thesis but the effects on the model in the tunnel was qualitatively measured at air speeds from 30 to 80 miles per hour at intervals of 10 miles per hour. Figure 12 is a plot of the amplitude and period of the over-all noise data and indicates that these effects increase with air speed. Brush recordings of tunnel noise are included in Appendix D.

The next step was to check the stability of the control surfaces. It was immediately apparent that the rudder, with tab fixed, was unstable. For this original configuration, shown in Fig. 9, C_{h_α} was positive and C_{h_δ} negative. The rudder system was made stable by increasing the tab chord dimension by 0.4 inch and this new tab configuration installed as indicated in Fig. 13. This tab will hereafter be referred to as the original tab.

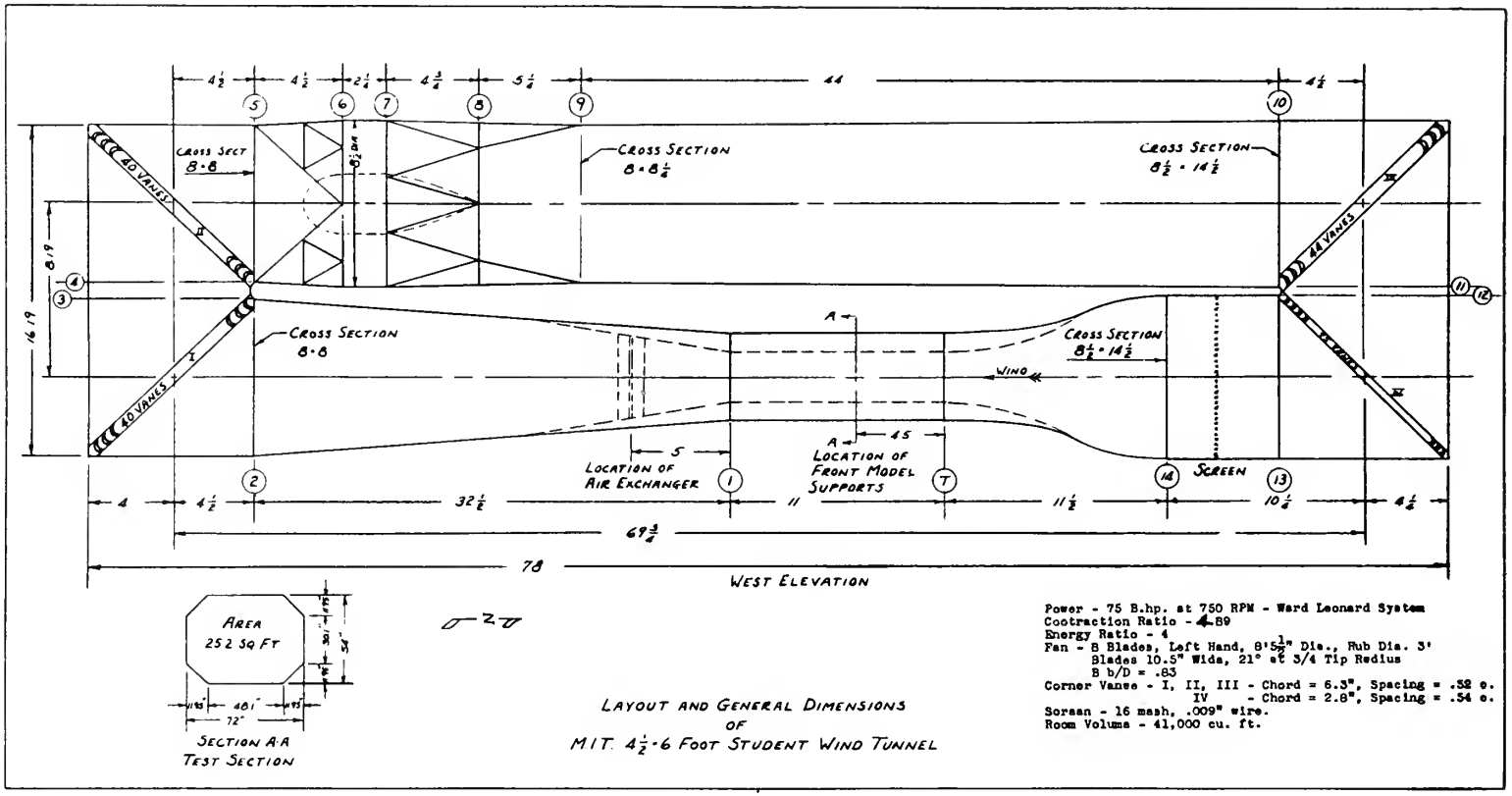
Cross Sect 8·8
Cross Section 8·8½
Cross Section 8½·14½
40 Vanes I
40 Vanes II
44 Vanes III
44 Vanes IV
Cross Section 8·8
Wind
Location of Air Exchanger
Location of Front Model Supports
Screen
West Elevation
Area 252 Sq Ft
Section A-A Test Section
Layout and General Dimensions of M.I.T. 4½-6 Foot Student Wind Tunnel
Power - 75 B.hp. at 750 RPM - Ward Leonard System
Contraction Ratio - 4.89
Energy Ratio - 4
Fan - 8 Blades, Left Hand, 8'5 1/8" Dia., Hub Dia. 3'
Blades 10.5" Wide, 21° at 3/4 Tip Radius
B b/D = .83
Corner Vanes - I, II, III - Chord = 6.3", Spacing = .52 c.
IV - Chord = 2.8", Spacing = .54 c.
Screen - 16 mesh, .009" wire.
Room Volume - 41,000 cu. ft.

FIG.-10

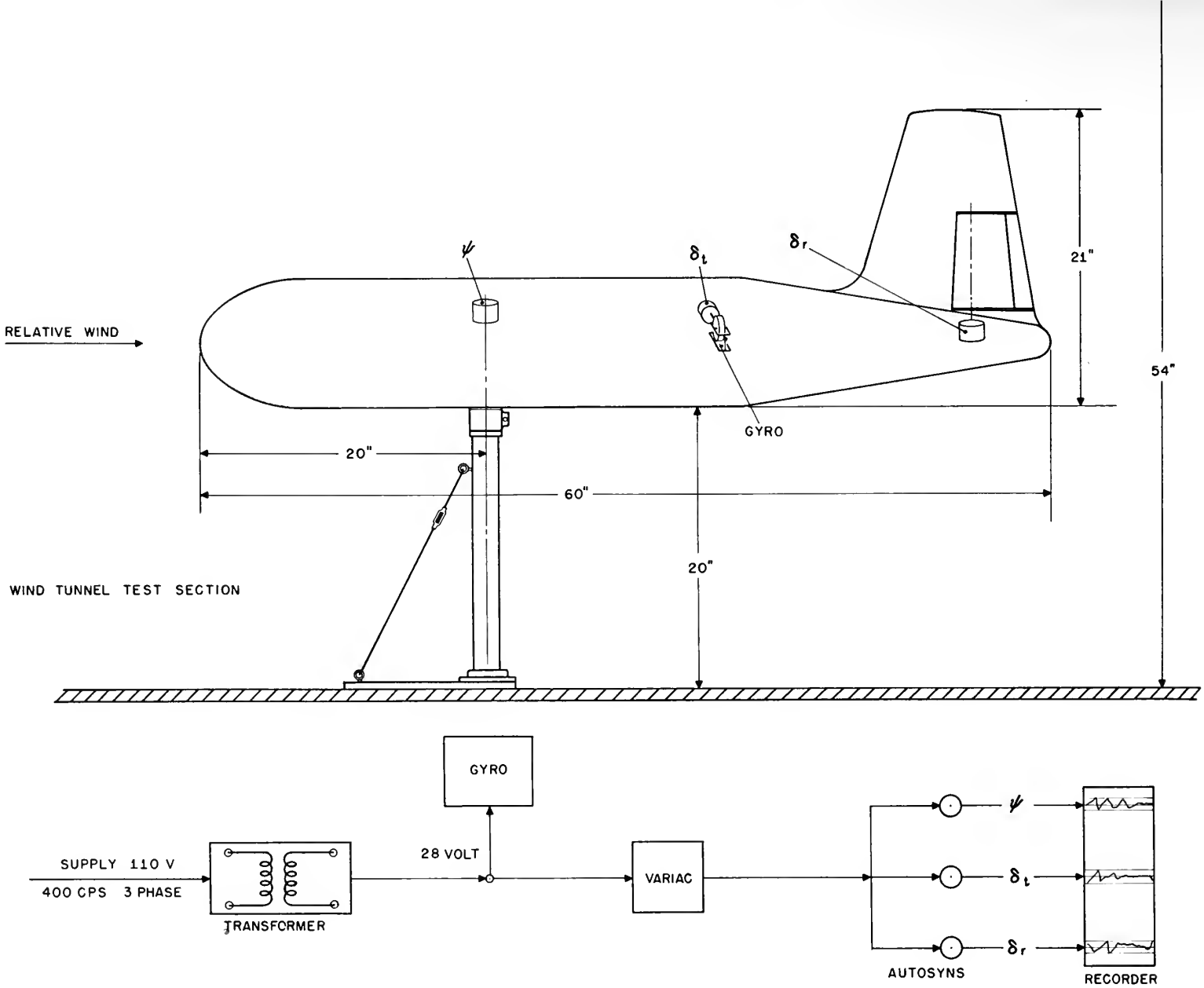

FIG. 11 INSTRUMENTATION AND MOUNTING FOR WIND TUNNEL MODEL

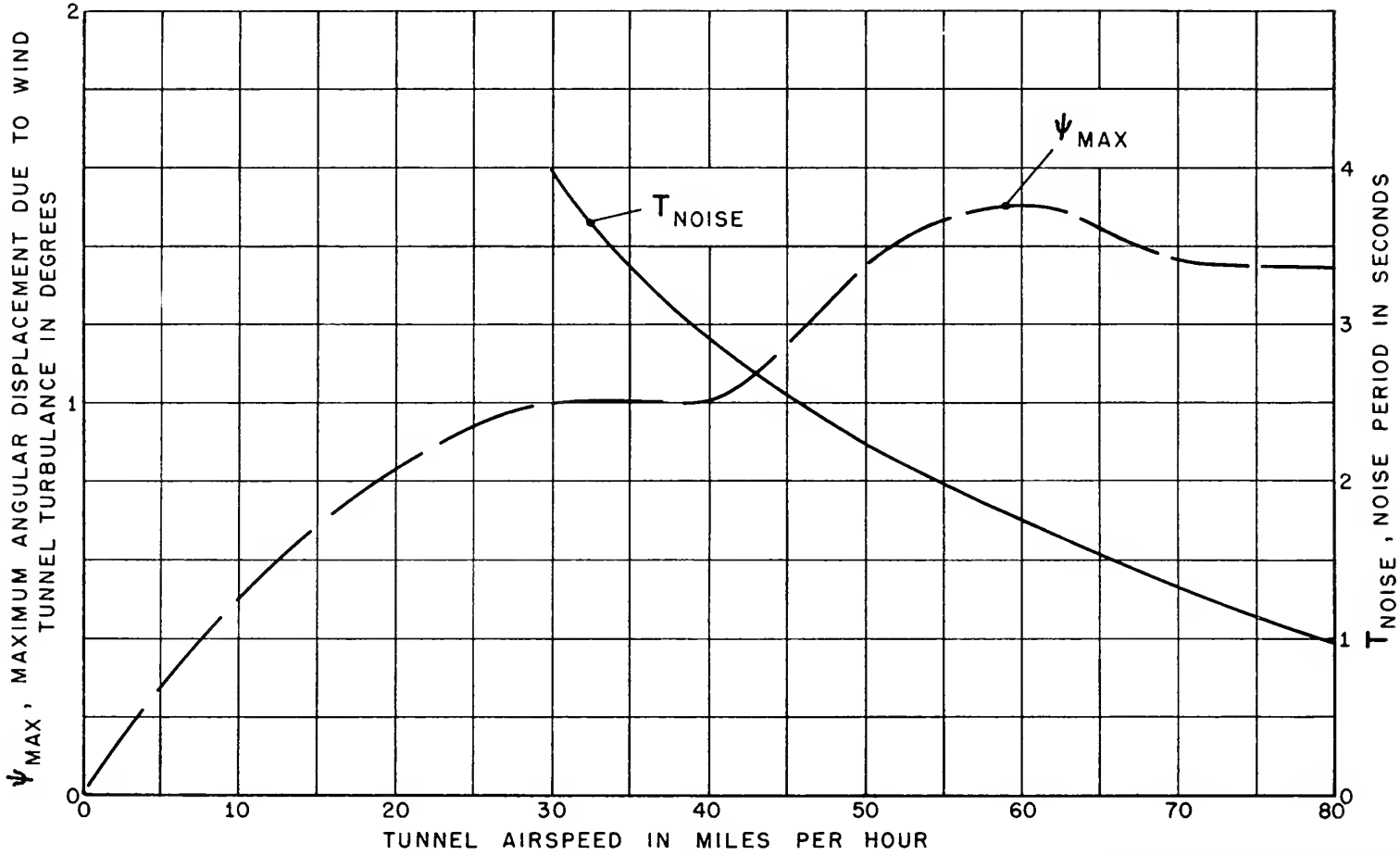

FIG. 12. PERIOD AND AMPLITUDE OF TUNNEL NOISE AS A FUNCTION OF TUNNEL AIRSPEED.

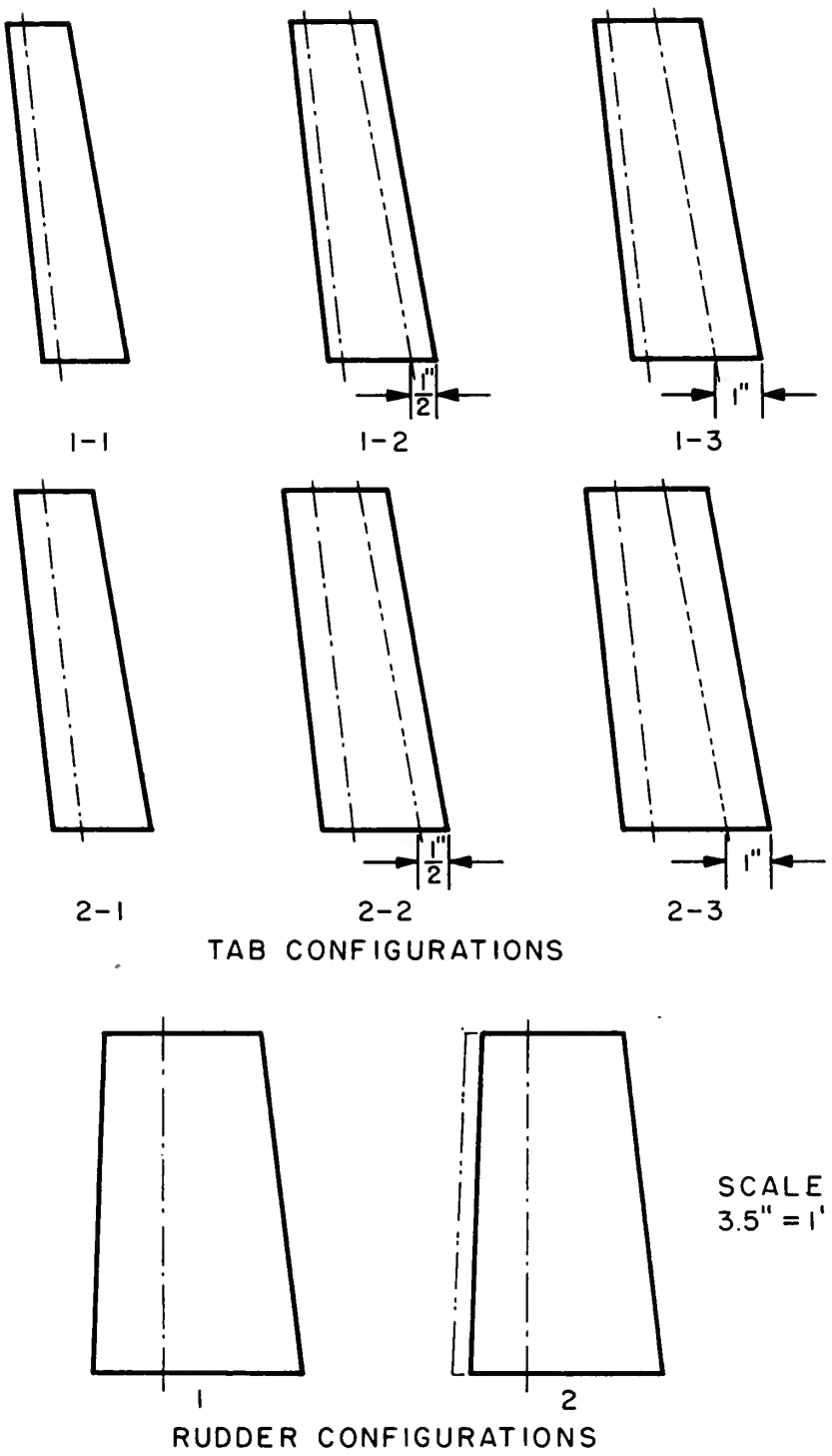

FIG. 13. MODIFICATION OF VERTICAL TAIL.

With this stable rudder arrangement, the rudder free and tab free system was next investigated. This combination was found to be unstable also. The thickness of the vertical tail was built up slightly to simulate the effect of sharpening the rudder nose and a slight improvement was noted. The rudder nose section was sharpened by shaving the balsa wood contours but no appreciable improvement was obtained.

On the basis of the negligible improvements observed, the aerodynamic balance of the rudder was reduced by removing the original nose section and replacing it with an aluminum nose cap. The new configuration is shown as number 2 in Fig. 13. At this point the rudder was only partially balanced statically by inserting lead weights in the nose section. Due to the small volume space within the nose cap and the reduced moment arm of the center of gravity of the nose section, a satisfactory static balance could not be obtained. Subsequent tests showed this configuration to be stable under both tab fixed and tab free conditions and no flutter tendency under the tunnel noise conditions was observed.

At the same time, a viscous damper was being installed to reduce the sensitivity of the controller linkage system to the high frequency tunnel noise excitation. This addition was found to improve the stability of the system and the viscous damper was therefore retained as a portion of this controller arrangement. Upon completion of these two alterations, this system configuration was selected as the basic yaw damper for testing purposes.

All data was available as output voltages while the aerodynamic yaw response and control surface positions were based on angular measurements. It was therefore necessary to obtain the calibration data for the autosyn voltages and the position angles. The permanent records were made on a Heiland photographic recorder actuated directly by the autosyn voltages and the response voltages were adjusted until all recording traces were within the tracing range for the maximum angular values previously outlined. All three traces were adjusted to the same reference center line for the calibrations and the rudder trace was then offset slightly to permit ready identification of the various traces. All data records have been included in Appendix D.

The moment of inertia of the model about the yaw axis was obtained from oscillations with a known spring restraint attached to the tail section. This was calculated to be 30.8×10^6 gm-cm^2 .

Upon completion of the instrumentation calibrations, the model was tested for control effectiveness factors. A tunnel airspeed of 60 miles per hour was selected for this data due to the velocity of 120 miles per hour which it represented for the full scale model, a value near the cruising flight condition. Data was obtained to determine static curves of ψ vs. δ_R, ψ vs. δ_T, and δ_R vs. δ_T. In addition, a record was made for fixed tab angles and free rudder and yaw. The respective control effectiveness curves are shown in Fig. 14.

Having completed all the basic work, the actual model tests were then begun. For comparison purposes, three tunnel speeds were selected for these runs. These speeds, 40-60-80 mph compare with full scale aircraft speeds of 80-120-160 mph. For light aircraft, these speeds will correspond to the landing approach, normal cruise, and fast cruise flight conditions. It is felt that this broad range of test speeds also provides a more comprehensive evaluation of the yaw damper control system.

Test data was obtained for the model yaw response from an initial yaw displacement of 15° for the following conditions:

1. Controls Fixed. No yaw damper operating.
2. Controls Free. The yaw damper is operating. Unless otherwise noted, all controls free tests are made with the gyro running.
3. Direct Control. This corresponds to controls free with the damping rudder fixed at zero deflection. The tab operates directly as the damping control.

The yaw damper system in condition 2 was found to oscillate in the zero yaw angle position. A temporary external rudder mass balance was added but did not improve the oscillation tendency. A trailing edge extension was added to the control tab to increase the tab hinge moment; this was not found to improve the situation. For the present control configuration, the oscillation appeared to be a function of the control linkage and the time lags in the system.

Further work to improve this tab and rudder control system was suspended and an amended approach initiated in which the tab control surface was operated directly by the gyro. For this approach, the rudder control surface was fixed in the zero deflection angle. Yaw response data was taken for the several tab configurations shown in Fig. 13. Basically, these tabs have two values of nose balance with two extensions added to the original trailing edge.

This direct control system was found to perform satisfactorily at the zero yaw angle position. As a final test, the tab system was operated in the balanced configuration with the half-inch extension and without the viscous damper in order to permit a comparison for the effect of the damper in the system.

At this point all tunnel tests were concluded. The effects of changes in the model moment of inertia and control system linkage ratio, while allowed for in the design of the model and anticipated as a part of the tunnel work, were not investigated due to the large volume of test data to be analyzed at this time.

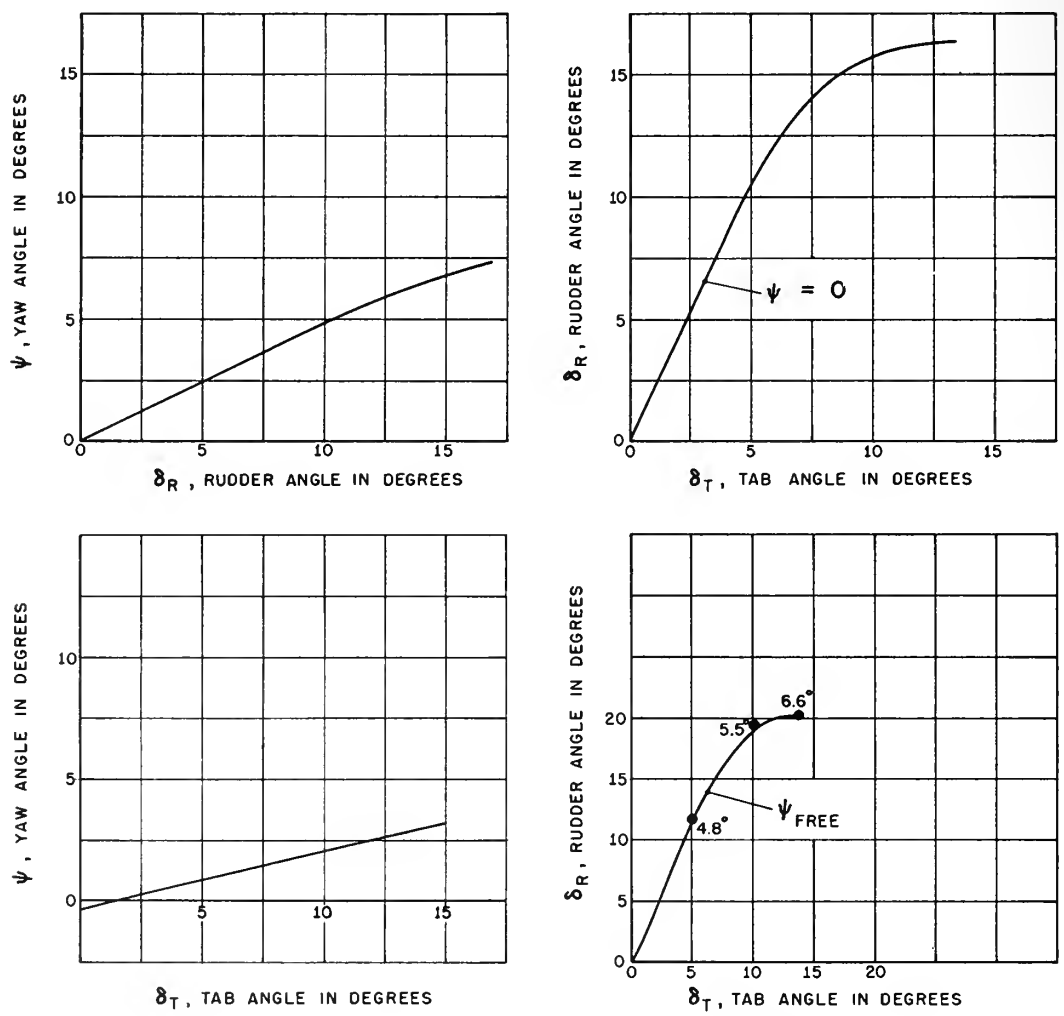

FIG. 14. CONTROL EFFECTIVENESS CURVES, SYSTEM 2-1-1.

Chapter 7

DISCUSSION OF RESULTS

In carrying out the investigation of a simplified yaw damping system for an airplane, it soon became apparent that the theoretical approach could not provide sufficient design information for an operating system. For this reason, the theoretical design was reproduced in a scale model and the system tested in the wind tunnel.

For testing purposes, the model was restricted to a fuselage and a vertical tail arrangement with a single degree of freedom in yaw only. In considering the motion of the model in the tunnel, the equations below describe the transient yaw response to a step input of yaw:

$$\frac{I_Z}{qSb}\ddot{\psi} + C_{n_{\dot{\psi}}}\dot{\psi} + C_{n_{\psi}}\psi = 0$$

$$\ddot{\psi} + \frac{C_{n_{\dot{\psi}}}}{C}\dot{\psi} + \frac{C_{n_{\psi}}}{C}\psi = 0 \qquad \text{Controls Fixed}$$

$$\ddot{\psi} + \frac{C'_{n_{\dot{\psi}}}}{C}\dot{\psi} + \frac{C'_{n_{\psi}}}{C}\psi = 0 \qquad \text{Yaw Damper Operating}$$

$$\ddot{\psi} + 2(DR)\omega_n\dot{\psi} + \omega_n^2\psi = 0$$

where: DR = damping ratio ω_n = undamped natural angular velocity

$$C = \frac{I_Z}{qSb} \qquad \omega_n = \sqrt{\frac{C_{n_{\psi}}}{C}}$$

$$DR = \frac{C_{n_{\dot{\psi}}}}{(2C)\omega_n} \qquad C_{n_{\dot{\psi}}} = \left(\frac{b}{2V}\right) C_{n_r}$$

[With negative sign of $C_{n_{\psi}}$ and $C_{n_{\dot{\psi}}}$ taken into account.]

With the Yaw Damper operating, the equations of motion become more complex than the simple second-order equation which describes the fixed-control case. This is because of the introduction of the non-linear damping term described in Appendix B. Since it was desired to compare the two systems, the response equation is assumed to remain a second-order function, and the primed coefficients reflect this effect.

In order to analyze the photographic data obtained on the Heiland recordings, all Yaw Damper tests were standardized as indicated in Chapter 6. The data has been correlated for three air speeds. This information is shown in the plots of Figs. 16 to 27, with the operating condition and configuration as indicated by Table I for each run. Specific configuration relationships may be obtained by referring to Figs. 9 and 13.

All plots have been presented in a non-dimensional form. The undamped natural period for the controls-fixed response at each airspeed was chosen as the non-dimensionalization time factor for all data at that airspeed. In this manner, the variations in undamped natural frequency due to changes in airspeed have been removed. In addition, the yaw response ordinate has been non-dimensionalized by taking the ratio of this angle to the initial yaw angle.

Figures 16, 17, and 18 show the comparative results for the three test conditions. All the test airspeeds have been shown, but, except for minor variations in the damping ratio, the general response data is similar for each of these speeds. The remaining figures show the response results obtained for the direct-control system with the tab extension dimension as the variable. Any other individual comparisons between the several tab configurations are readily obtained by overlaying the desired response curves. Figure 15 is a non-dimensional plot of the response of a second-order system to a step input as a function of damping ratio. The response curves of Figs. 16 to 27 inclusive may be compared with a second-order system by overlaying a specific response curve on Fig. 15.

From these tests, the Yaw Damper installation was found to greatly increase the effective damping of the model response from the initial yaw angle of 15 degrees. The response plots show that the model returns to a zero yaw angle position with no overshoot. However, at this position the control system oscillated and did not possess the smooth performance characteristics

desired. Under similar conditions in an actual aircraft, this installation would not contribute to pilot or passenger comfort and might eventually destroy itself.

In order to improve the system characteristics, the vertical tail fin thickness was increased and a small viscous damper added to the control linkage. Both effects acted to smooth the system, but reduced the effective damping sufficiently to cause a slight overshoot to occur.

The damper rudder was fixed at a zero deflection angle, and the tab then operated directly as a control surface. This direct control with viscous damper arrangement produced the smoothest operating system, but reduced the effective damping still further and increased the magnitude of the overshoot.

Because of the large initial yaw angle, response rates were sufficiently high to cause the tab to operate in the limit stops. In most cases, the yawing rate after the first peak overshoot was small enough to operate the tab within the 15-degree limit stops. For this reason, a measure of the direct control system effectiveness is difficult to obtain.

The comparative effectiveness of the various control conditions and configurations is shown in Table II. This table lists the time, T, in seconds necessary to damp the fuselage yaw angle to ten percent of its initial amplitude at each of the test airspeeds. A response time to damp to five percent initial amplitude is normally used for comparison purposes. Because of the small scale factors in the later portions of the response curves, the level has been increased to ten percent. An approximate method of conversion to this five percent basis is to estimate this level by an exponential decay from the ten percent position.

A time ratio T/T_{fixed} is arbitrarily selected as a figure of merit, where T_{fixed} is the time for the controls-fixed response to damp to ten percent. For evaluation, the smaller numbers correspond to the more effective system. In order to remove the variations due to airspeed, a similar time ratio based on T_N (the undamped natural period of the controls-fixed response) is also shown. Both ratios are included in the data of Table II.

Based on these figures of merit, it may be seen that the tab-rudder-gyro system is the most effective yaw damping control. Because of the instability

that arises near the zero yaw angle, this system at present is not feasible for an actual installation.

The direct tab control system is a simple and workable system. It was found that the configuration 2-2 is the most effective of all of the tabs considered.

Based on real time considerations, the direct tab control effectiveness appears to increase with airspeed. The tab rudder effectiveness decreases with airspeed. For all tab configurations, the control effectiveness changed through a range of only 30 percent.

The small viscous damper installed in the control system noticeably increased the effectiveness of the control.

As a representative conventional airplane, the B-26C has formed the basis of the theoretical approach in the investigation of the yaw damper design herein described. Comparative data for this aircraft and the wind tunnel model are shown in Table III.

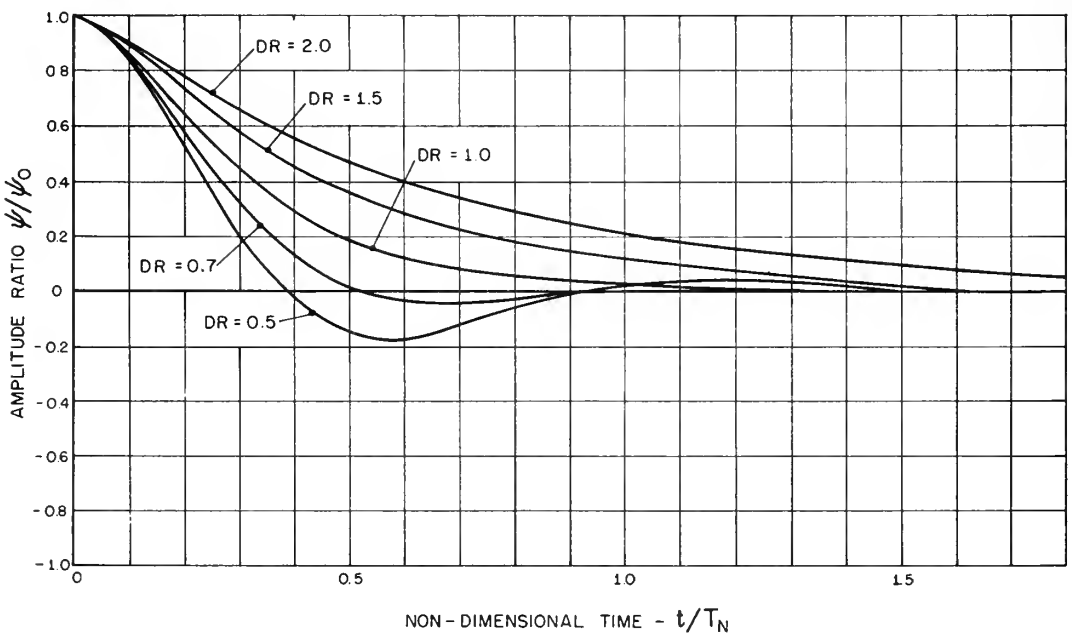

FIG.-15

NON-DIMENSIONAL AMPLITUDE RATIO ψ/ψ_0 VS NON-DIMENSIONAL TIME RATIO t/T_N FOR VARIOUS VALUES OF DAMPING RATIO DR OF A SECOND ORDER SYSTEM WHEN THE FORCING FUNCTION IS A STEP INPUT.

TABLE I

MODEL CONFIGURATIONS FOR NONDIMENSIONAL YAW RESPONSE CURVES

Number	Control	Speed	Rudder	Tab	Viscous Damper
1	Fixed	80	2	1-1	In
2	Free	80	2	1-1	In
3	Direct	80	2	1-1	In
4	Fixed	60	2	1-1	In
5	Free	60	2	1-1	In
6	Direct	60	2	1-1	In
7	Fixed	40	2	1-1	In
8	Free	40	2	1-1	In
9	Direct	40	2	1-1	In
10	Direct	80	2	1-2	In
11	Direct	80	2	1-3	In
12	Direct	60	2	1-2	In
13	Direct	60	2	1-3	In
14	Direct	40	2	1-2	In
15	Direct	40	2	1-3	In
16	Direct	80	2	2-1	In
17	Direct	80	2	2-2	In
18	Direct	80	2	2-3	In
19	Direct	60	2	2-1	In
20	Direct	60	2	2-2	In
21	Direct	60	2	2-3	In
22	Direct	40	2	2-1	In
23	Direct	40	2	2-2	In
24	Direct	40	2	2-3	In
25	Direct	80	2	2-2	Out
26	Direct	60	2	2-2	Out
27	Direct	40	2	2-2	Out
A	Fixed	80	1	1-1	Out
B	Fixed	60	1	1-1	Out
C	Fixed	40	1	1-1	Out
D†	Free	80	2	1-1	In
E†	Free	60	2	1-1	In
F†	Free	40	2	1-1	In
G	Direct	80	1	1-1	In
H	Direct	60	1	1-1	In
I	Direct	40	1	1-1	In
J†*	Free	50	1	1-1	In
K*	Free	50	1	1-1	In
L*	Free	40	1	1-1	In
M†*	Free	40	1	1-1	In
N	Free	40	1	1-1	Out
O†	Free	40	1	1-1	Out
P	Free	40	1	1-1	In

† Gyro Not Running

* Spoiler on Vertical Tail

Table II

CONTROL EFFECTIVENESS COMPARISON

Condition	Configuration Viscous Damper in Rudder	Tab	Tunnel Airspeed in mph 40	60	80
Controls Fixed	2	1-1			
T			4.62	4.05	3.04
T/T_{fixed}			1.0	1.0	1.0
T/T_N			1.96	2.62	2.58
Controls Free	2	1-1			
T			0.5	.76	.58
T/T_{fixed}			.108	.1875	.191
T/T_N			.212	.49	.492
Direct Control	Fixed	1-1			
T			1.5	1.16	.67
T/T_{fixed}			.324	.286	.22
T/T_N			.635	.748	.568
Direct Control	Fixed	1-2			
T			1.66	.88	.9
T/T_{fixed}			.36	.217	.296
T/T_N			.704	.568	.763
Direct Control	Fixed	1-3			
T			1.62	1.16	.88
T/T_{fixed}			.351	.286	.29
T/T_N			.686	.749	.746

Table II (cont'd)

Condition	Configuration Viscous Damper in Rudder	Tab	Tunnel Airspeed in mph 40	60	80
Direct Control	Fixed	2-1			
T			1.55	.98	.73
T/T_{fixed}			.335	.242	.24
T/T_N			.657	.633	.619
Direct Control	Fixed	2-2			
T			1.47	1.06	.91
T/T_{fixed}			.318	.262	.299
T/T_N			.623	.684	.771
Direct Control	Fixed	2-3			
T			1.4	1.26	.92
T/T_{fixed}			.303	.311	.302
T/T_N			.594	.813	.78
	No Viscous Damper Installed				
Direct Control	Fixed	2-2			
T			2.2	1.35	1.12
T/T_{fixed}			.476	.333	.368
T/T_N			.932	.871	.949
T_N (sec)			2.36	1.55	1.18

where

T = Time to damp to 10 percent amplitude in seconds.

T_N = Undamped natural period for controls fixed.

Table III

COMPARISON OF WIND TUNNEL MODEL AND B-26C DATA

	MODEL	B-26C
Speed in mph	60	265
Altitude in feet	0	10,000
ω_n in radians per second	4.05	3.95
DR	0.15	0.149
C_{n_ψ}	-.0694	-.0735
$C_{n_{\dot{\psi}}} \cdot (\frac{2V}{b})$	-0.123	-0.106
C_L	0.3*	0.3

*Corresponds to airplane of Piper "Clipper" type at 120 mph, from which scale model was derived.

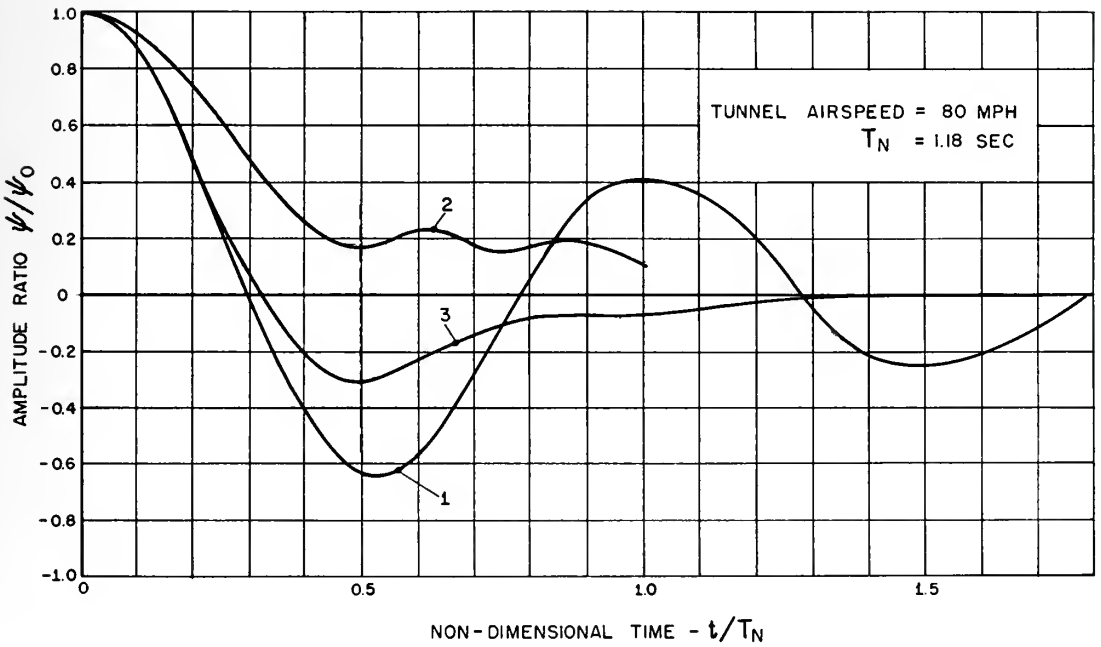

FIG. -16

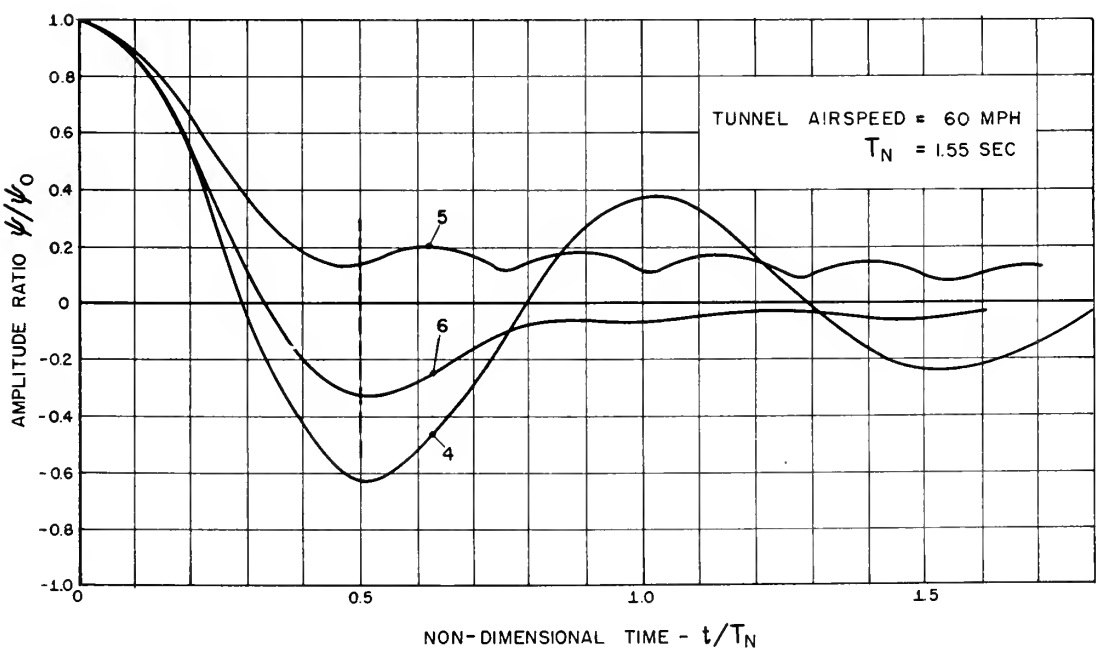

FIG.-17

NON-DIMENSIONAL PLOT OF WIND TUNNEL MODEL YAW RESPONSE TO A STEP INPUT.

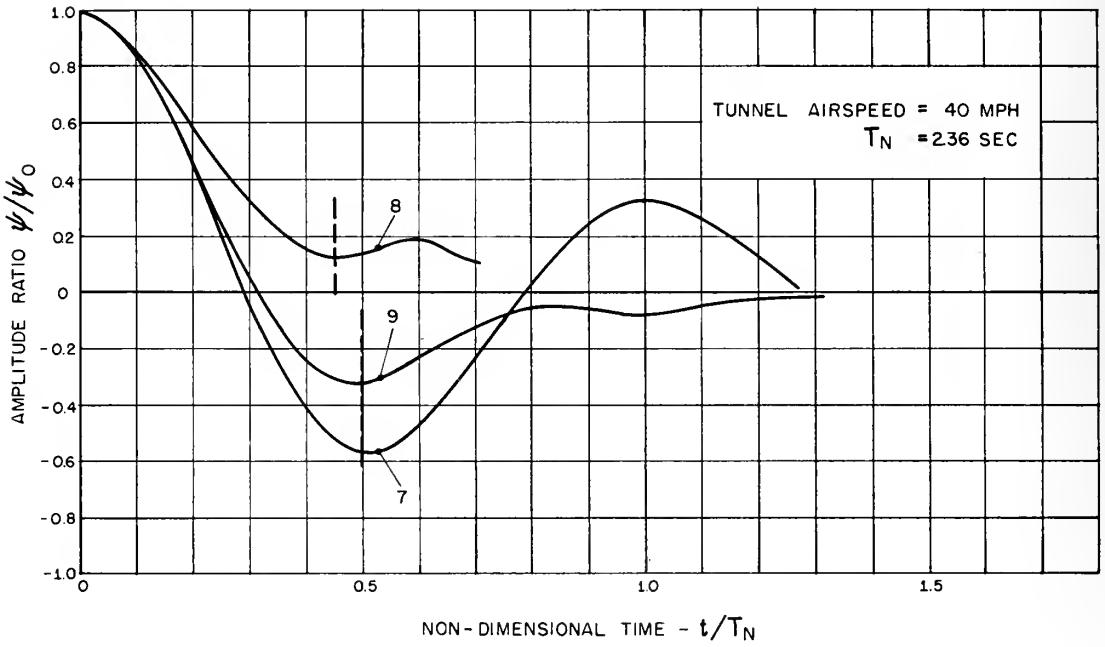

FIG.- 18

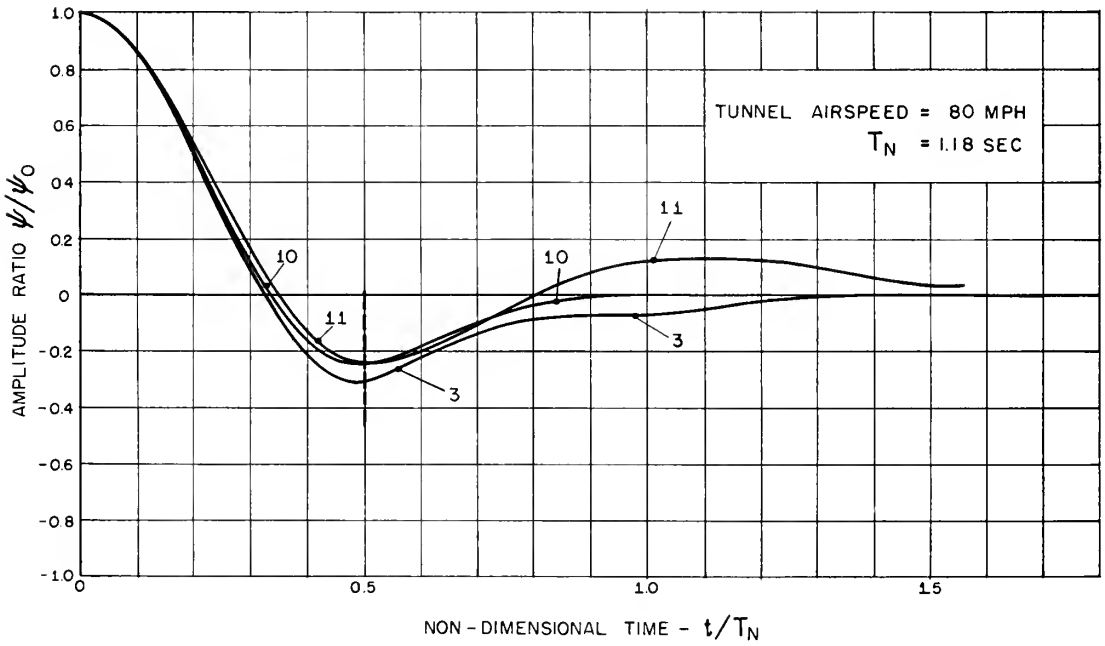

FIG.- 19

NON-DIMENSIONAL PLOT OF WIND TUNNEL MODEL YAW RESPONSE TO A STEP INPUT.

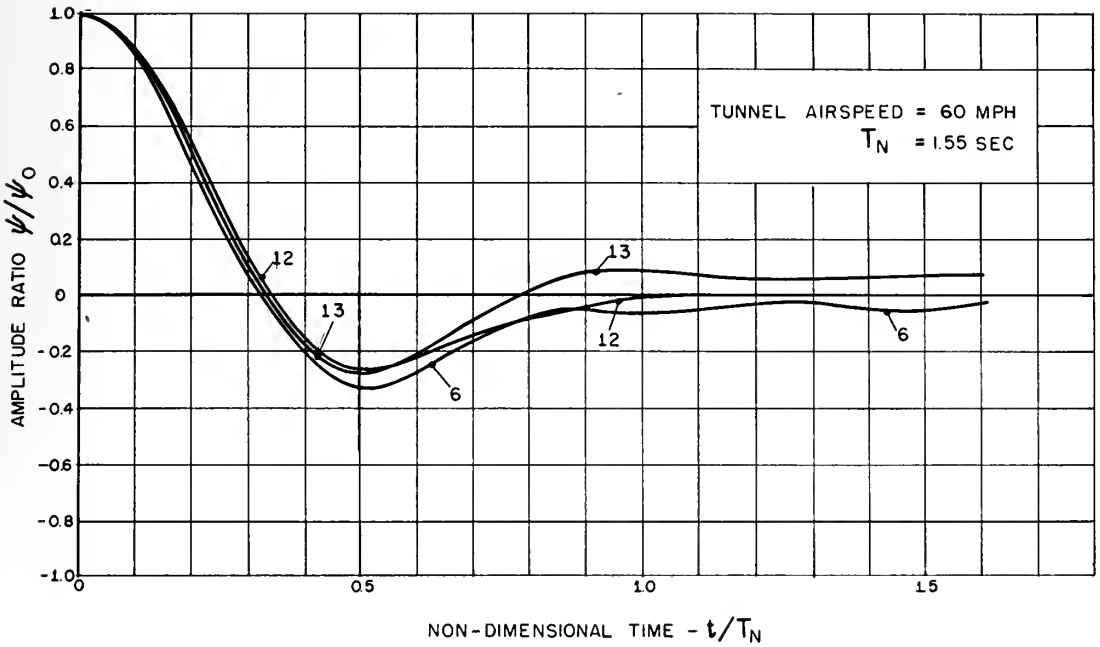

FIG. - 20

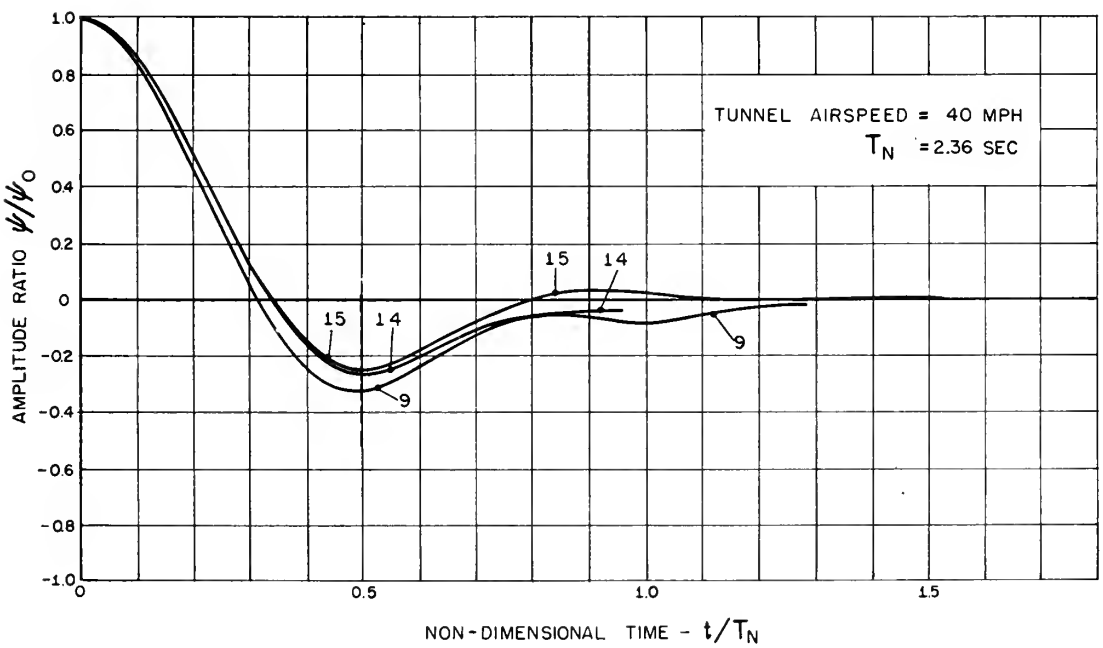

FIG. - 21

NON-DIMENSIONAL PLOT OF WIND TUNNEL MODEL YAW RESPONSE TO A STEP INPUT.

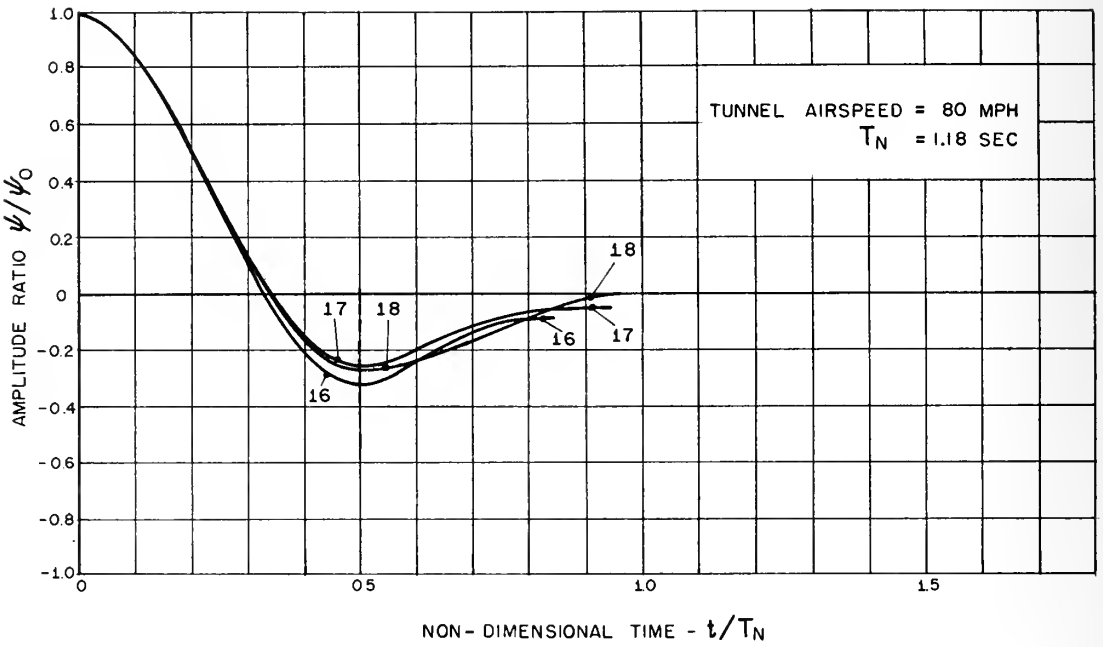

FIG. – 22

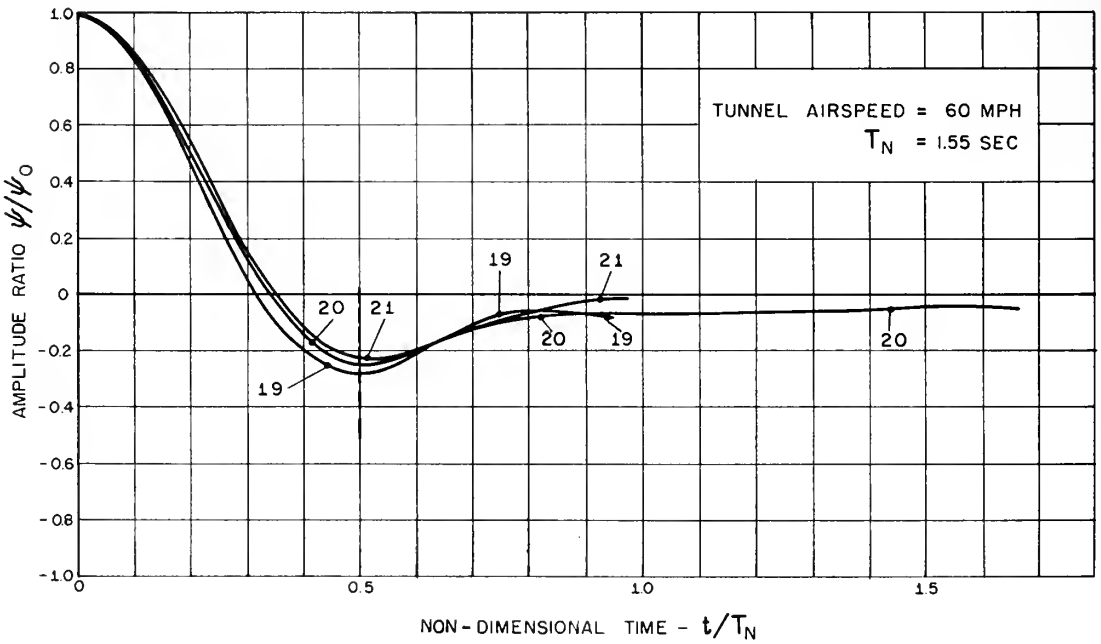

FIG.– 23

NON-DIMENSIONAL PLOT OF WIND TUNNEL MODEL YAW RESPONSE TO A STEP INPUT.

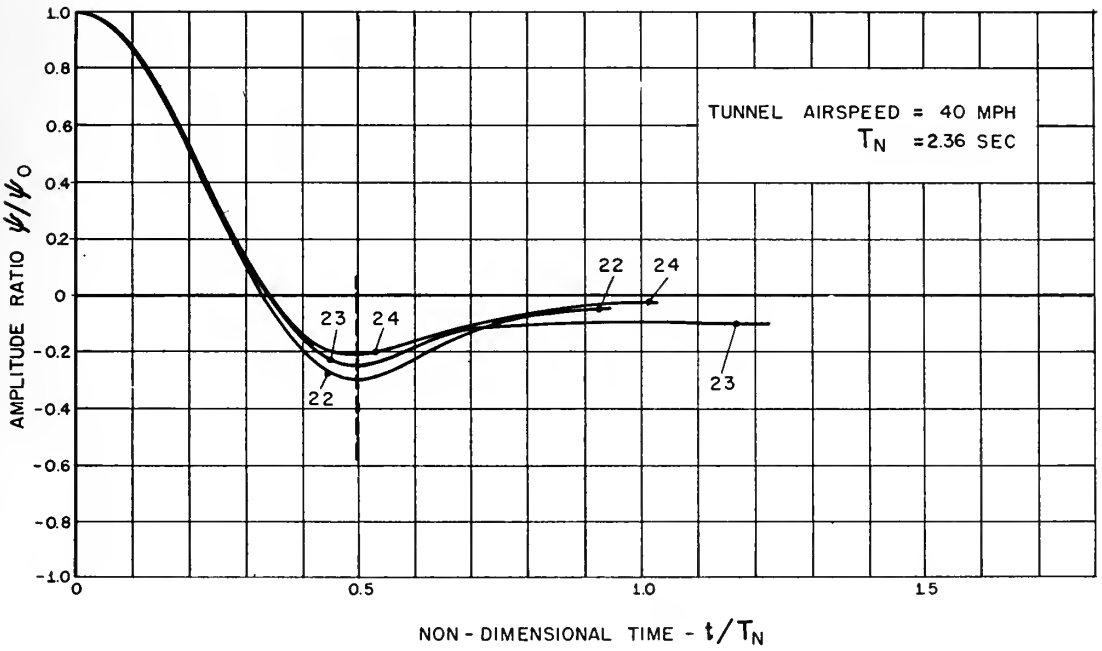

FIG. – 24

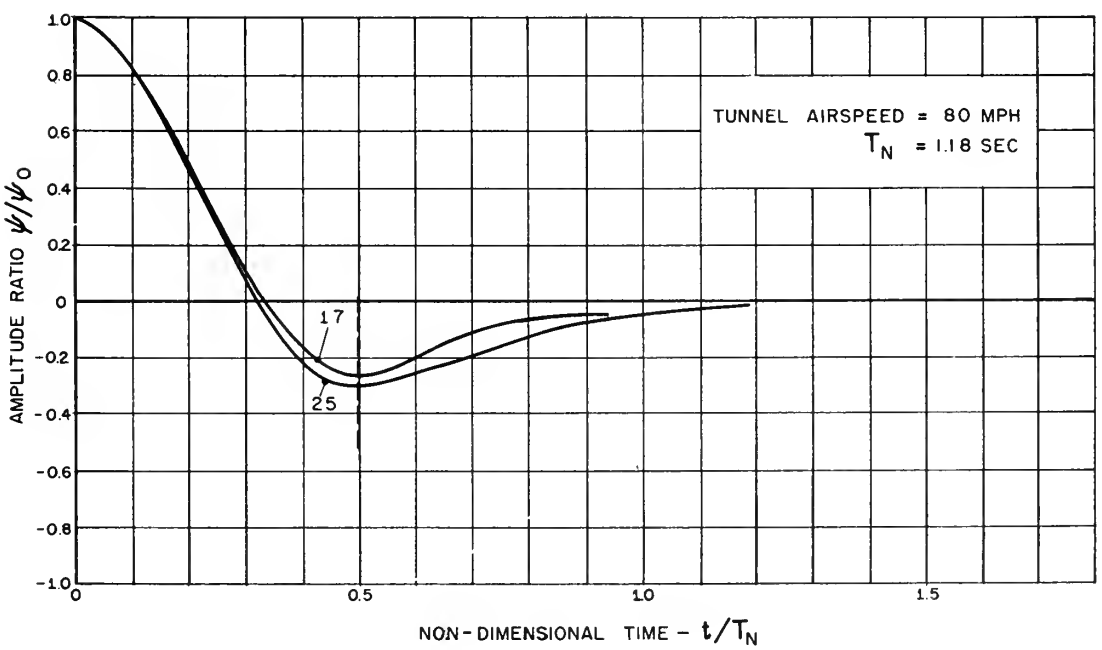

FIG. – 25

NON-DIMENSIONAL PLOT OF WIND TUNNEL MODEL YAW RESPONSE TO A STEP INPUT.

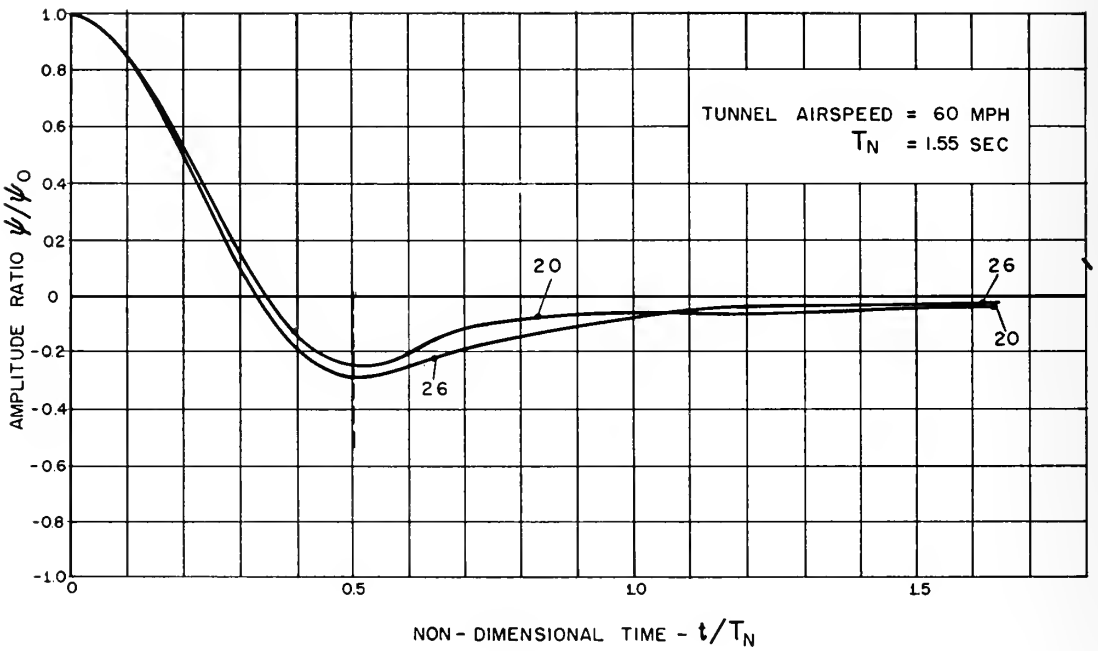

FIG.- 26

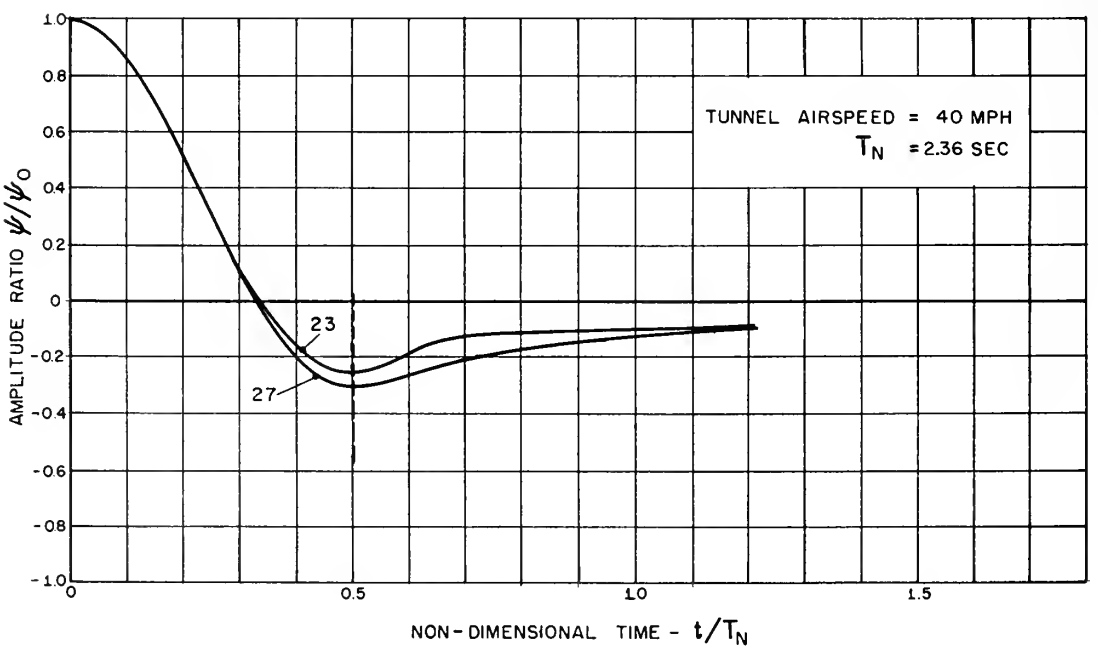

FIG.- 27

NON-DIMENSIONAL PLOT OF WIND TUNNEL MODEL YAW RESPONSE TO A STEP INPUT.

Chapter 8

CONCLUSIONS AND RECOMMENDATIONS

The object of this investigation was to develop a method for improving the lateral stability characteristics of an aircraft by means of a Yaw Damper.

The results of an analytical study made in Appendix A, and a simulator study reported in Appendix C, illustrate the marked improvement in the lateral response of an aircraft as a result of increased damping in yaw. Not only has the spiral stability of the aircraft been greatly increased, but the Dutch Roll oscillation has been highly damped. On the basis of these two studies, it is concluded that increased damping in yaw is desirable.

The results of the wind tunnel model tests indicate that increased damping in yaw can be obtained from a control surface moving in response to a disturbing yaw rate input so as to oppose the motion initiated by the disturbance. The amount of damping obtained is a function of the Yaw Damper control system configuration. Power amplification can be obtained by causing a large surface to move as the result of the deflection of a smaller surface. In the case of a single surface, the amount of damping obtained is a function of the aerodynamic balance and the area of that surface. This means that the amount of damping is directly related to the hinge moment and the aerodynamic efficiency of the surface being moved.

An important conclusion based on the results of the wind tunnel test is that one surface moving in response to the disturbing input can provide increased damping, and this direct control configuration results in a simple, smooth-working system. A single control surface system is simple to design and operates smoothly because the complexities associated with moving a second surface as a function of the position of the first have been eliminated.

The tab-rudder control system gives the maximum damping but also produces an unsatisfactory oscillation at the zero yaw position in response to the tunnel noise or turbulent air. Further investigation and study of the unsteady forces associated with circulation lags (which result in a time delay between

the tab position and the rudder response, and between rudder position and fuselage response) could possibly bring about the development of a smoothly working, non-oscillating, tab-rudder system that would provide more damping than that obtainable from a direct control system.

It is concluded that the direct control tab configuration which gave the most effective damping could, when linked to a gyro having an H value of 72×10^6 dyne-centimeter-seconds, adequately stabilize a light aircraft of the Piper "Clipper" class so that it would be spirally stable at all airspeeds and would have a highly damped Dutch Roll oscillation.

Higher performance aircraft could also use the same system, provided the hinge moments were of the same order of magnitude. Low hinge moment is a function of aerodynamic balance and surface design. If a low hinge moment could not be obtained through design, a direct-control mechanical system would require a gyro with a larger value of angular momentum, H. One way to increase H is to increase the angular velocity of spin. If the size of the gyro were bounded by dimensions or weight, a servo system could be installed to provide an irreversible control with the desired amplification so as to meet design specifications.

It is recommended that the possibility of making the Yaw Damper operate smoothly at the zero yaw angular position be further investigated. The following steps are suggested:

1. The linkage ratio should be varied to determine its effect on the smoothing of the system.

2. The effect of the viscous damper in the control linkage system should be further examined.

3. Time lags in the surface control positions and the aerodynamic forces which form, should be investigated to determine their effects on the system design.

4. The effect of friction and mechanical backlash in the control linkage should be studied as these effects will contribute control lags that may be destabilizing the system.

For further wind tunnel investigations it is recommended that the tests be made with smaller yawing rates and larger scale factors. Such a procedure would permit a more accurate evaluation of the effectiveness of the various control systems in damping in yaw.

Finally, on the basis of the results of the wind tunnel tests, it is recommended that a direct-control system similar to the 2-2 tab configuration with the 72×10^6 dyne-centimeter-seconds gyro be installed in an aircraft and that the system be given a complete and thorough flight test.

APPENDIX A

CALCULATION OF THE ROOTS OF THE AIRPLANE LATERAL STABILITY EQUATION, CONTROLS FIXED

Lateral equations for the airplane motion are given in reference (1). These equations and notations will be used with slight modifications. It can be shown that for an aircraft flying at cruising speed and above, the product of inertia, I_{xz}, has but a small influence on the lateral stability.

At speeds below cruising the terms involving this product have a greater effect on the lateral stability. However, if these terms are neglected, the results will be more conservative than if they are included. The calculations of reference (2) indicate that the inclination of the principal longitudinal axis above the flight path causes a stabilizing shift in the oscillatory-stability boundary. Therefore, for reasons of simplicity the product of inertia I_{xz} and terms involving this product are neglected, and the following equations of motion result:

$$\left.\begin{aligned} &(C_{y_\beta} - 2d)\beta - 2d\psi + C_L\varphi = 0 \\ &\mu C_{l_\beta}\beta + \frac{C_{l_r}}{2} d\psi + \left[\frac{C_{l_p}}{2} d - J_x d^2\right] \varphi = 0 \\ &\mu C_{n_\beta}\beta + \left[\frac{C_{n_r}}{2} - J_z d\right] d\psi + \frac{C_{n_p}}{2} d\varphi = 0 \end{aligned}\right\} \quad (1)$$

where

$$J_x = 2\left[\frac{k_x}{b}\right]^2$$

$$J_z = 2\left[\frac{k_z}{b}\right]^2$$

These equations may be written in the determinant form as:

$$\begin{vmatrix} C_{y_\beta} - 2\lambda & -2 & C_L \\ \mu C_{l_\beta} & \frac{C_{l_r}}{2} & \frac{C_{l_p}}{2}\lambda - J_x\lambda^2 \\ \mu C_{n_\beta} & \frac{C_{n_r}}{2} - J_z\lambda & \frac{C_{n_p}\lambda}{2} \end{vmatrix} = 0 \quad (2)$$

Expanding this determinant, a quartic in λ is obtained:

$$A\lambda^4 + B\lambda^3 + C\lambda^2 + D\lambda + E = 0 \qquad (3)$$

where

$$A = 1$$

$$B = -\tfrac{1}{2}\left(C_{y_\beta} + C_{n_r}/J_Z + C_{l_p}/J_X\right)$$

$$C = \frac{1}{4J_XJ_Z}\left(C_{l_p}C_{n_r} - C_{l_r}C_{n_p}\right) + \frac{C_{y_\beta}}{4}\left[\frac{C_{n_r}}{J_Z} + \frac{C_{l_p}}{J_X}\right] + \frac{\mu C_{n_\beta}}{J_Z}$$

$$D = -\frac{\mu}{2J_XJ_Z}\left(C_{n_\beta}C_{l_p} - C_{l_\beta}C_{n_p}\right) - \frac{\mu}{2J_X}C_LC_{l_\beta} - \frac{C_{y_\beta}}{8J_XJ_Z}\left(C_{l_p}C_{n_r} - C_{l_r}C_{n_p}\right)$$

$$E = \frac{\mu C_L}{4J_XJ_Z}\left(C_{l_\beta}C_{n_r} - C_{n_\beta}C_{l_r}\right)$$

The coefficients of the quartic in λ given in eq. (3) above are constants depending for their values on the inertia terms, the airplane relative density parameter μ, and the partial, or stability, derivatives. The values of these derivatives are listed in Table I. The coefficients of the quartic in λ are listed in Table II.

The quartic stability equation, (3), is readily solved by use of the approximate factorization formula:

$$(\lambda_1 + B)\left(\lambda_2 + \frac{E}{D}\right)\left(\lambda^2_{3,4} + \frac{R}{B^2D}\lambda + \frac{D}{B}\right) = 0 , \qquad (4)$$

the roots being:

$$\lambda_1 = -B$$

$$\lambda_2 = -\frac{E}{D}$$

$$\lambda_{3,4} = -\frac{R}{2B^2D} \pm \sqrt{\frac{R^2}{4B^4D^2} - \frac{D}{B}}$$

where $R \triangleq BCD - D^2 - B^2E \triangleq$ Routh's Discriminant.

From the roots of equation (4), it is possible to calculate the period, the time to damp to one-half amplitude, the number of cycles to damp to one-half amplitude, and the damping ratio, DR, by use of the following equations:

$$\lambda_{1,2} = \alpha_{1,2}$$

$$\lambda_{3,4} = \alpha \pm \beta i$$

$$T_{1/2} = \frac{\log_e 2}{\alpha/\tau} \text{ seconds}$$

$$P = \frac{2\pi}{\beta/\tau} \text{ seconds/cycle}$$

$$N_{1/2} = \frac{T_{1/2}}{P} \text{ cycle}$$

$$DR = \frac{.11}{N_{1/2}}$$

The value of the roots $\lambda_{1,2,3,4}$, the time to damp to one-half amplitude $T_{1/2}$, and the period of the Dutch Roll oscillation, are tabulated in Table III for the four flight conditions. The root λ_1 indicates the rapid roll subsidence. The root λ_2 indicates spiral subsidence, which in most airplanes is generally a small spiral divergence. This root gets more positive as the speed is decreased. The roots $\lambda_{3,4}$ represent the complex Dutch Roll oscillation.

As a check on the approximate factorization method of determining the roots of the quartic, the exact roots have been calculated for flight condition (4) by synthetic division methods and found to be:

$$\lambda_1 = -4.97$$

$$\lambda_2 = -0.495$$

$$\lambda_{3,4} = -0.77 \pm 1.44i$$

The exact roots indicate that the plane is even more stable than the approximate factorization methods indicate, both from the spiral stability and the Dutch Roll considerations. This is shown in Table III under flight condition (4).

TABLE A-I

AIRPLANE STABILITY DERIVATIVES

Flight Condition	(1)* B-26 IAS = 256 mph 10,000 Ft	(2) Small Airplane IAS = 120 mph Sea Level	(3) Small Airplane IAS = 120 mph Sea Level C_{n_r} increased 4x	(4) Small Airplane IAS = 120 mph Sea Level C_{n_r} & C_{l_β} increased 4x
C_L	0.3	0.3	0.3	0.3
b(ft)	70.22	32	32	32
μ	13.05	3.12**	3.12**	3.12**
τ (sec)	2.02	0.567	0.567	0.567
J_x	0.0313	0.0546	0.0546	0.0546
J_z	0.0598	0.1048	0.1048	0.1048
C_{y_β}	-0.720	-0.720	-0.720	-0.720
C_{l_β}	-0.096	-0.096	-0.096	-0.384
C_{n_β}	0.0735	0.0735	0.0735	0.0735
C_{l_r}	0.055	0.055	0.055	0.055
C_{n_r}	-0.106	-0.106	-0.424	-0.424
C_{l_p}	-0.505	-0.505	-0.505	-0.505
C_{n_p}	-0.0168	-0.0168	-0.0168	-0.0168

* From ref. (3)

** From ref. (5)

TABLE A-II

AIRPLANE STABILITY COEFFICIENTS

Flight Condition	(1)	(2)	(3)	(4)
A	1	1	1	1
B	9.31	5.49	7.01	7.01
C	26.53	6.31	13.54	13.54
D	144.17	12.13	14.56	18.35
E	3.93	0.253	1.51	6.54
R	14520	281	1096	1084

TABLE A-III

AIRPLANE RESPONSE

	Flight Condition	(1)	(2)	(3)	(4) Approx. Roots	(4) Exact Roots
Roll Stability	$\lambda_1 = -B$	-9.31	-5.49	-7.01	-7.01	-4.97
	$T_{1/2}$ (sec)	.15	.0717	.0562	.0562	.079
Spiral Stability	$\lambda_2 = -\frac{E}{D}$	-.0272	-.0208	-.104	-.356	-.495
	$T_{1/2}$ (sec)	51.5	18.6	3.78	1.09	.795
Dutch Roll Oscillation	$\lambda_{3,4}$	$-.58 \pm 3.88i$	$-.38 \pm 1.44i$	$-.77 \pm 1.23i$	$-.6 \pm 1.5i$	$.77 \pm 1.44i$
	$T_{1/2}$ (sec)	2.42	1.035	.511	.647	.511
	P (sec)	3.27	2.48	2.91	2.36	2.48
	$N_{1/2}$ (cycle)	.738	.417	.176	.275	.206
	DR, damping ratio	.149	.264	.625	.400	.534

Appendix B

PRELIMINARY DESIGN STUDY FOR THE VERTICAL TAIL OF THE WIND TUNNEL MODEL

In designing the vertical tail for incorporation of the proposed yaw damper, it was necessary to investigate the left effects of various combinations of geometric airfoil surfaces so as to find the combination that would produce the greatest lift per unit of control torque. The control torque was to be produced directly from the gyro linkage system. The aerodynamic lift was to be obtained through the use of a tab-rudder-fin combination. As has been previously explained, the tab was to be controlled by the gyro, and act as an aerodynamic amplifier in moving the rudder. The change in the airfoil camber produced by the deflection of the tab and rudder was for the purpose of increasing the lift in such a direction as to always oppose the angular yaw motion of the aircraft.

The design study was therefore reduced primarily to the selection of a tab-rudder-vertical tail configuration that would produce the maximum lift per unit of tab hinge moment.

Since the vertical tail design was to include both a pilot-controlled rudder and a gyro-controlled rudder, it was decided to make the two rudder areas approximately equal. In an attempt to give the pilot the same amount of controllability that he now has in most conventional aircraft, (i.e., rudder deflections capable of holding a 15° sideslip angle) the area of the vertical tail was increased by a factor of about 20 percent. It is apparent that with this increase of vertical tail area, the weather-vane tendencies of the plane have been increased. Since the pilot-controlled rudder has not been increased in the same proportion, it is admitted that the pilot could not hold the same steady-state sideslip angle that he could hold with a tail of conventional design. The controllability of the airplane for this dual rudder configuration is a subject for further analysis. The pilot-controlled section was fixed at $\delta_R = 0$ throughout the remainder of this investigation.

The tab hinge moment is the sum of four effects; that is,

$$C_{H_T} = \frac{\partial C_{H_T}}{\partial \delta_T} \delta_T + \frac{\partial C_{H_T}}{\partial \delta_R} \delta_R + \frac{\partial C_{H_T}}{\partial \alpha} \alpha + C_{H_{T(\text{friction})}}$$

From Ref. 14 we find that, by using a balanced rudder and a partially balanced tab, the tab hinge moment coefficient can be expected to be in the order of magnitude of:

$$C_{H_T} = 0.01/\text{degree}$$

where

$$\frac{\partial C_{H_T}}{\partial \delta_T} = -0.009/\text{ degree}$$

$$\frac{\partial C_{H_T}}{\partial \delta_R} = -0.002/\text{degree}$$

$$\frac{\partial C_{H_T}}{\partial \alpha} = -0.001/\text{degree}$$

For

$$\delta_{R(\max)} = 15 \text{ degrees}$$

$$\delta_{T(\max)} = 15 \text{ degrees}$$

$$\alpha_{(\max)} = 5 \text{ degrees}$$

$$C_{H_{T(\max)(\text{aero})}} = -0.17$$

These hinge moment coefficients are based on the area and chord of the control tab.

The actual tab hinge moment for the wind tunnel model tab, based on the dimensions shown in Fig. 9 and a q corresponding to 60 miles per hour, becomes:

$$M_{T_{(max)(aero)}} = C_{H_T} S_T q C_T = -0.17 \times \frac{.002378}{2} \times \left(\frac{88}{12}\right)^2 \times .75 \times 5.25$$

$$= 0.043 \text{ in-lbs.}$$

For the steady-state condition in which the aerodynamic moments on the tab are balanced by the control moment from the gyro linkage system:

$$\sum M_T = 0 = M_{T(aero)} + M_{T(gyro\ link)}$$

The gyro output torque can be determined as follows:

$$\overline{M}_{(gyro)} = \overline{W}_{(Z\ axis)} \times \overline{H}_{(gyro\ wheel)}$$

or

$$M_{(gyro)} = W_{(Z\ axis)} H_{(gyro\ wheel)} \cos(A_g)$$

Assuming perpendicularity between $\overline{M}$, $\overline{W}$, and $\overline{H}$, since the angle A_g is restricted to plus or minus 7.5 degrees because of the setting of the gyro stops, we may write this equation in the form:

$$M_{(gyro)} = W_{(Z\ axis)} H_{(gyro\ wheel)}$$

When the gyro is installed in the model, the gyro output torque and the control moment at the tab are related by the following sensitivity:

$$M_{(gyro\ link)} = M_{(gyro)} \times S_{(link)}$$

where

$$S_{(link)} = 0.482$$

The damping in yaw of an aircraft consists of three component parts; that due to the wing, that due to the fuselage, and that due to the vertical tail. Expressing this in terms of the damping coefficient in yaw, we have:

$$C_{n_r} = C_{n_{r(wing)}} + C_{n_{r(fuselage)}} + C_{n_{r(vertical\ tail)}}$$

where the yawing moment coefficient due to the vertical tail is simply

$$C_{n_r} = -2 \left[\frac{dC_L}{d\alpha}\right]_{(VT)} \frac{S_{(VT)}}{S_{(W)}} \left[\frac{l_{(VT)}}{b}\right]^2 \eta_{(VT)}$$

From the equation it can be seen that the damping can be increased by lengthening the distance from the center of gravity of the aircraft to the center of pressure of the vertical tail, by increasing the tail area, or by increasing the slope of the lift curve of the vertical tail. The yaw damper changes the lift of the vertical tail by changing the camber of the lift surface, thereby increasing the effective angle of attack and the slope of the lift curve.

The increase in damping due to the yaw damper is proportional to the increase in the damping force, that is:

$$\Delta M_{(damp)} = \left\{\left[\frac{dC_L}{d\alpha_{eff}}\right]_{(VT)} \alpha_{eff} - \left[\frac{dC_L}{d\alpha}\right]_{(VT)} \alpha\right\} qS_{(VT)}\, l_{(VT)}$$

Since the tail of the wind-tunnel model is designed so that only one-half of the tail is controlled by the yaw damper, it becomes apparent that the damping will be made up of two parts:

$$M_{(damp)} = [C_{n_{r(gyro\ cont)}} + C_{n_{r(pilot\ cont)}}]\, qSb$$

If we are to increase the damping coefficient four times, the merits of which were discussed in Chapter 2, it means that the damping force must be increased four times. Since the areas of the two controlled rudders are the same, and since the damping force on the pilot-controlled rudder remains the same as for the fixed-control case, it follows that the damping force on the gyro-controlled rudder must be increased seven times, i.e.;

$$C_{n_{r(gyro\ cont)}} = 7C_{n_{r(pilot\ cont)}}$$

Now, if the gyro were infinitely sensitive to angular rate of yaw, and powerful enough to overcome the friction inherent in the linkage system, it

would cause the tab to swing to its designed stops as the fuselage sensed an infinitesimal yaw rate. The tab would deflect the rudder, and the fin-rudder-tab combination would produce an effective angle of attack that is a function of angular rate of yaw. If this effective angle of attack is seven times as great as the angle of attack experienced by the fixed control surface due to the same angular rate, (i.e., $\frac{l_{VT}\, r}{V_A}$) we have effectively increased our damping coefficient by a factor of four. It can be shown that the damping coefficient will be a non-linear function having its greatest values for small angular rates of yaw and rapidly decreasing values for increasing angular rates. As will be seen later, the aerodynamic lift coefficients are also non-linear, especially for large angular deflections of the control surfaces. The fact that the damping is non-linear makes the system more difficult to analyze, but it does not detract in any way from the merit of the damping system. This analysis indicates that the damper will be most efficient at low angular rates of yaw and that the damper efficiency reduces to zero as the angular rate increases without limits. (See Fig. B-1 below.)

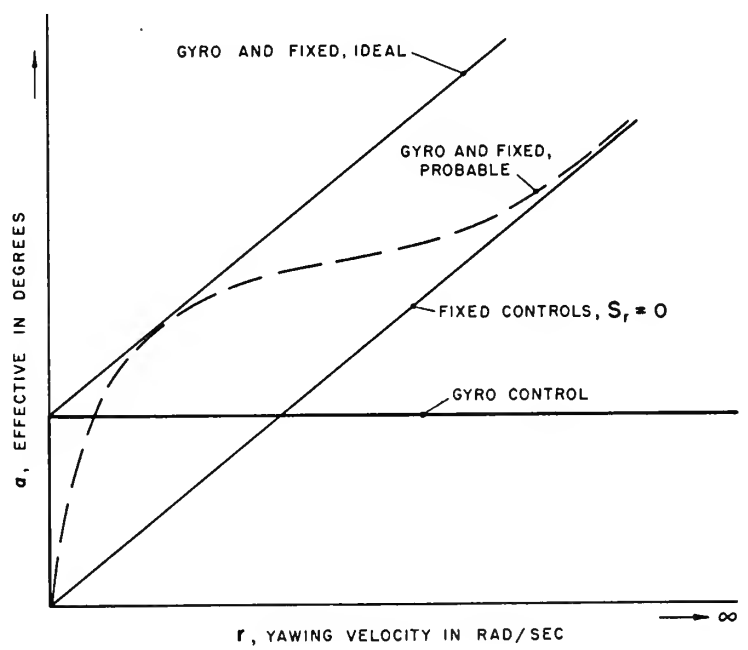

FIG. B-1. QUALITATIVE CURVES OF EFFECTIVE ANGLE OF ATTACK AS A FUNCTION OF YAW RATE.

In the gyro-controlled portion of the vertical tail it was desired to determine the minimum control force for the maximum lift of a fin-rudder-tab combination. It has been found that the optimum design in obtaining a given amount of lift results from keeping the control surface within the linear range of operation. The lift effectiveness after stall is always less than the values obtained just before stall. The maximum control surface deflection of the rudder was the first thing to be determined in the design problem.

Figure B-2 from reference (14), Fig. 3, shows the maximum rudder deflection as a function of c_R/c_{VT} and α. Since $\alpha = \frac{l_{(VT)}\, r}{V_A}$, we may design for an $\alpha_{(max)}$ of two degrees which corresponds approximately to an angular rate of 1 radian per second for V_A = 60 mph. Entering Fig. B-2, we see that a fifteen-degree rudder deflection is well within the stall limit for a chord ratio of c_R/c_{VT} of 0.33 and an angle of attack, α, of 2 degrees. This α will always be positive for the purposes of using Fig. B-2, since the rudder will always act in such a manner as to move into the relative wind. Fifteen degrees maximum rudder deflection is considered a conservative estimate since Refs. (9), (10), and (11) indicate that in most cases rudder stall is delayed when the tab moves in a direction opposite to that of the rudder. It is to be noted that the tab deflection limits and the rudder deflection limits depend upon the aspect ratio of the vertical tail, the plan form, and the scale size. No attempt was made to correct for these variables. Figure B-2 is based on information obtained from an NACA 0009 airfoil; an NACA 0012 airfoil was used on the wind-tunnel model tail, no correction being made for the difference.

The amount of tab deflection necessary to produce fifteen degrees of rudder deflection (or the most effective rudder angle) under the dynamic conditions of flight was so difficult to estimate that the tab link was made adjustable so that the maximum angular throw of the tab could be controlled. It is to be noted also that the relative angular deflection of tab and rudder is a function of aerodynamic balance on the two control surfaces.

It can be shown that aerodynamic balance on the control surfaces can greatly reduce the control hinge moment. The more closely the controls are balanced, the more apt they are to become unstable. For example, if the

rudder is overbalanced to the extent that C_{h_R} is a positive number, the aerodynamic forces no longer act as a spring restraint, but act in the same direction as the control moment. This would result in rudder lock, and a non-stable control system. Figure B-3 reproduced from Fig. 144-b of Ref. (15), is indicative of the merits derived from using various values of aerodynamic balance, i.e., c_b/c_R. If c_b/c_R is selected to equal 0.3, and c_R/c_{VT} to equal 0.3, values of $C_{h_{R_{\delta_R}}} = -0.006$ and $C_{h_{R_\alpha}} = -0.0045$ can be taken directly from the figure.

Figure B-4, reproduced from Fig. 106, Ref. (10), shows that by choosing aerodynamic parameters of c_b/c_R equal to 0.3 and c_R/c_{VT} equal to 0.26 for a blunt-nosed overhang with a 0.001-inch gap, we might expect a small negative value for $C_{h_{R_\alpha}}$, and a lift coefficient of 1.0 for an angle of attack of 5 degrees and a $\delta_R = 15°$. It is to be noted that this curve is plotted for an NACA 66-009 airfoil with infinite aspect ratio. No attempt was made to reduce this data to a finite aspect ratio for the NACA 0012 airfoil. Figure B-4 shows that for rudder angles greater than ten degrees, the lift effectiveness of the airfoil falls off rapidly and the hinge moment rises rapidly. In an attempt to delay this stalled condition, the nose of the rudder and tab of the model was made elliptical. The combination of the balsawood rudder and pine tab was designed so as to lend itself to easy modification if wind tunnel tests proved it desirable to sharpen the nose.

Figure B-5 from Fig. 143-b of Ref. (15) is an indication of the airfoil lift coefficient $C_{l_{VT}}$ and the lift effectiveness parameter α_δ as a function of balance. Here, again, the blunt-nosed configuration appears to be the most efficient.

The optimum size and balance of the tab must be determined from lift considerations and tab hinge moments, as well as from rudder hinge moments, since the gyro linkage output must produce the desired tab hinge moments. In a sense, the gyro output forces can be compared to the control tab forces of Fig. B-6 from Fig. 148 of Ref. (15). From this figure it can be seen that the optimum size of the balancing tab is about 20 percent of c_R. The lift effectiveness of the resulting combination is about two-thirds that of the rudder without the tab.

References (11), (12), and (13) indicate that, for a constant tab chord, using a large span tab at a small deflection angle is superior to using a small span tab at a large deflection angle. The tab on the wind tunnel model was designed for full span (i.e., controlled tab and controlled rudder had the same height).

Reference (15) indicates that for a given amount of overhang, the blunt-nosed control surface gives the greatest amount of balance. When the nose of any balanced control surface unports itself because of the deflection of the surface, regardless of the nose shape, large increases of hinge moment and decreases in lift result. Based on these considerations, a balanced rudder with a blunt elliptical nose was used. The unporting angle of 25 degrees was much greater than the designed 15-degree maximum rudder deflection. The tab nose was made similar to the rudder nose.

It can be seen that the tail design resulted from a study of various combinations of tab and rudder configurations as found in NACA reports. Representative curves showing some of the most important parameter ratios as functions of the lift efficien cy have been included in this report. The final model configuration chosen as a result of this study has the following geometric dimension ratios:

$$\frac{c_R}{c_{VT}} = 0.30 \qquad \frac{c_b}{c_R} = 0.27$$

$$\frac{c_T}{c_R} = 0.20 \qquad \frac{c_b}{c_T} = 0.31$$

The actual tail design can be seen in Fig. 9.

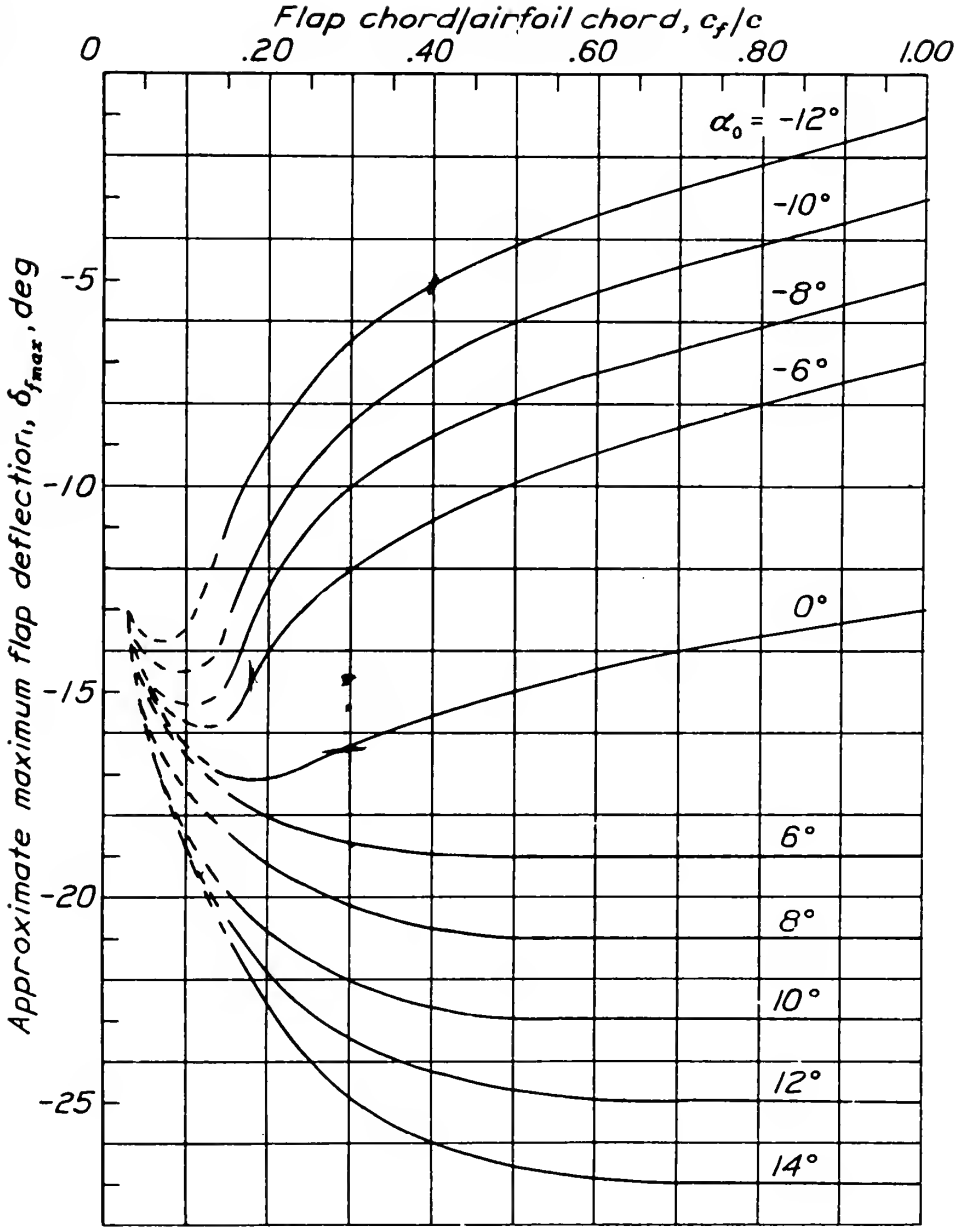

Figure 3.- Approximate maximum allowable flap deflections for linear limits of airfoil characteristics at various angles of attack. Data for NACA 0009 airfoil with infinite aspect ratio and at an effective Reynolds number of 3,410,000.

FIG. B-2

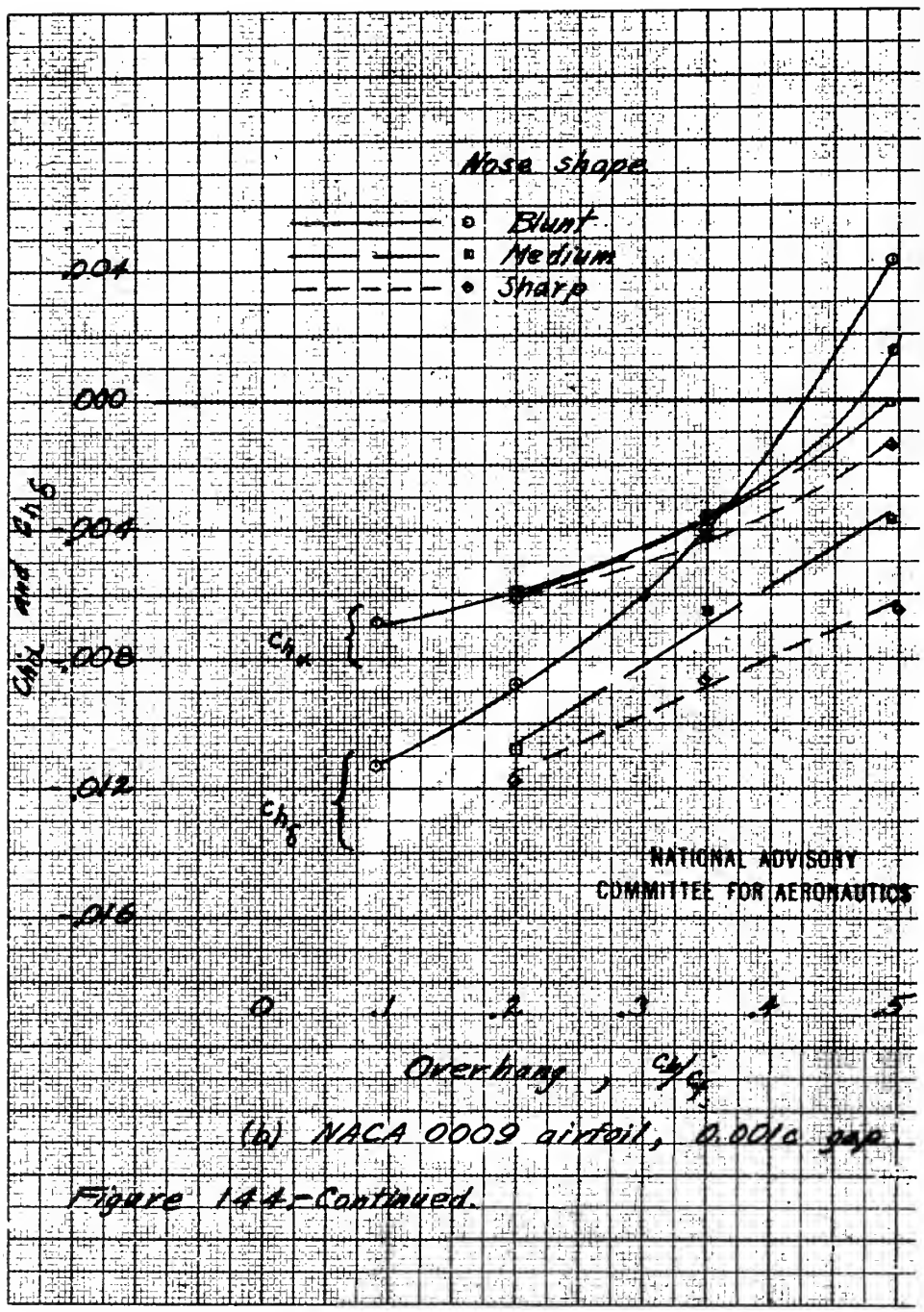

(b) NACA 0009 airfoil, 0.001c gap.

Figure 144.-Continued.

FIG. B-3

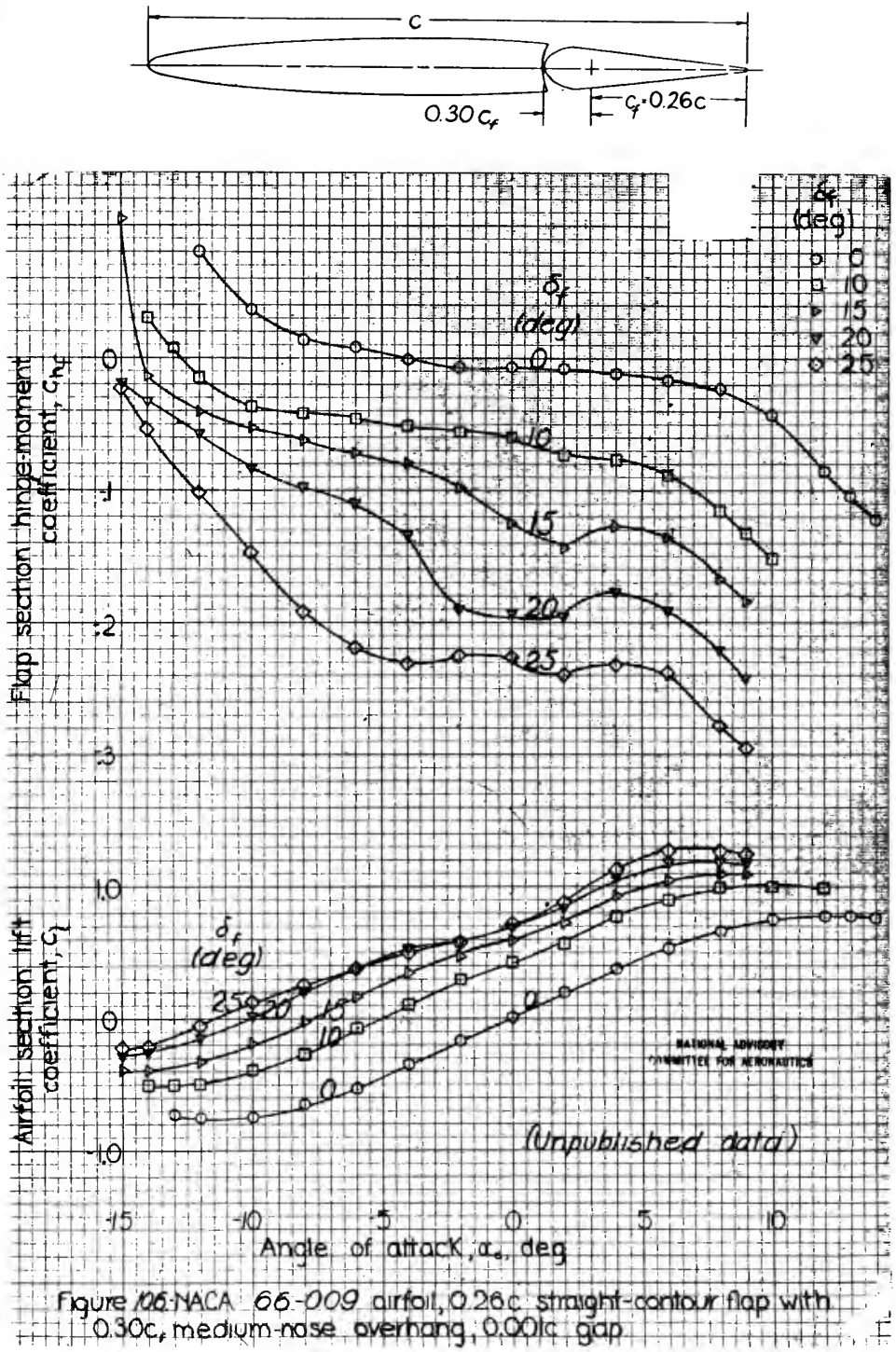

Figure 106.-NACA 66-009 airfoil, 0.26c straight-contour flap with 0.30c_f medium-nose overhang, 0.001c gap

FIG. B-4

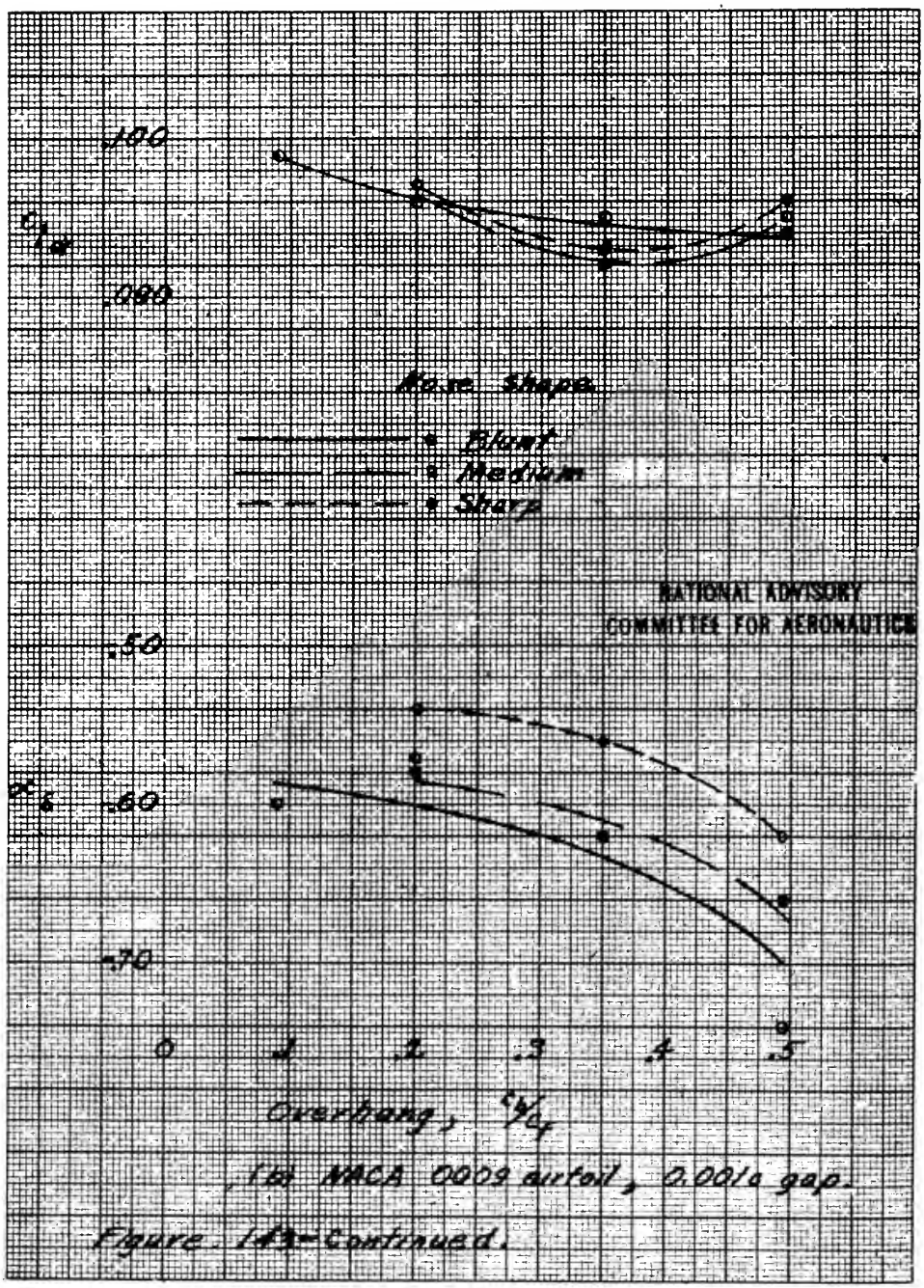
.100
$c_{l_{max}}$
.090
Nose Shape
Blunt
Medium
Sharp
NATIONAL ADVISORY
COMMITTEE FOR AERONAUTICS
.50
$c'_{l_{max}}$
.60
.70
0
.1
.2
.3
.4
.5
Overhang, c_4/c
(a) NACA 0009 airfoil, 0.001c gap.
Figure 14.- Continued.

FIG. B-5

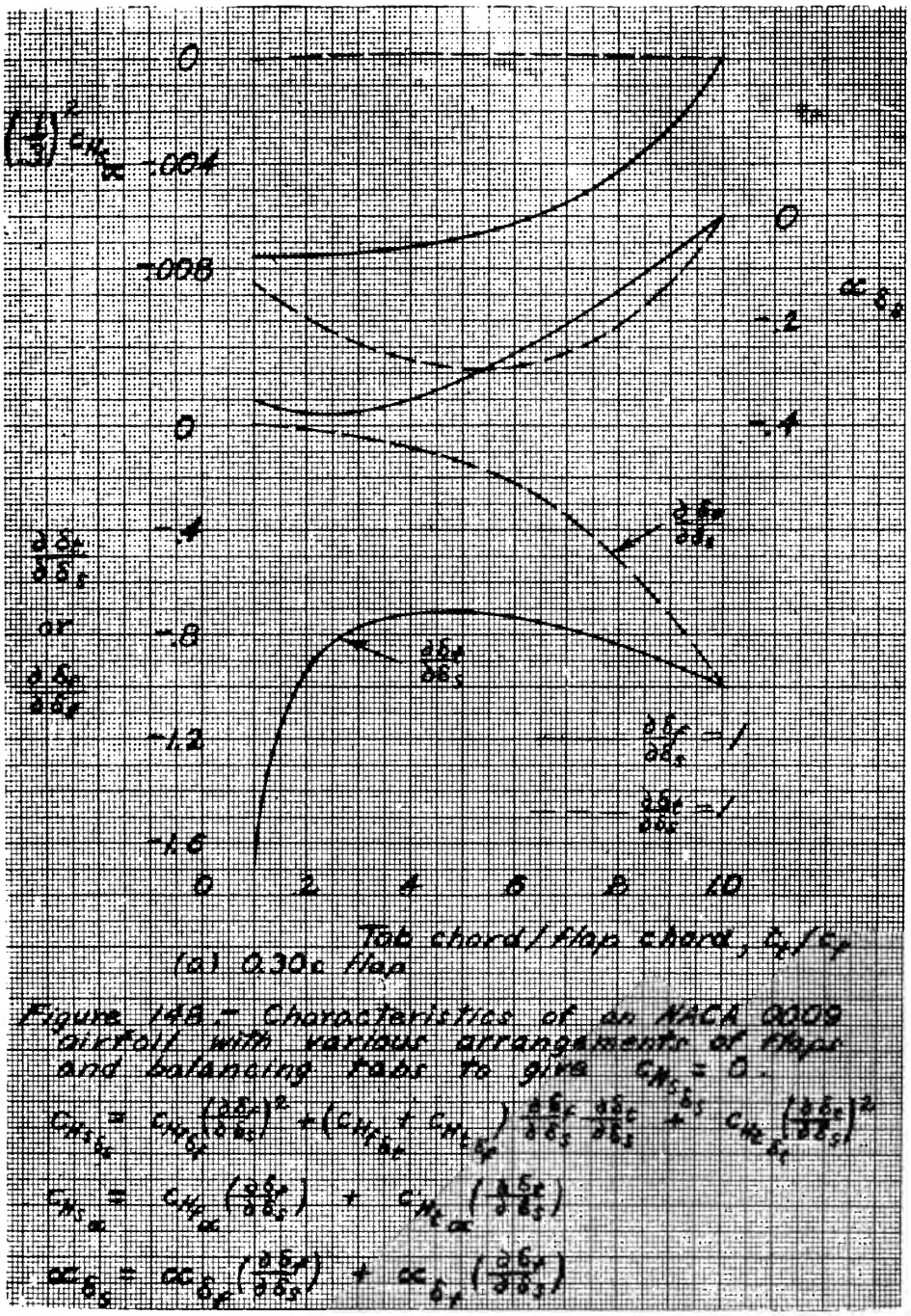

Figure 148.- Characteristics of an NACA 0009 airfoil with various arrangements of flaps and balancing tabs to give $c_{h_{\delta_s}} = 0$.

$$c_{h_{\delta_s}} = c_{h_{\delta_f}}\left(\frac{\partial \delta_f}{\partial \delta_s}\right)^2 + \left(c_{h_{\delta_f}} + c_{h_{\delta_t}}\right)\frac{\partial \delta_f}{\partial \delta_s}\frac{\partial \delta_t}{\partial \delta_s} + c_{h_{\delta_t}}\left(\frac{\partial \delta_t}{\partial \delta_s}\right)^2$$

$$c_{h_\alpha} = c_{h_{\alpha_f}}\left(\frac{\partial \delta_f}{\partial \delta_s}\right) + c_{h_{\alpha_t}}\left(\frac{\partial \delta_t}{\partial \delta_s}\right)$$

$$c_{\alpha_{\delta_s}} = c_{\alpha_{\delta_f}}\left(\frac{\partial \delta_f}{\partial \delta_s}\right) + c_{\alpha_{\delta_t}}\left(\frac{\partial \delta_t}{\partial \delta_s}\right)$$

FIG. B-6

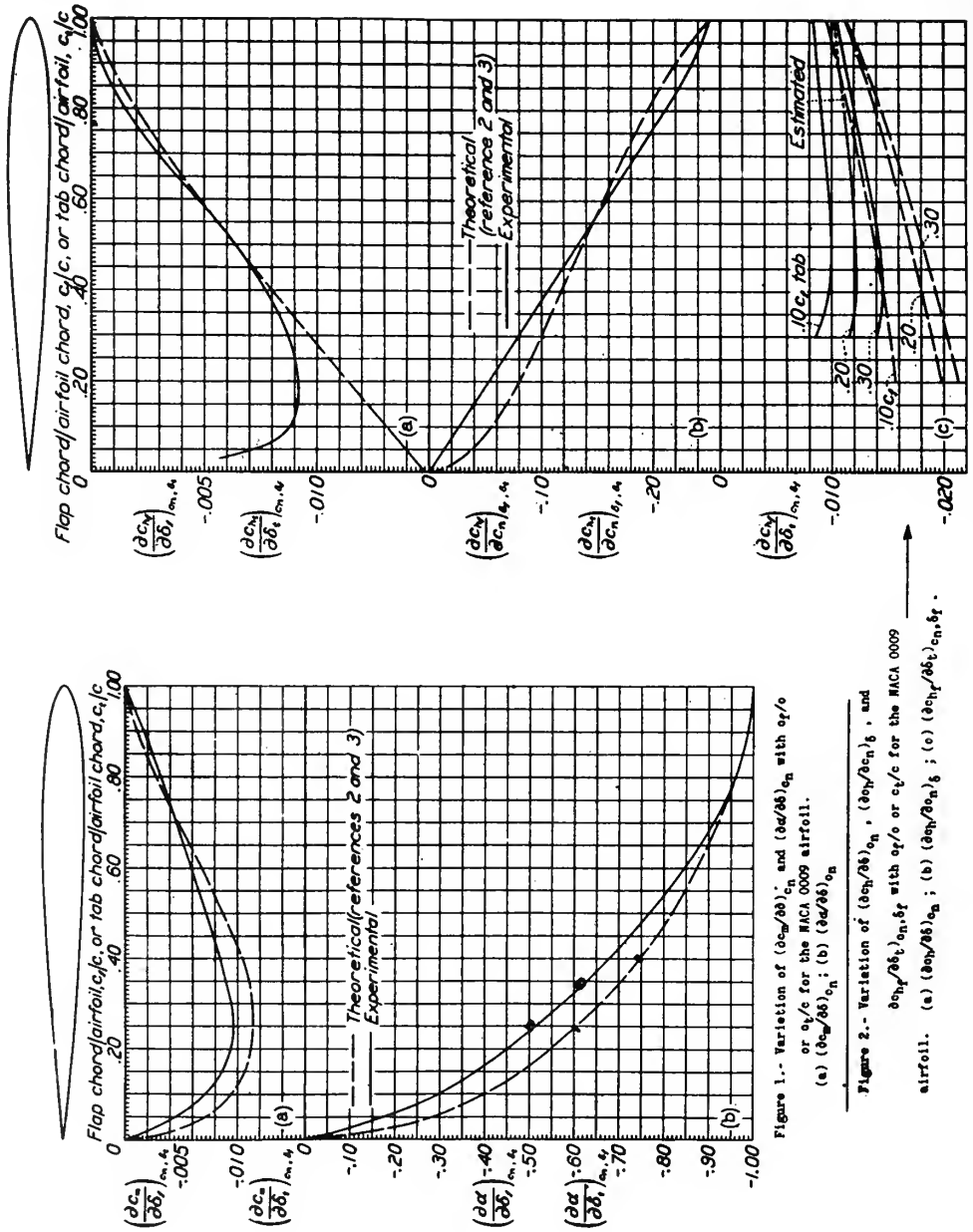

Figure 1.- Variation of $(\partial c_m/\partial\delta)'_{c_n}$ and $(\partial\alpha/\partial\delta)'_{c_n}$ with o_f/o or o_t/o for the NACA 0009 airfoil. (a) $(\partial c_m/\partial\delta)_{o_n}$; (b) $(\partial\alpha/\partial\delta)_{o_n}$

Figure 2.- Variation of $(\partial c_h/\partial\delta)_{o_n}$, $(\partial c_h/\partial c_n)'_\delta$, and $\partial c_{h_f}/\partial\delta_t)_{o_n,\delta_f}$ with o_f/o or c_f/c for the NACA 0009 airfoil. (a) $(\partial c_h/\partial\delta)_{o_n}$; (b) $(\partial c_h/\partial c_n)'_\delta$; (c) $(\partial c_{h_f}/\partial\delta_t)_{o_n,\delta_f}$.

FIG. B-7

SYMBOLS

C_l	Airfoil section lift coefficient
C_h	Hinge moment coefficient of control surface
C_{h_f}	Flap section hinge moment coefficient (in this investigation C_{h_f} and C_{h_r} are synonymous).
C_{h_r}	Rudder section hinge moment coefficient
C_{h_R}	Rudder hinge moment coefficient
S_W	Wing area
S_T	Tab area
S_R	Rudder area
q	Dynamic pressure of free air
c	Chord of airfoil section
c_{VT}	Chord of vertical tail*
c_R	Chord of rudder*
c_T	Chord of tab*
c_f	Chord of flap*
α	Angle of attack of finite span wing (angle between zero lift line and relative wind).
α_{eff}	Effective angle of attack
α_o	Angle of attack for infinite aspect ratio
α_δ	Flap or rudder effectiveness
ψ	Angle of yaw
$r, \dot{\psi}$	Angular rate of yaw

$\ddot{\psi}$	Angular acceleration of yaw
δ	Control surface deflection
δ_T	Tab deflection for model investigated
δ_R	Rudder deflection for model investigated
b	Span of surface
A	Aspect ratio
c_b	Chord of overhang
C_{l_α}	$\left[\frac{\partial C_l}{\partial \alpha}\right]_\delta^+$
C_{h_α}	$\left[\frac{\partial C_h}{\partial \alpha}\right]_\delta^+$
C_{h_δ}	$\left[\frac{\partial C_h}{\partial \delta}\right]_\alpha^+$
M	Moment
H	Angular momentum
V_A	Aircraft velocity
ρ	Air density
S_{link}	Linkage ratio
VT	Vertical tail
s	Control force, or stick force
η	Tail efficiency
l_{VT}	Length from center of gravity of aircraft to center of pressure of vertical tail
A_g	Angle between spin reference axis and gyro spin axis

NOTE:

* Measured from hinge axis to trailing edge of airfoil. + Subscripts outside of parentheses around the partial derivatives indicate the variables held constant when the derivatives are taken. A straight line over a symbol means the symbol is a vector quantity.

Appendix C

SIMULATION OF THE LATERAL AIRCRAFT RESPONSE ON THE GENERAL PURPOSE SIMULATOR

In order to more clearly illustrate the effect on the aircraft lateral response of increasing C_{n_r} and C_{l_β} by a factor of four, a simulator study using the equations of motion was made. The General Purpose Simulator of the Instrumentation Laboratory, Massachusetts Institute of Technology, was used for this study. The assistance of Mr. Samuel Giser and Mr. Frank Spada in setting up the problem is gratefully acknowledged.

The aircraft lateral equations of motion when written in the dimensional form appear as follows:

$$[Y_\beta - D]\beta - (\frac{g}{V_A})\varphi + D\psi = Y_{\delta_r} \tag{1}$$

$$L_\beta\beta + [L_p D - D^2]\varphi + [L_r D + \frac{I_{XZ}}{I_X} D^2]\psi = -L_{\delta_a} \tag{2}$$

$$N_\beta\beta + [N_p D + \frac{I_{XZ}}{I_Z} D^2]\varphi + [N_r D - I_Z D^2]\psi = -N_{\delta_r} - N_{\delta_a} \tag{3}$$

These equations may be rewritten:

$$D\beta = K_1 D\psi - K_2\delta_r - K_3\varphi + K_4\beta \tag{4}$$

$$D^2\varphi = K_5 D\psi + K_6 D^2\psi + K_7\delta_a + K_8 D\varphi - K_9\beta \tag{5}$$

$$D^2\psi = K_{10}\delta_a + K_{11}\delta_r + K_{12}\beta + K_{13} D\varphi + K_{14} D^2\varphi + K_{15} D\psi \tag{6}$$

For the B-26C airplane at 265 mph IAS, at a density altitude of 10,000 feet, the dimensional coefficients have the following values:

COEFFICIENT	CONSTANT	VALUE	UNITS
-	K_1	1	-
Y_{δ_r}	K_2	.0444	sec^{-1}
g/V_A	K_3	.0709	sec^{-1}
Y_β	K_4	-.1772	sec^{-1}
L_r	K_5	.4320	sec^{-1}
I_{XZ}/I_X	K_6	.121	-
L_{δ_a}	K_7	-6.901	sec^{-2}
L_p	K_8	-3.961	sec^{-1}
L_β	K_9	-10.757	sec^{-2}
N_{δ_a}	K_{10}	.2043	sec^{-2}
N_{δ_r}	K_{11}	-4.110	sec^{-2}
N_β	K_{12}	3.881	sec^{-2}
N_p	K_{13}	-.06852	sec^{-1}
I_{XZ}/I_Z	K_{14}	.064	-
N_r	K_{15}	-.4327	sec^{-1}

The method of simulation will not be discussed in this appendix. Suffice to say that the equations were simulated in such a manner that the constants K_9 and K_{15} could be increased by a factor of four. In addition, constants K_6

and K_{14}, which represent the products of inertia, could be set equal to zero.

The simulated response of the B-26C airplane for a rudder pulse input and an aileron pulse input were photographed from the trace appearing on a cathode ray oscilloscope. Response pictures were taken for Sideslip, β; Roll, φ, and Yaw, ψ. These photographs are described as they appear on the following pages.

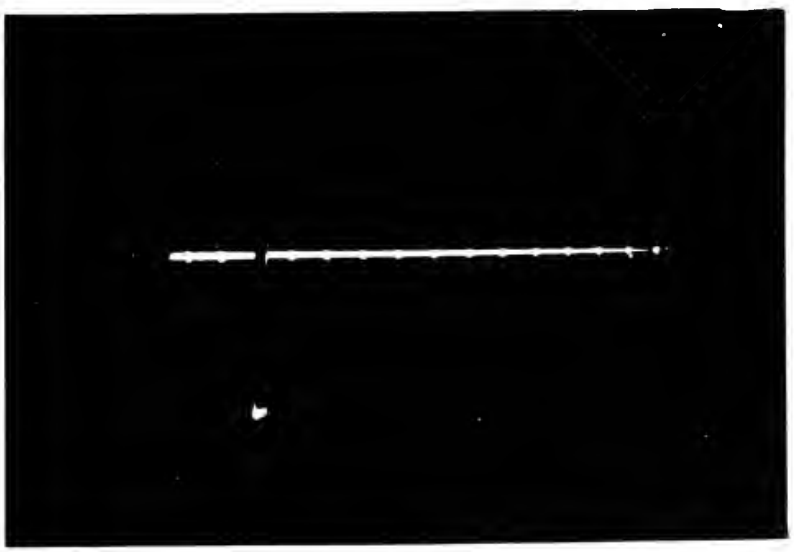

Fig. C-1. Pulse Input = 1/4 sec

Note:

1. Same pulse applied to aileron and rudder.
2. Timing dots are 2 seconds apart.

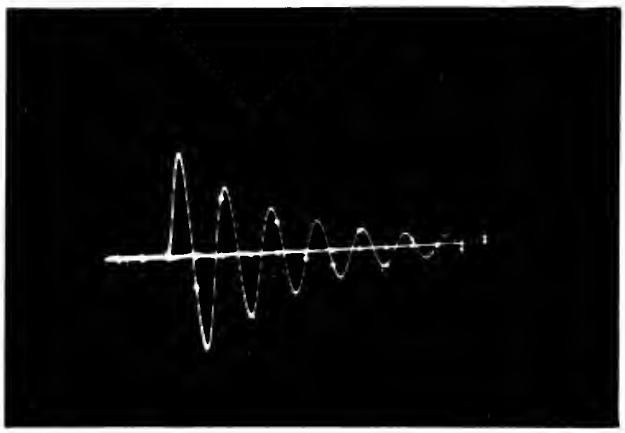

Comments:
Oscillation is Dutch Roll.
DR = 0.15

Sideslip Response

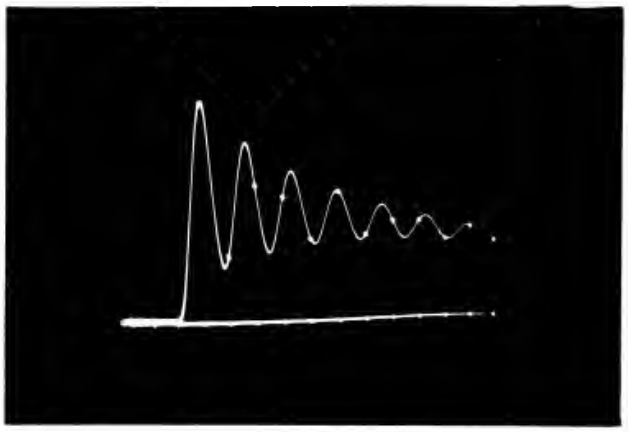

Roll Response

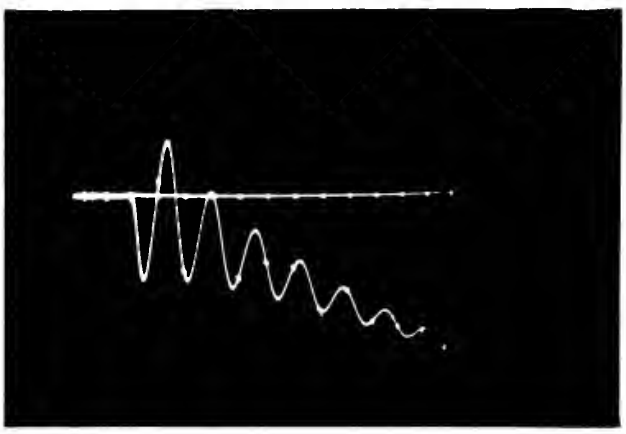

Yaw Response

Fig. C-2 Response of B-26C to a Rudder Pulse Input
Normal Configuration

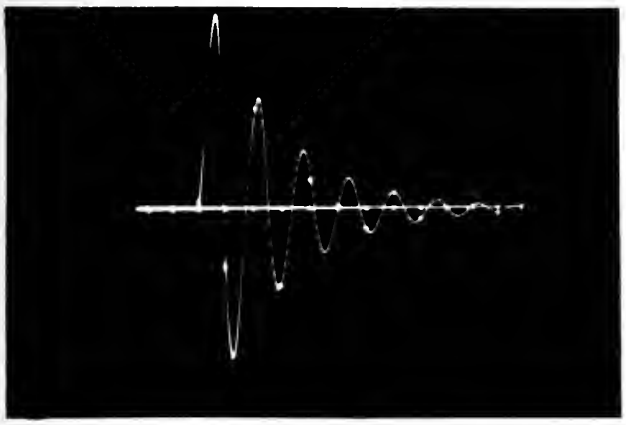

Sideslip Response

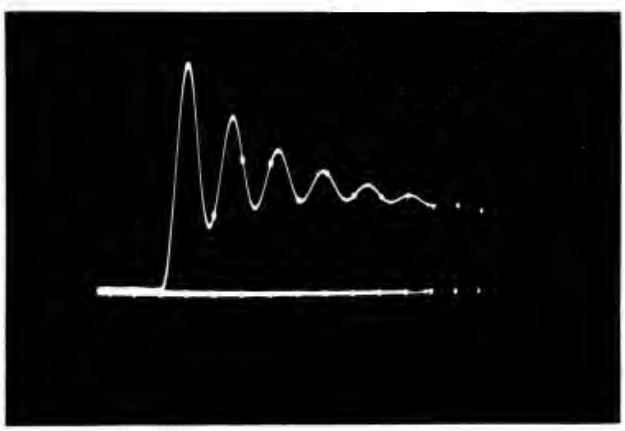

Roll Response

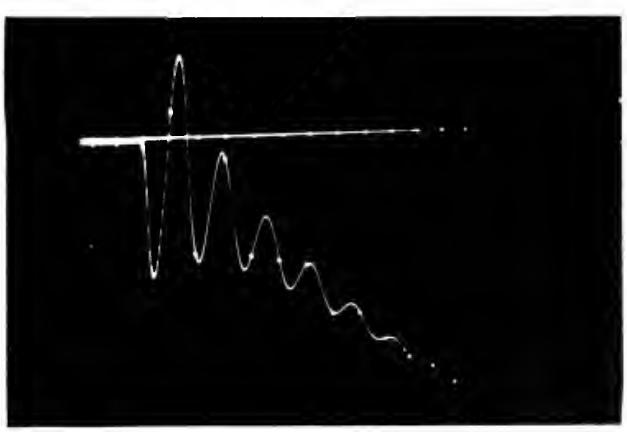

Yaw Response

Comments:

Neglecting Products of Inertia, I_{XZ} has only a small effect.

Fig. C-3. Response of B-26C to a Rudder Pulse Input
Normal Configuration with $I_{XZ} = 0$

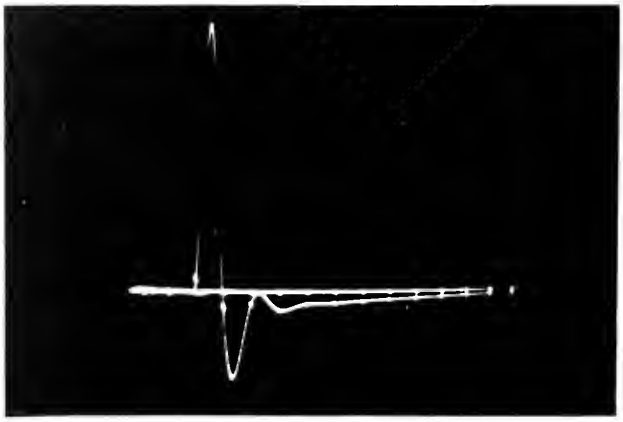

Comments:

Increasing C_{n_r} by a factor of four has damped Dutch Roll Oscillation

Sideslip Response

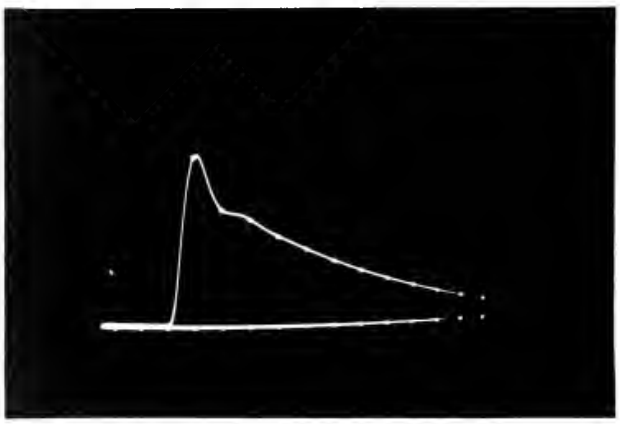

Roll Response

Note improvement in spiral mode.

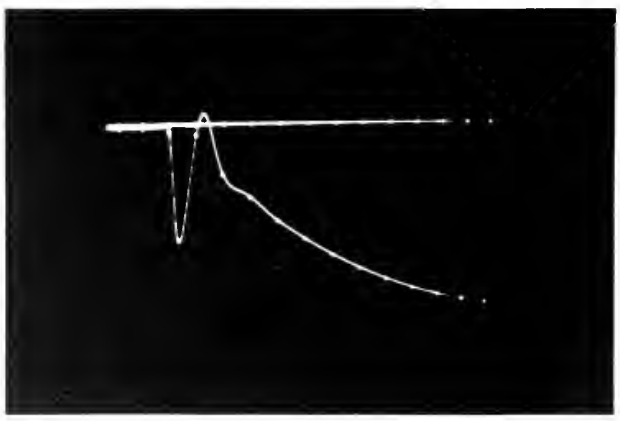

Yaw Response

Fig. C-4. Response of B-26C to a Rudder Pulse Input with $I_{XZ} = 0$ and Yaw Damping Increased by a Factor of Four

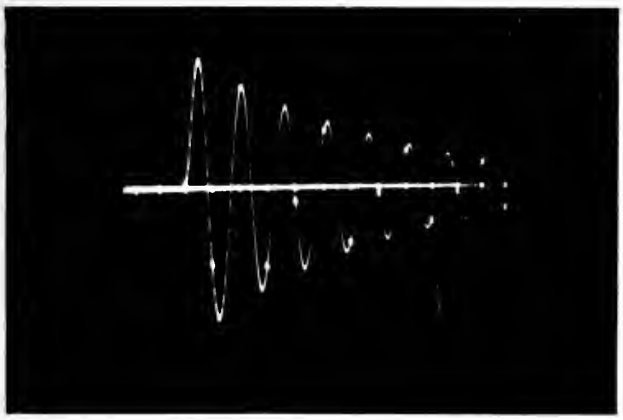

Comments:

Increasing C_{l_β} by a factor of four has increased Dutch Roll Oscillation

Sideslip Response

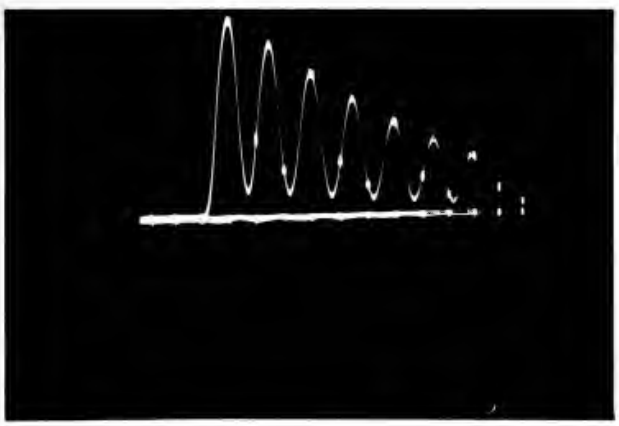

Roll Response

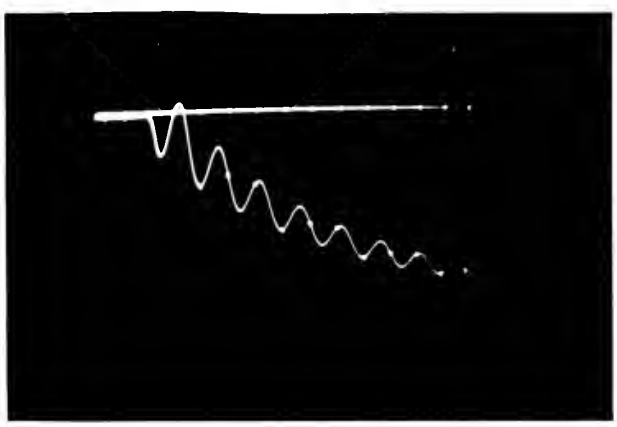

Yaw Response

Fig. C-5. Response of B-26C to Rudder Pulse Input with $I_{XZ} = 0$ and Dihedral Increased by a Factor of Four

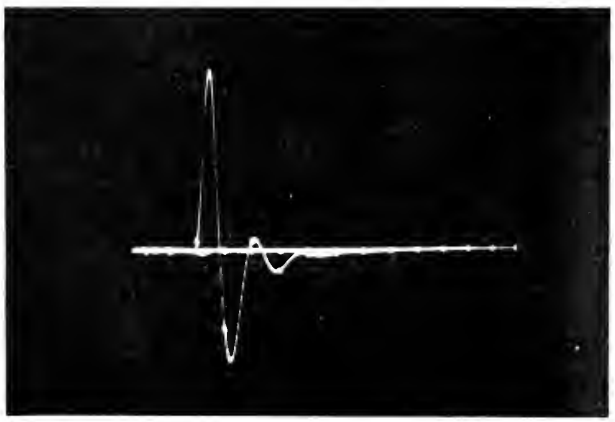

Comments:

Increasing C_{n_r} and C_{l_β} by a factor of four has damped Dutch Roll and improved Spiral Stability

Sideslip Response

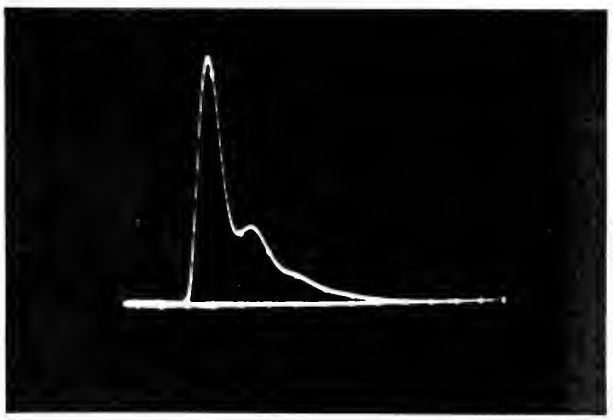

Roll Response

Note improvement in spiral mode.

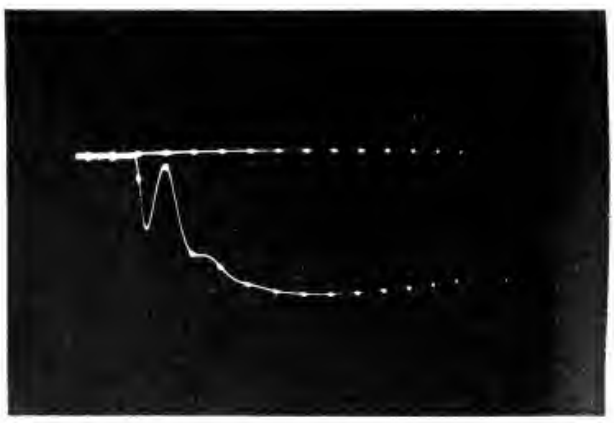

Yaw Response

Fig. C-6. Response of B-26C to a Rudder Pulse Input with $I_{XZ} = 0$ Dihedral and Yaw Damping Increased by a Factor of Four

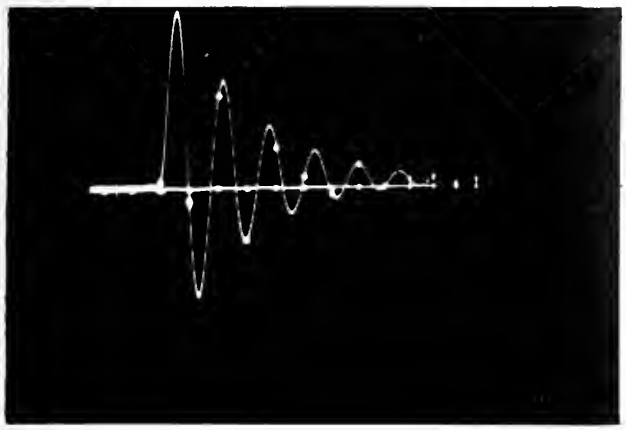

Comments:

Normal configuration DR = 0.15

Sideslip Response

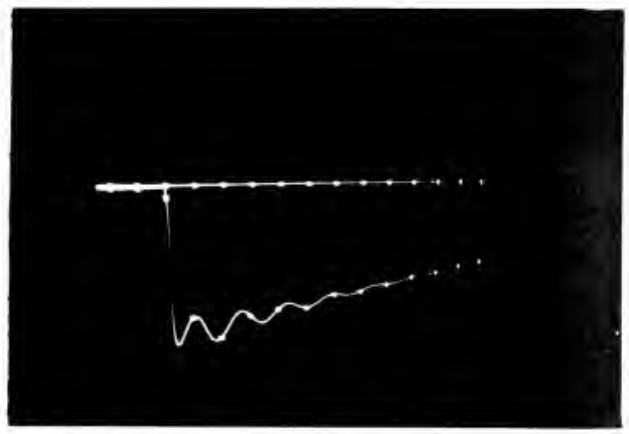

Roll Response

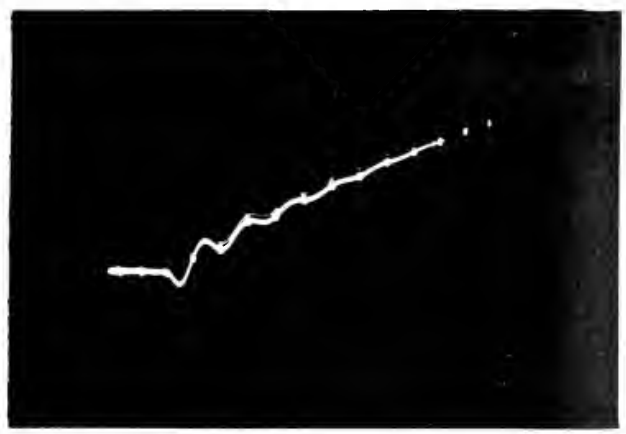

Yaw Response

Fig. C-7. Response of B-26C to Aileron Pulse Input with $I_{XZ} = 0$

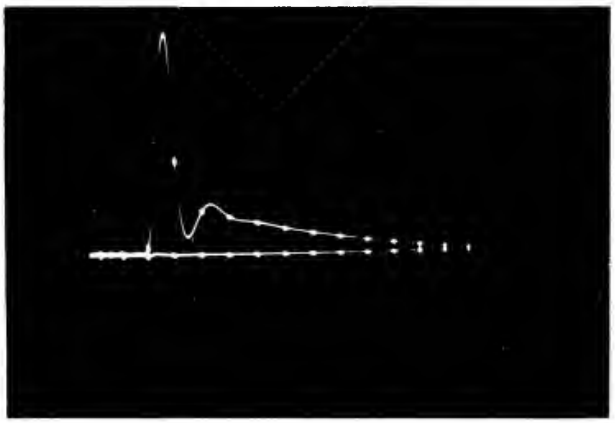

Comments:

Increasing C_{n_r} has damped Dutch Roll. Spiral Stability is improved.

Sideslip Response

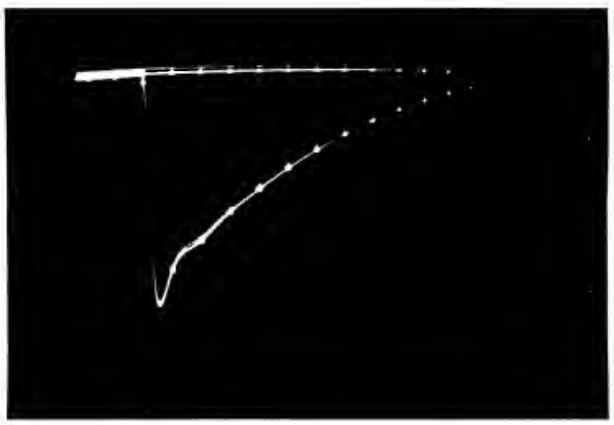

Roll Response

Note improvement in spiral mode.

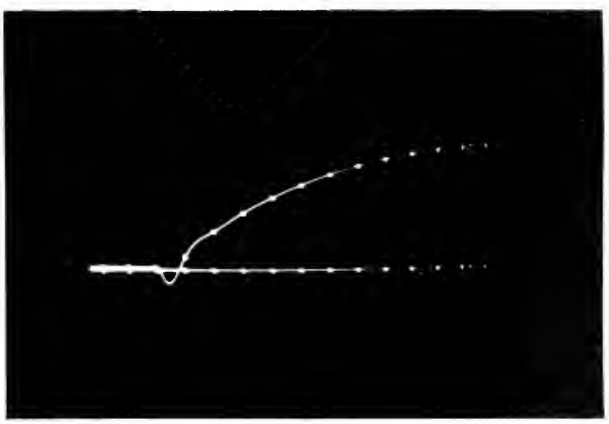

Yaw Response

Fig. C-8. Response of B-26C to Aileron Pulse Input with $I_{XZ} = 0$ and Yaw Damping Increased by a Factor of Four

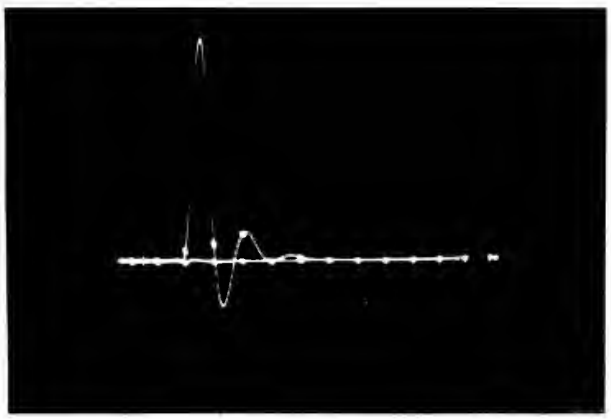

Comments:

Increasing C_{n_r} and C_{l_β} by a factor of four results in a high stable system.

Sideslip Response

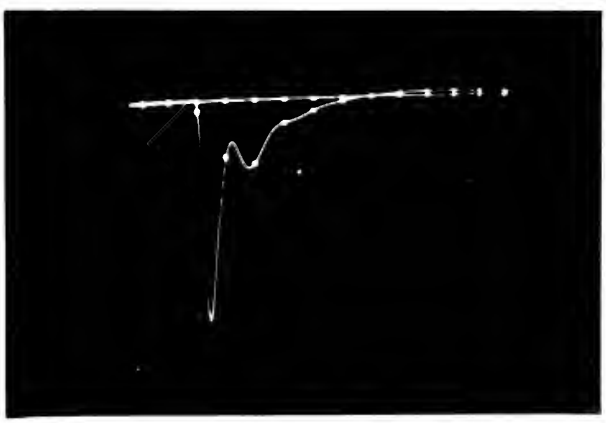

Roll Response

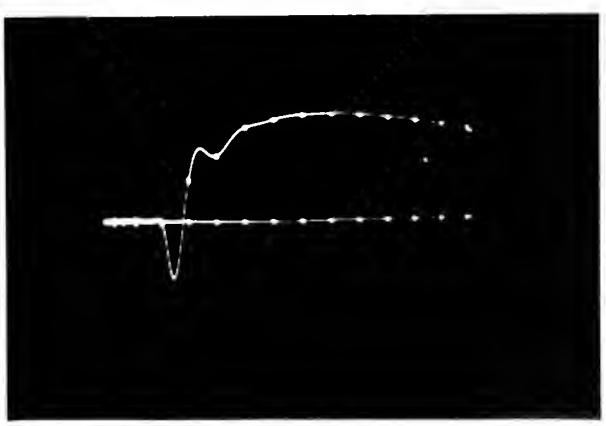

Yaw Response

Fig. C-9. Response of B-26C to Aileron Pulse Input with $I_{XZ} = 0$, Dihedral and Yaw Damping Increased by a Factor of Four

APPENDIX D

RESPONSE RECORDS

Numbers on Individual Records Correspond to
Information in Table I, Chapter 7

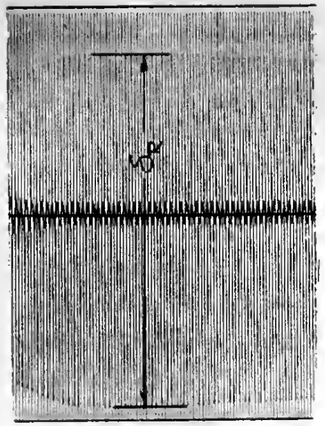

δ_R = 15° R

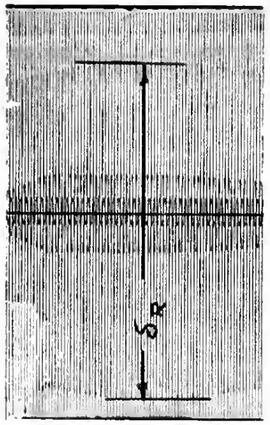

δ_R=15° L

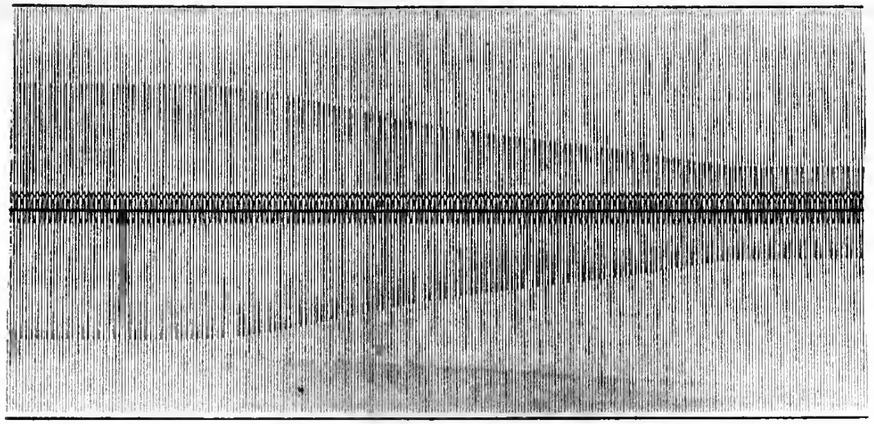

ψ = 15° R

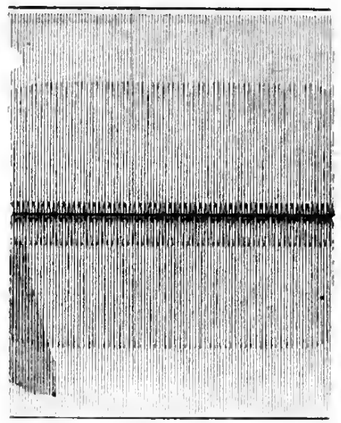

δ_T=14° L

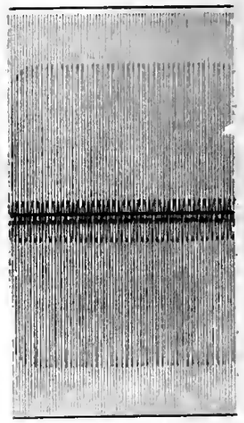

δ_T=13.5° R

CALIBRATION FOR RUDDER NO. 1

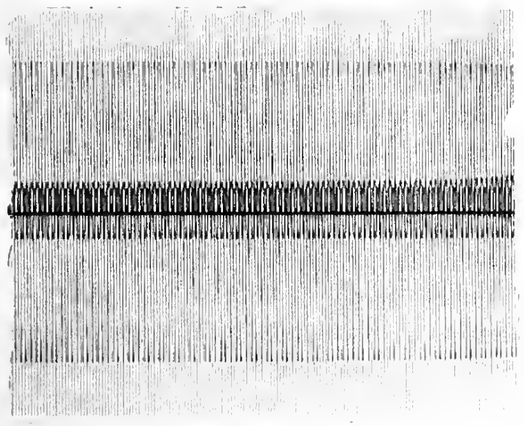

ψ = 15° R

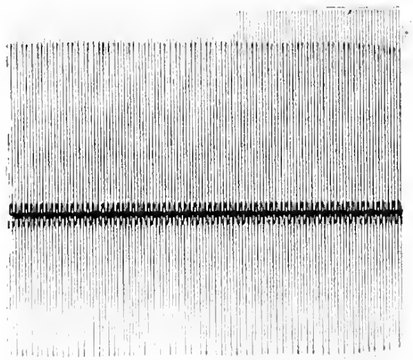

δ_R = 25° R

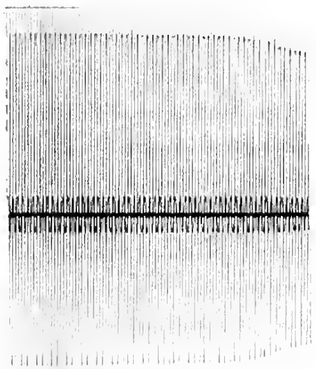

δ_R = 25° L

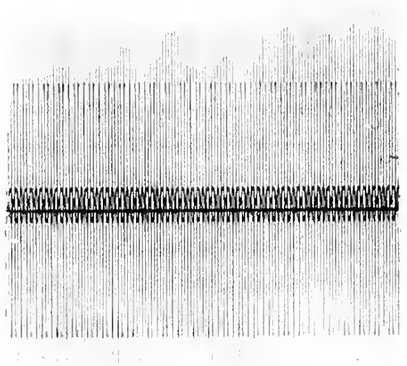

δ_T = 13.5° R

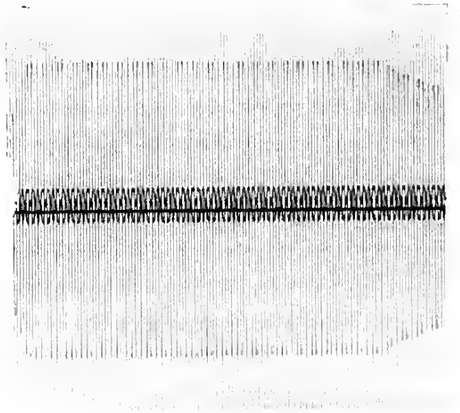

δ_T = 14° L

CALIBRATION FOR RUDDER NO. 2

CALIBRATION DATA FOR PHOTOGRAPHIC RECORDS

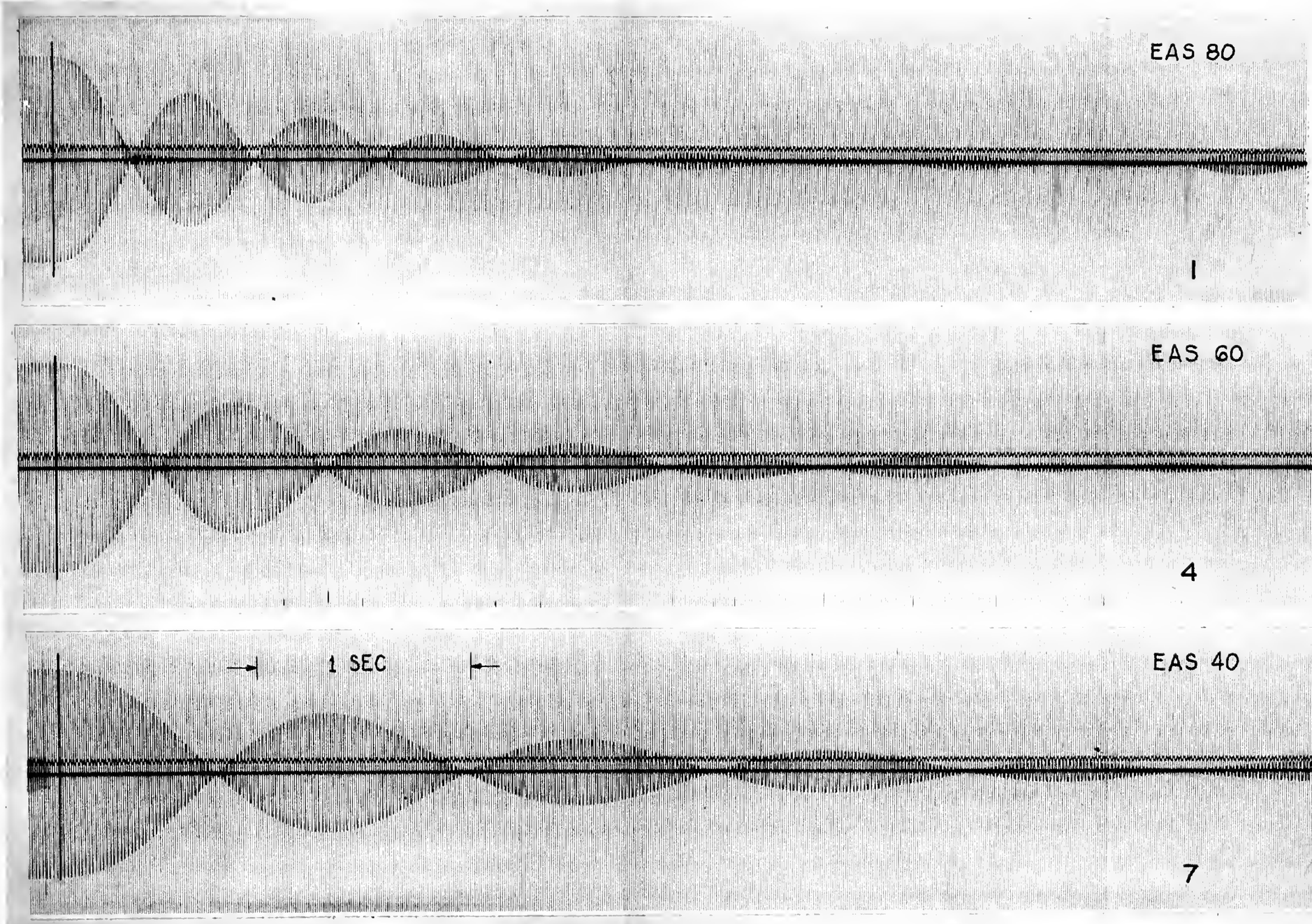

RESPONSE RECORD for FIXED CONTROLS
RUDDER 2 TAB 1-1 VISCOUS DAMPER IN

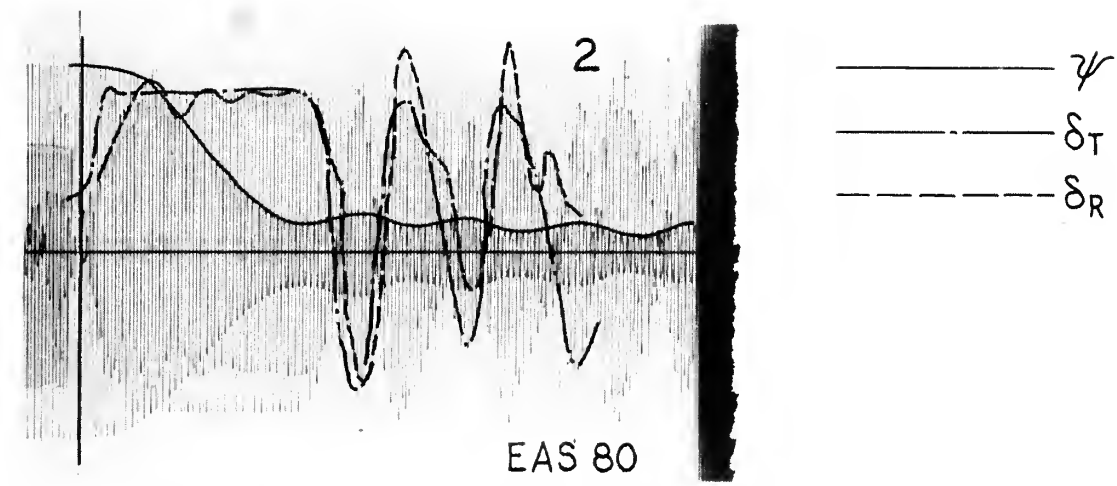

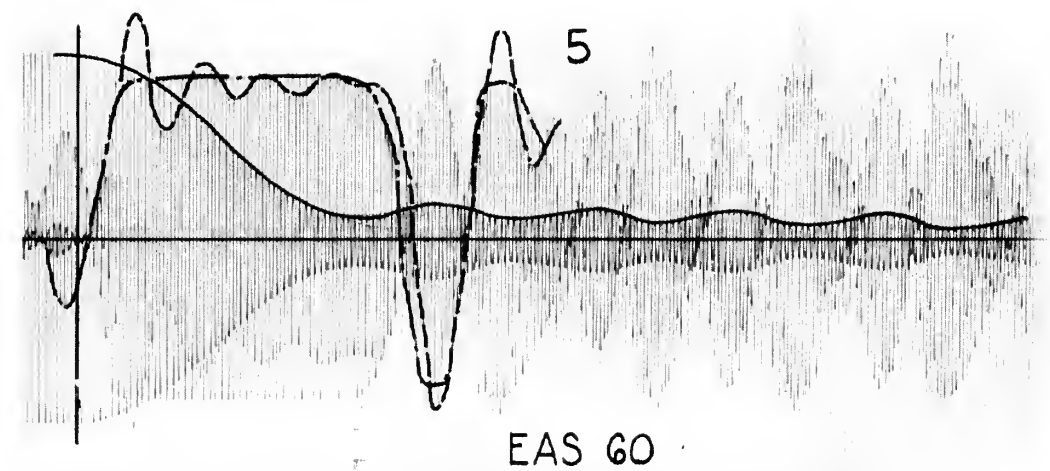

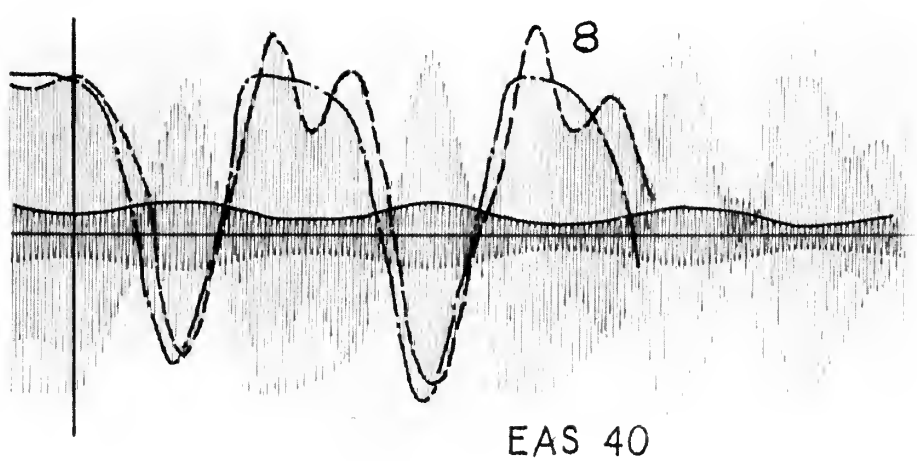

RESPONSE RECORDS for FREE CONTROL SYSTEM RUDDER 2 TAB.1-1 VISCOUS DAMPER IN GYRO ON

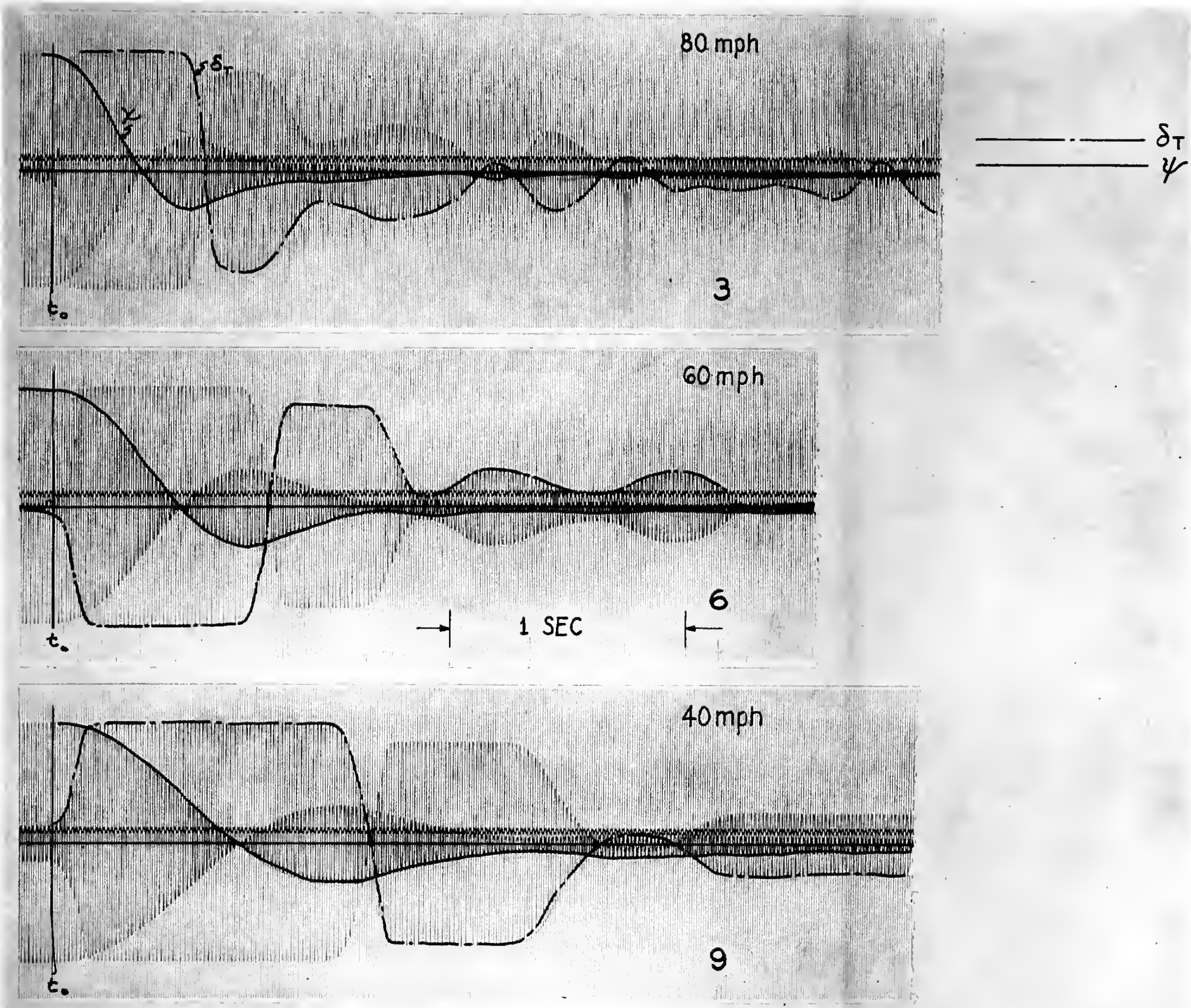

RESPONSE RECORD for DIRECT CONTROL SYSTEM
RUDDER 2 TAB 1-1 VISCOUS DAMPER IN

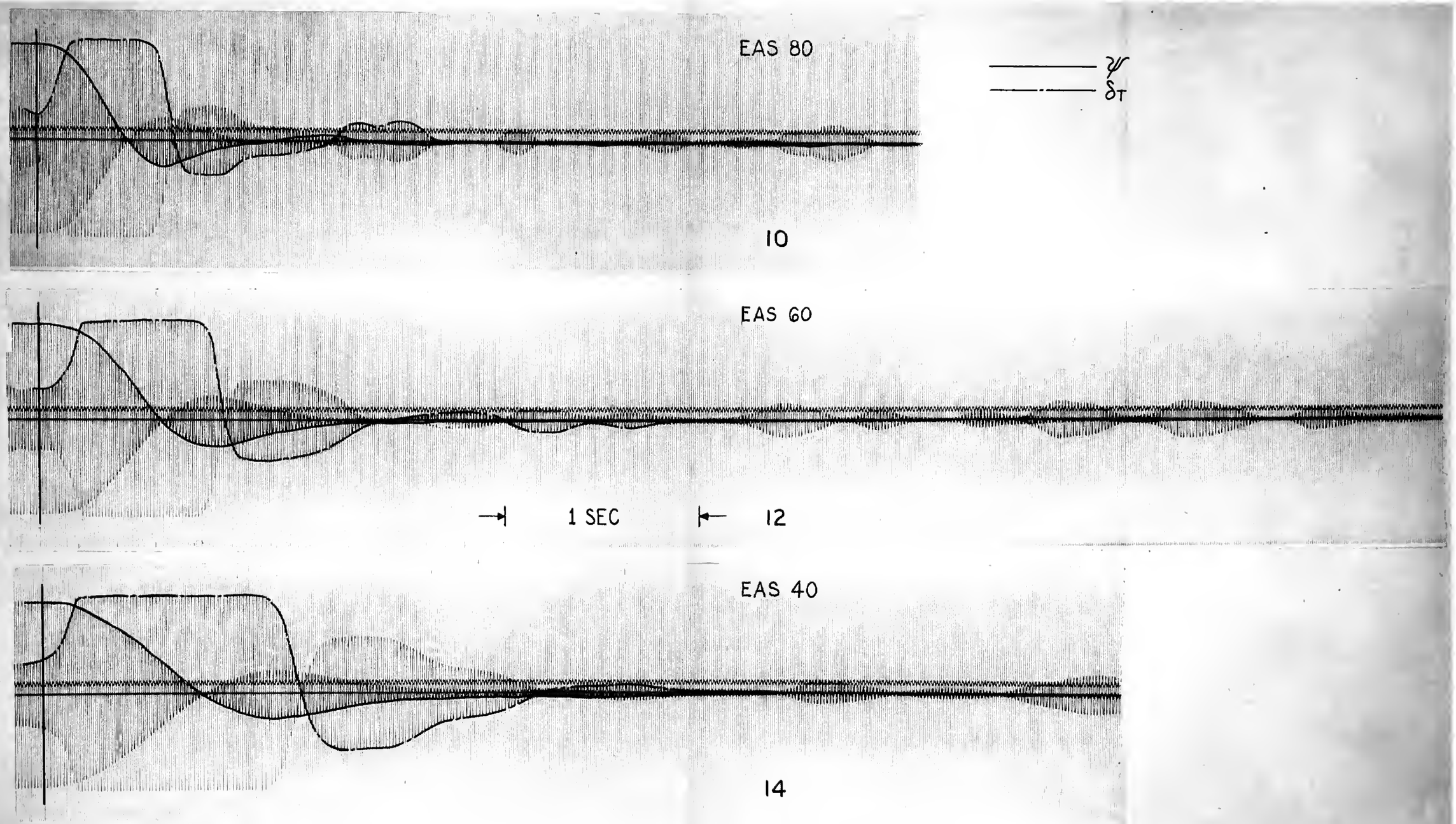

RESPONSE RECORD for DIRECT CONTROL SYSTEM
RUDDER 2 TAB. 1-2 VISCOUS DAMPER IN

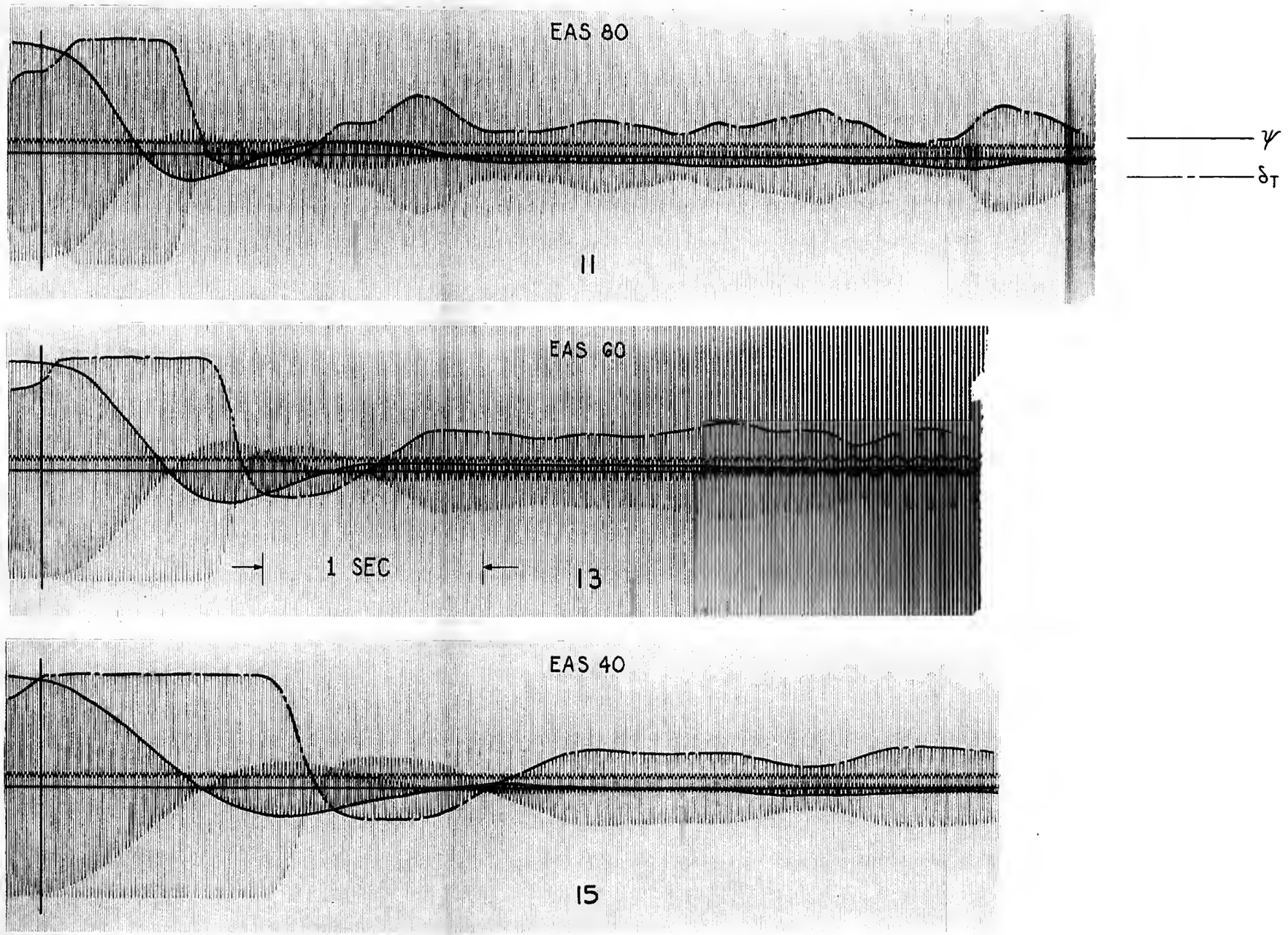

RESPONSE RECORD for DIRECT CONTROL SYSTEM
RUDDER 2 TAB. 1-3 VISCOUS DAMPER IN

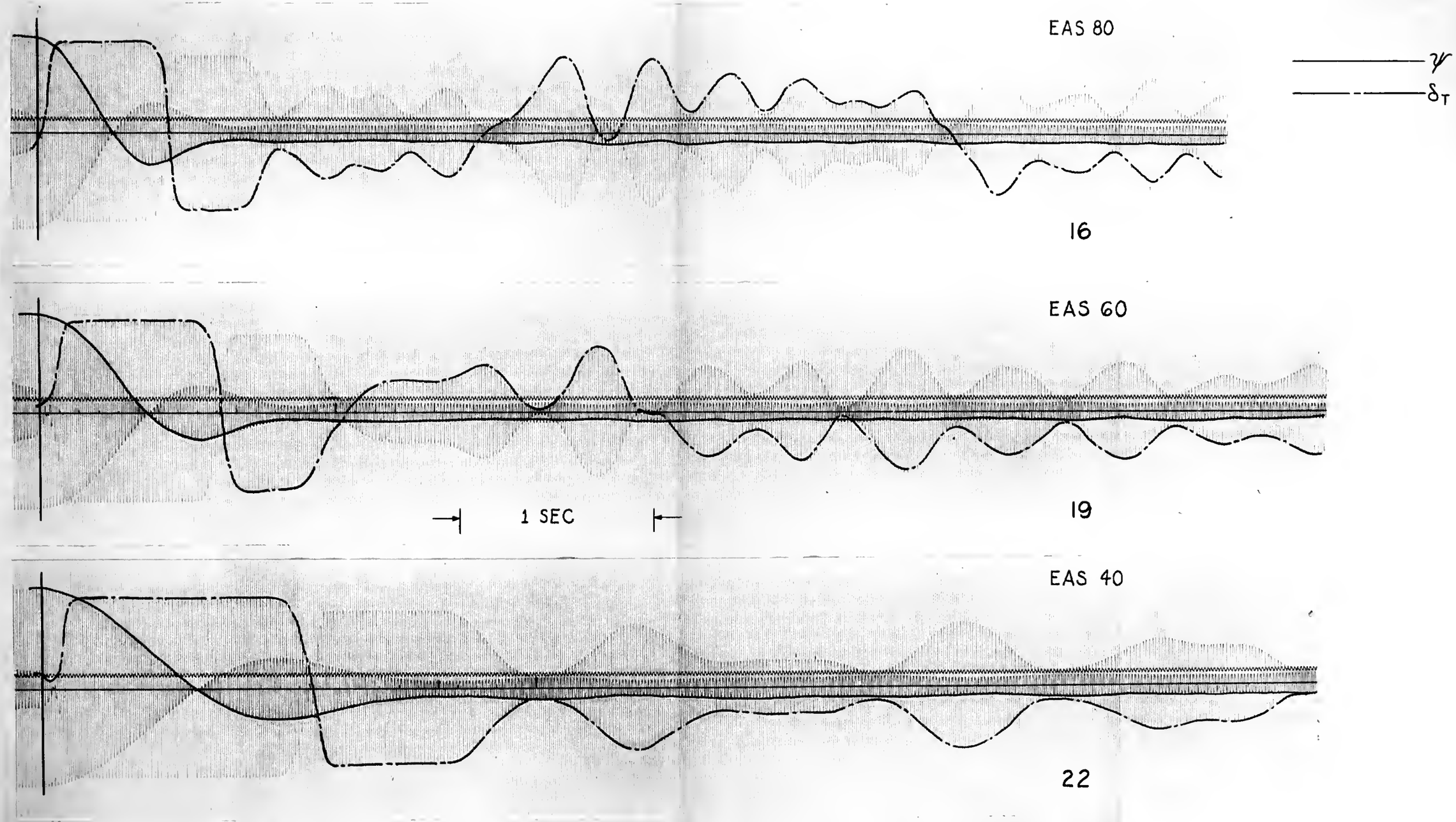

RESPONSE RECORD for DIRECT CONTROL SYSTEM
RUDDER 2 TAB. 2-1 VISCOUS DAMPER IN

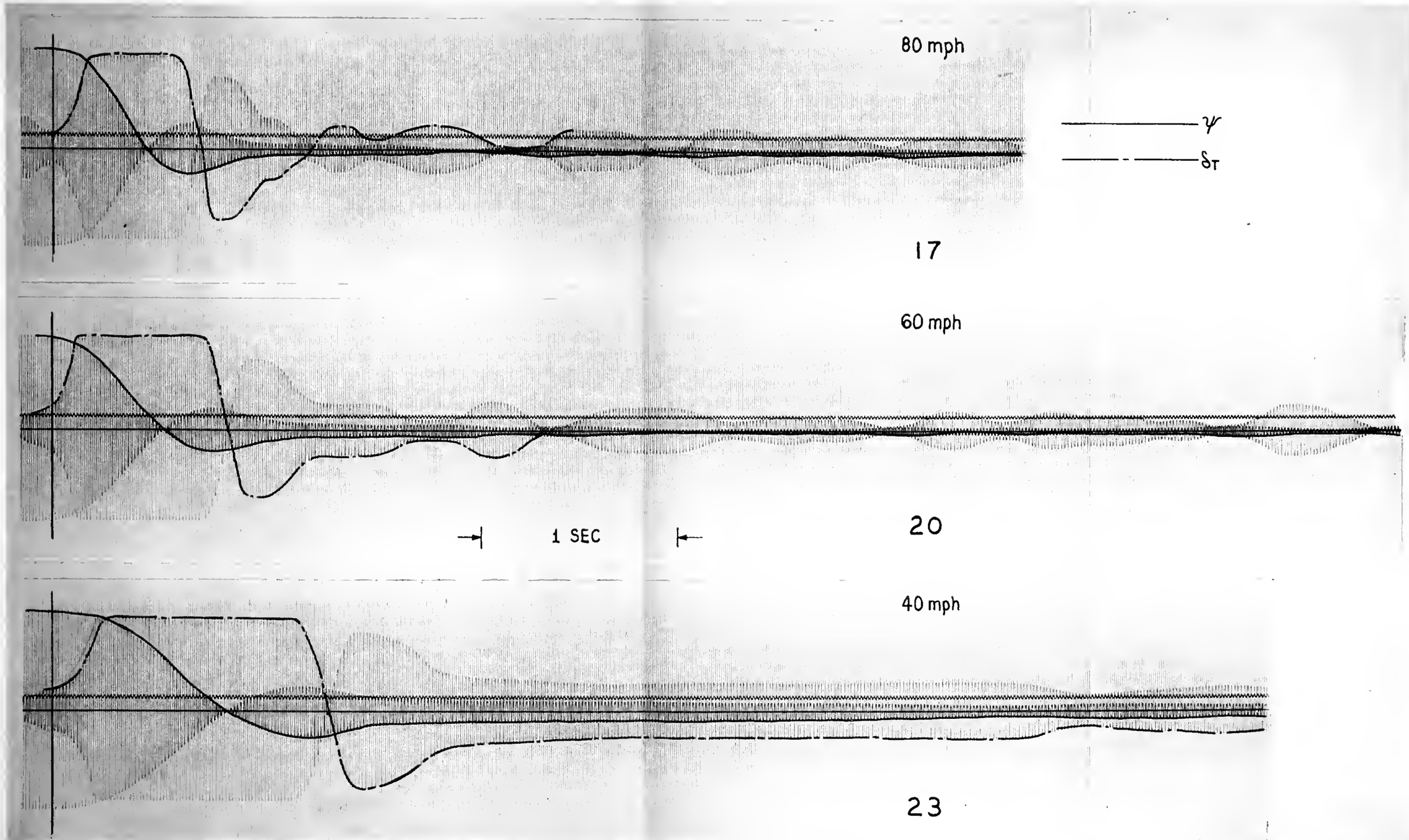

RESPONSE RECORD for DIRECT CONTROL SYSTEM
RUDDER 2 TAB. 2-2 VISCOUS DAMPER IN

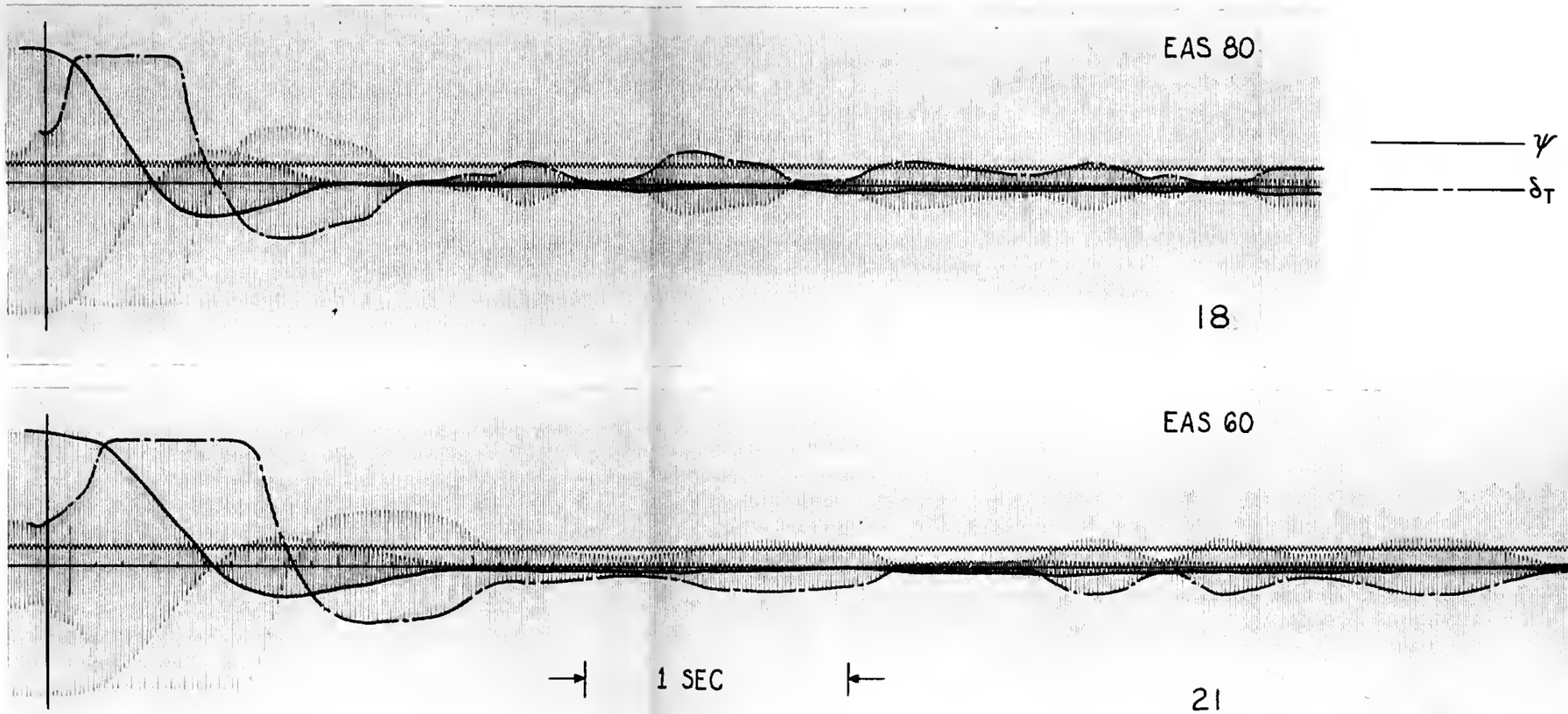

RESPONSE RECORD for DIRECT CONTROL SYSTEM
RUDDER 2 TAB. 2-3 VISCOUS DAMPER IN

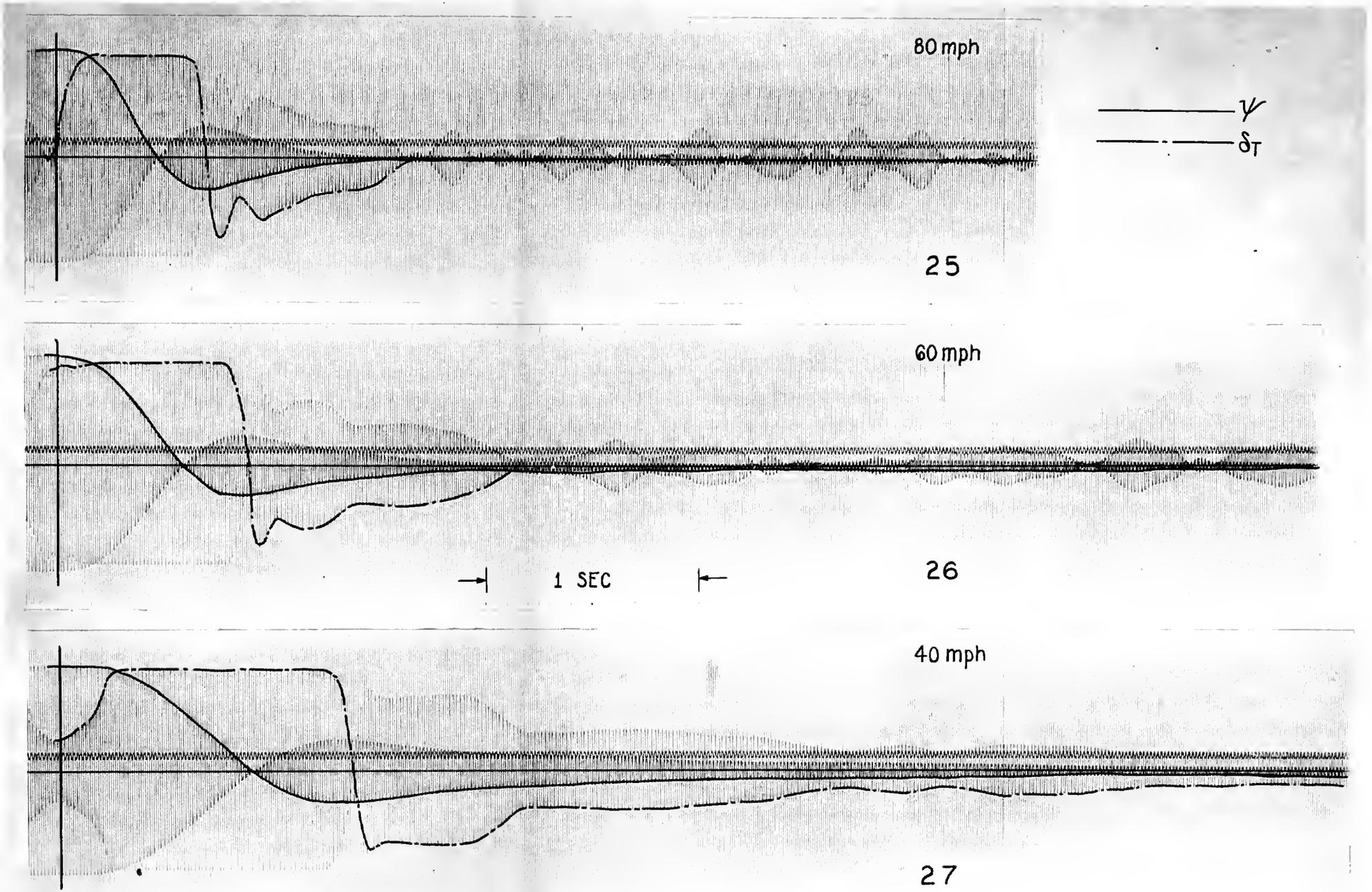

RESPONSE RECORD for DIRECT CONTROL SYSTEM
RUDDER 2 TAB. 2-2 NO VISCOUS DAMPER

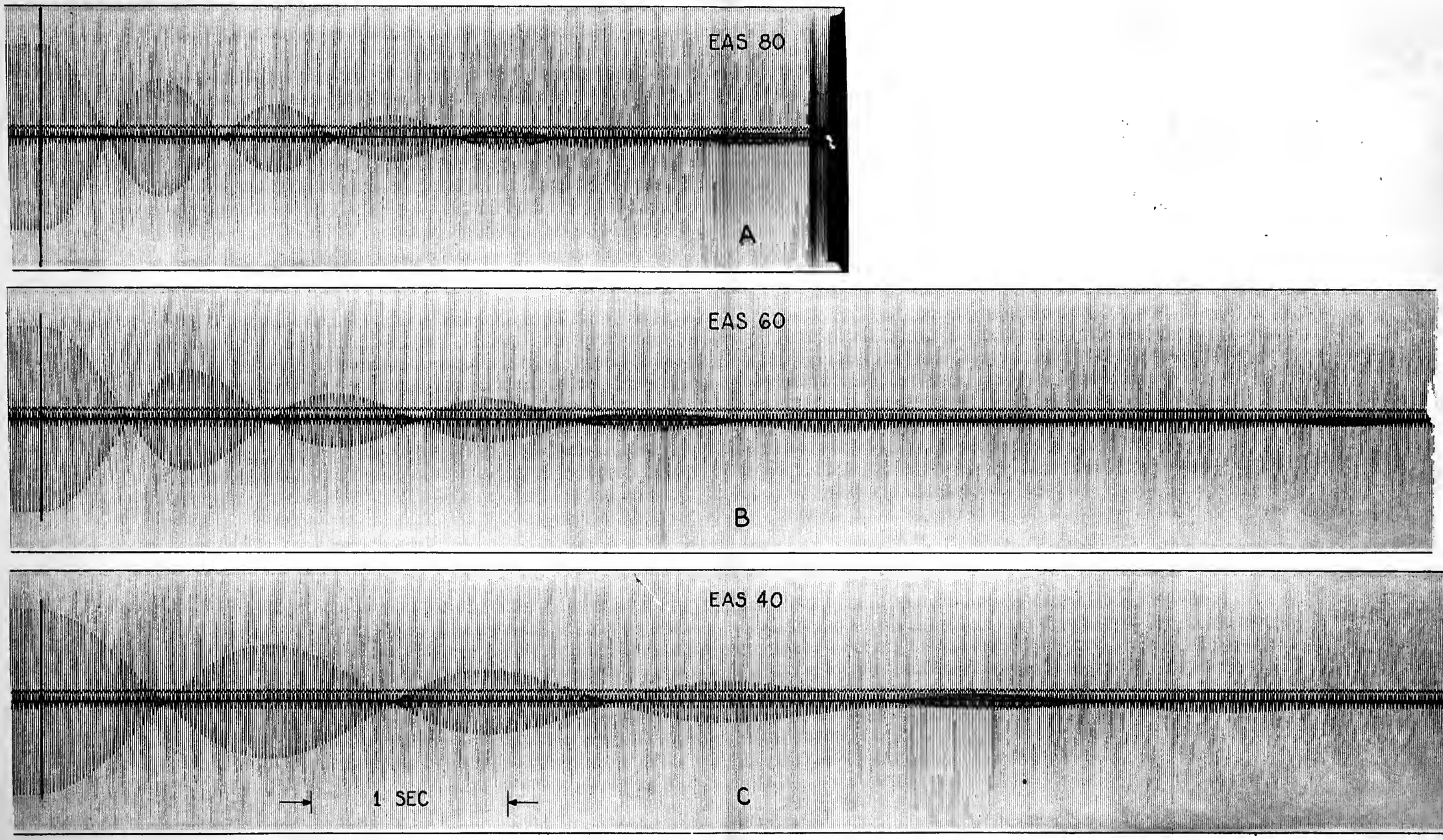

RESPONSE RECORD for FIXED CONTROL SYSTEM
RUDDER 1 TAB 1-1 NO VISCOUS DAMPER

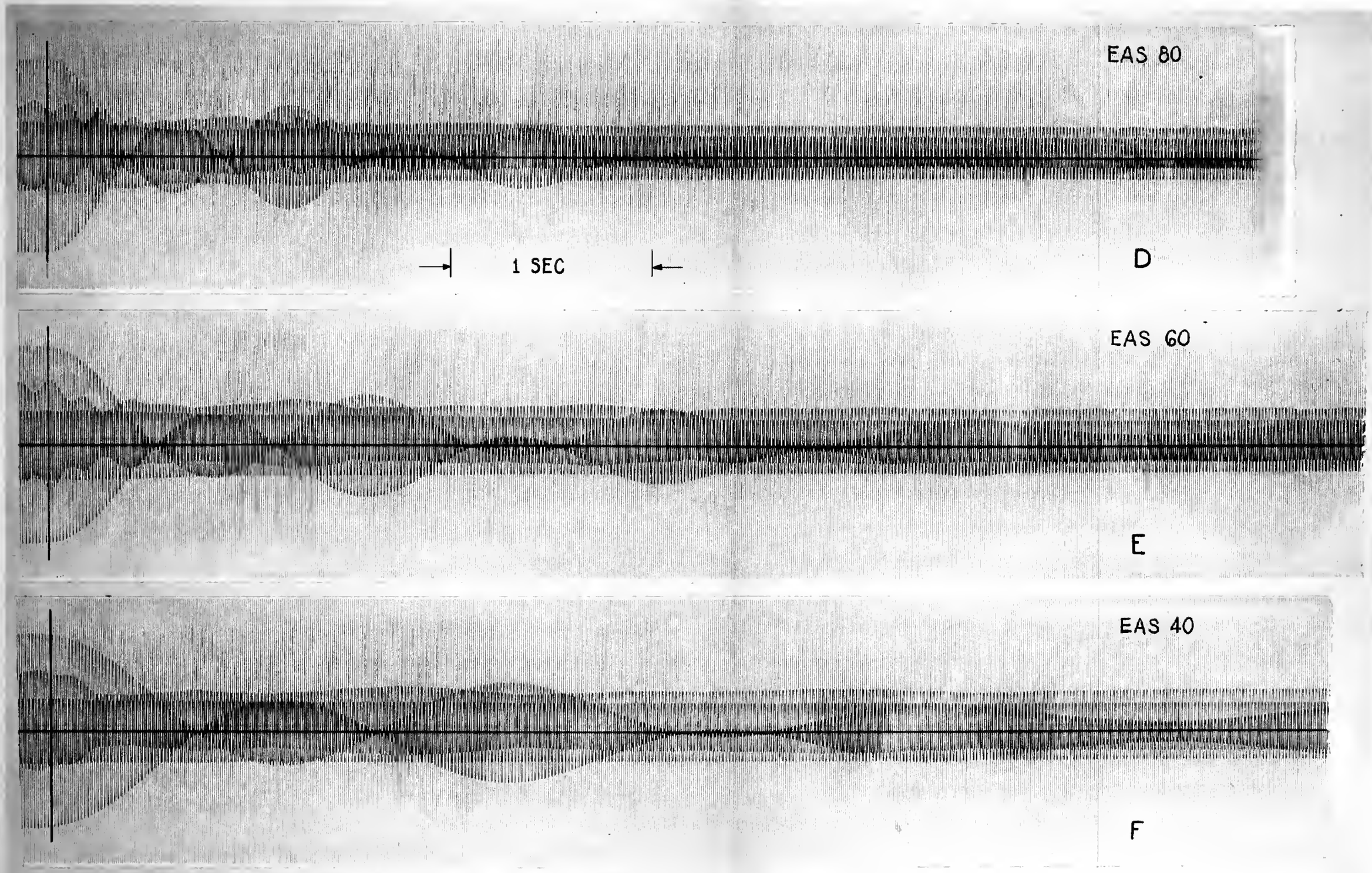

RESPONSE RECORDS for FREE CONTROL SYSTEM
RUDDER 2 TAB. 1-1 VISCOUS DAMPER IN
GYRO OFF

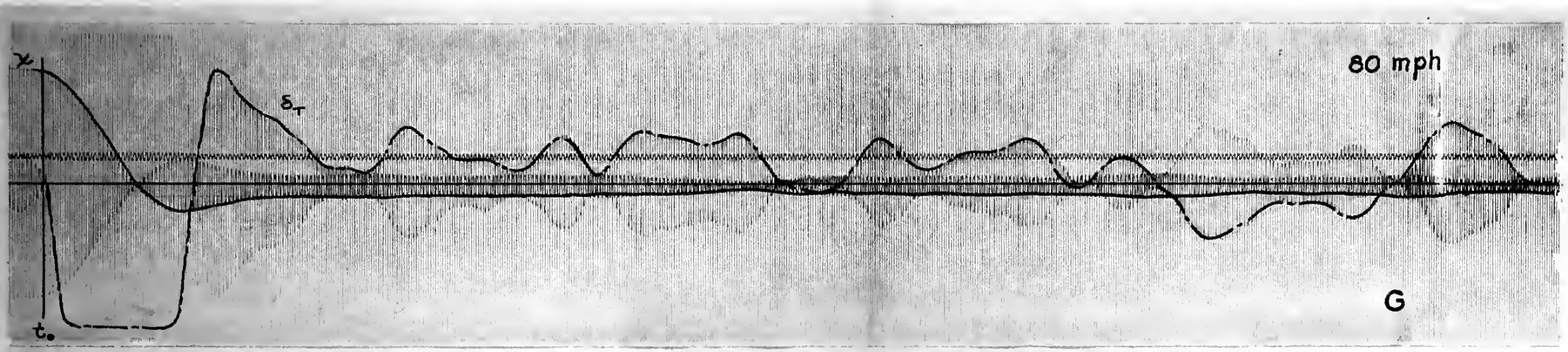

δ_T

ψ

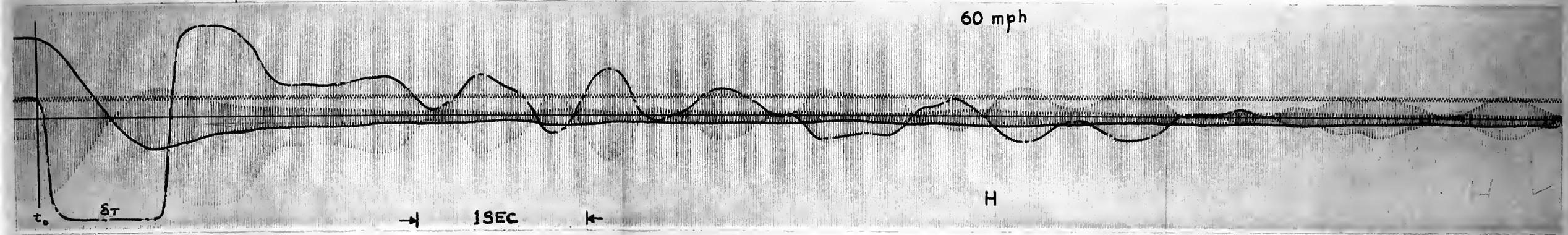

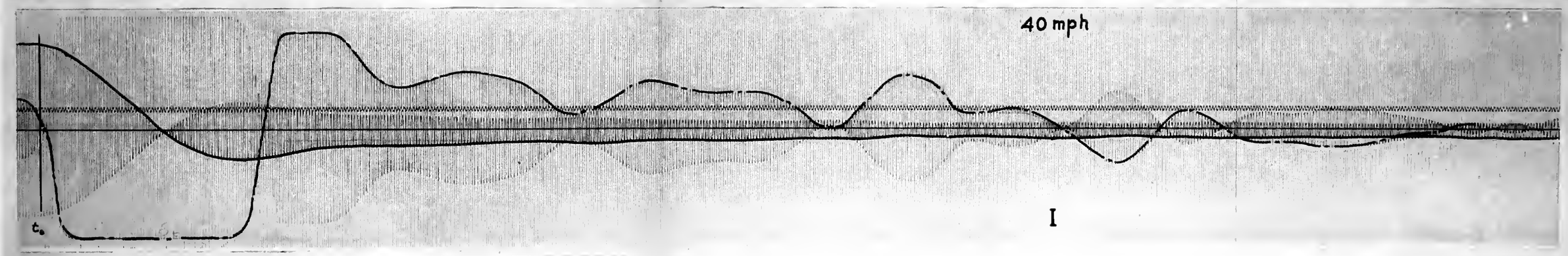

RESPONSE RECORD for DIRECT CONTROL SYSTEM
RUDDER 1 TAB 1-1 VISCOUS DAMPER IN

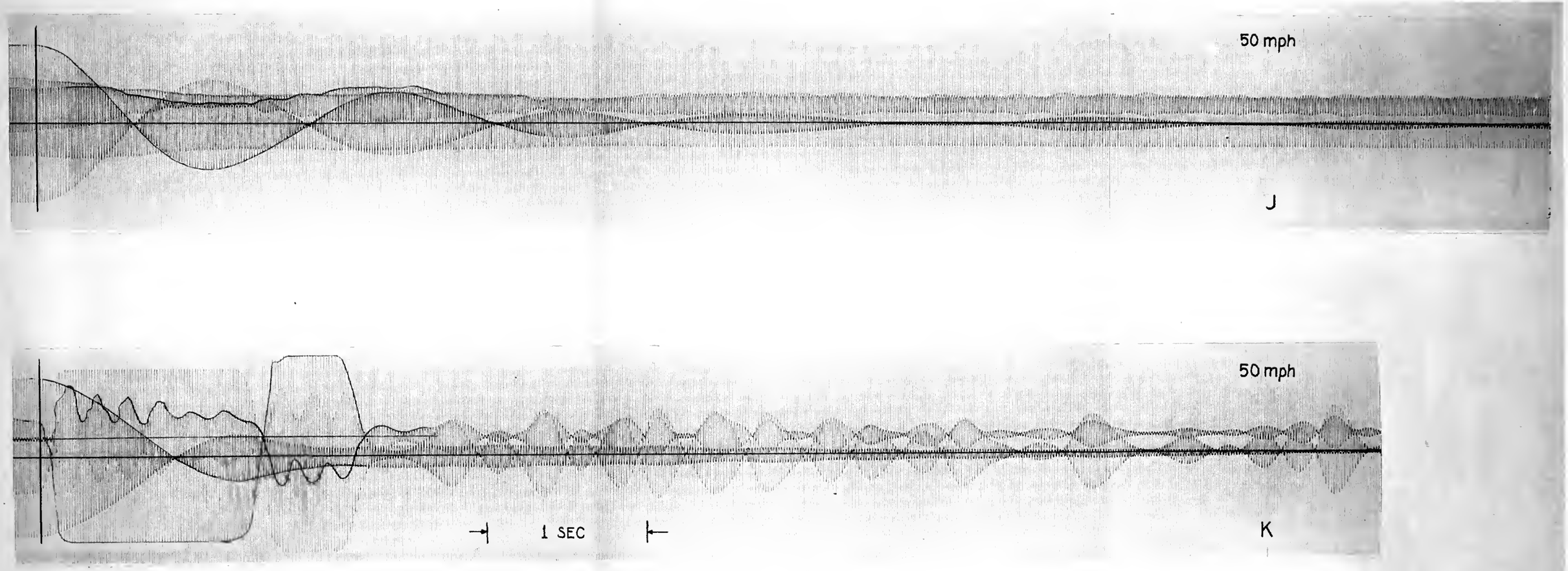

RESPONSE RECORD for FREE CONTROL SYSTEM
RUDDER 1 TAB. 1-1 VISCOUS DAMPER IN
SPOILER ON

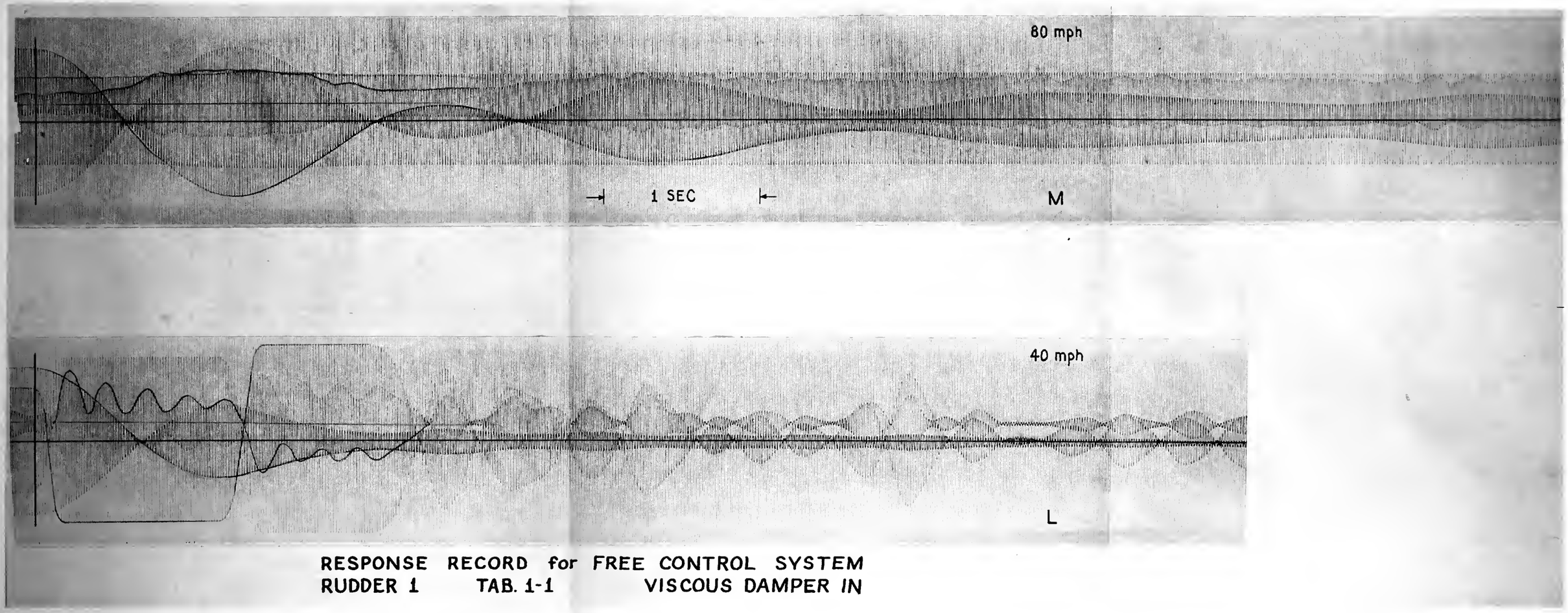

RESPONSE RECORD for FREE CONTROL SYSTEM
RUDDER 1 TAB. 1-1 VISCOUS DAMPER IN

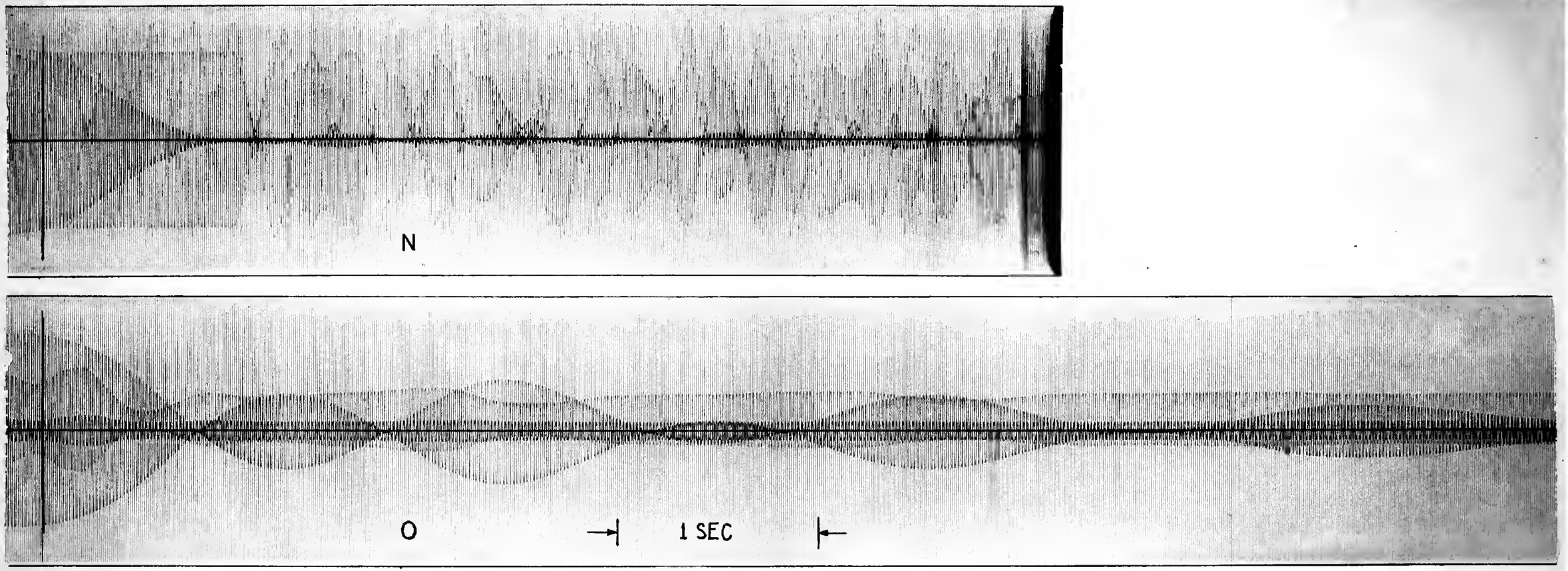

RESPONSE RECORD for FREE CONTROL SYSTEM
RUDDER 1 TAB. 1-1 40mph

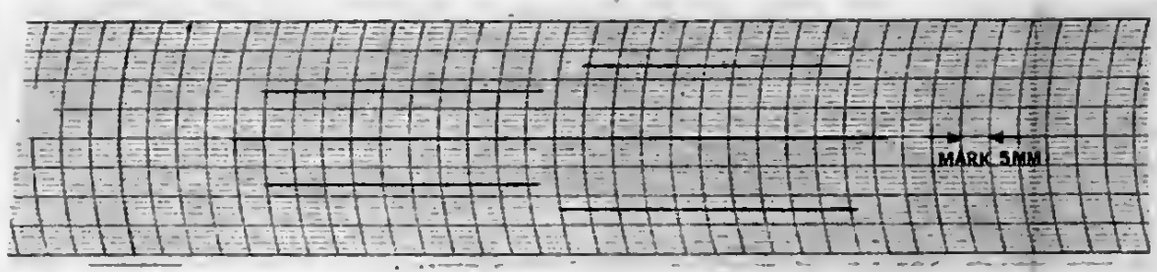

NOISE CALIBRATION 2° YAW 3° YAW

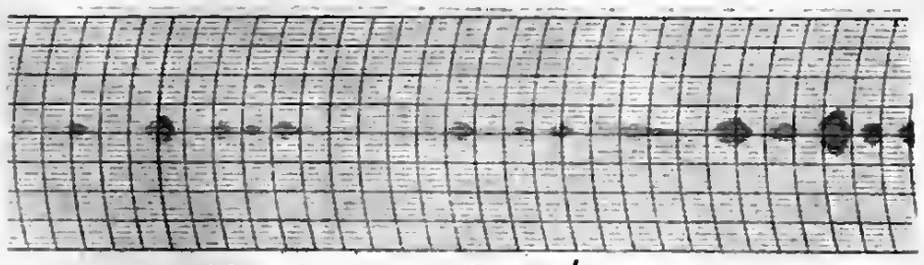

30 mph 5 MM/SEC

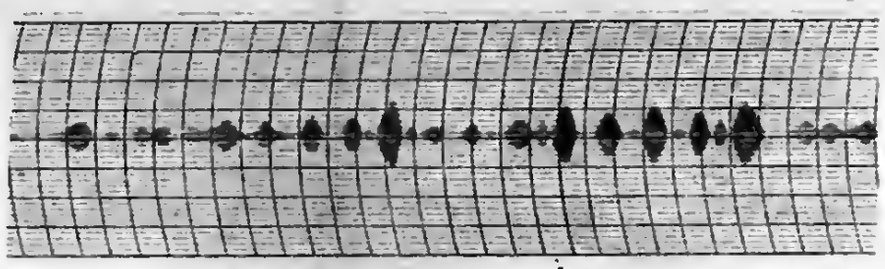

60 mph 5 MM/SEC

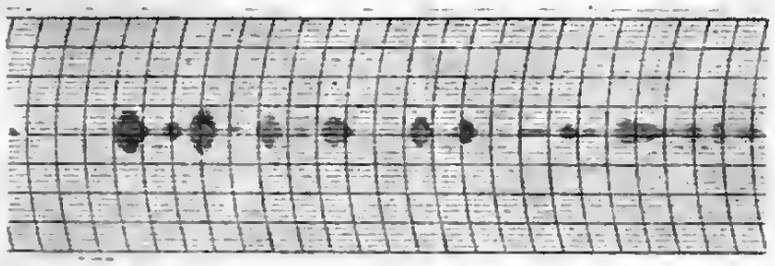

40 mph 5 MM/SEC

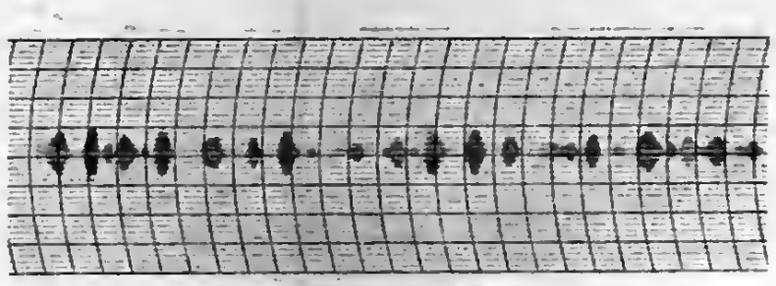

70 mph 5 MM/SEC

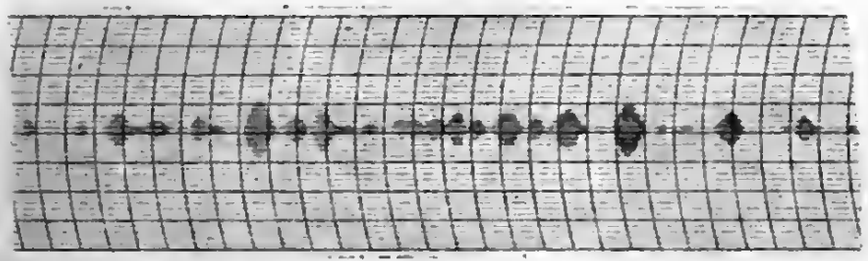

50 mph 5 MM/SEC

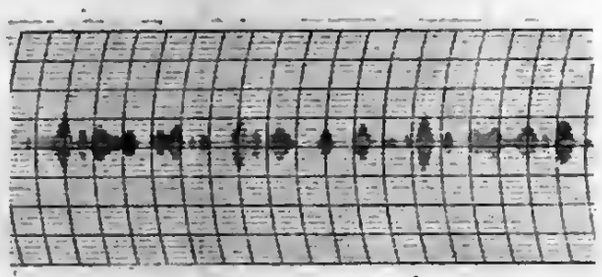

80 mph 5 MM/SEC

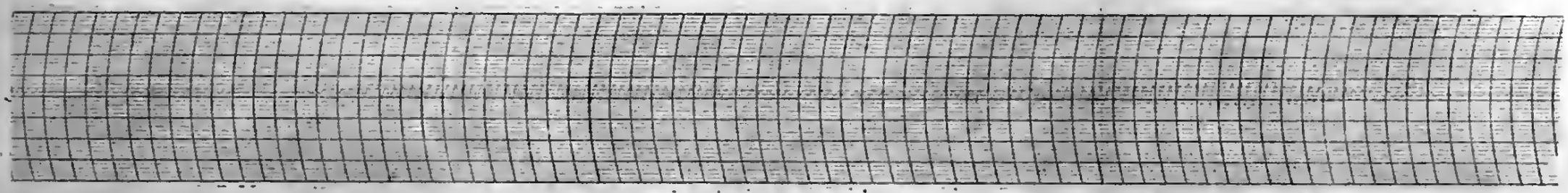

60 mph 125 MM/SEC

80 mph 125 MM/SEC

WIND TUNNEL NOISE DATA
MODEL RESPONSE

REFERENCES

1. Perkins, Courtland D., and Hage, Robert F., Airplane Performance, Stability, and Control, John Wiley and Sons, Inc. (1949).

2. Sternfield, Leonard, "Effect of Product of Inertia on Lateral Stability," NACA TN No. 1193, March 1947.

3. Stone, D. G., and Muse, T. C., Memorandum Report of the Air Materiel Command, USAF, "Power-off and Power-on Tests of the .2375 Scale Model of the Douglas XA-26 Airplane in the N.A.C.A. 19-Foot Pressure Tunnel, Part II, Stability Characteristics."

4. White, Roland J., "Investigation of Lateral Dynamic Stability in the XB-47 Airplane," Institute of the Aeronautical Sciences Preprint No. 241.

5. McKinney, Marion O., Jr., and Maggin, Bernard, "Experimental Verification of the Rudder-Free Stability Theory for an Airplane Model Equipped with Rudders Having Negative Floating Tendency and Negligible Friction," NACA ARR No. L4J05a, November 1944, (Declassified).

6. Liddell, Charles J., Jr.; Van Dyke, Rudolph D., Jr.; and Heinle, Donovan R., "A Flight Determination of the Tolerable Range of Effective Dihedral on a Conventional Fighter Airplane," NACA TN No. 1936, August 1949.

7. Weems, William R., "An Introduction to the Study of Gyroscopic Instruments," M.I.T. Instrument Section, Dept. of Aeronautical Engineering.

8. Street, William G. and Ames, Milton B., Jr., "Pressure Distribution Investigation of a N.A.C.A. 0009 Airfoil With a 50 - Percent - Chord Plain Flap and Three Tabs," T.N. No. 734, NACA, 1939.

9. Ames, Milton B., Jr., and Sears, Richard I., "Pressure Distribution Investigation of an N.A.C.A. 0009 Airfoil with a 30 - Percent - Chord Plain Flap and Three Tabs," T.N. No. 759, NACA, 1940.

10. Ames, Milton B., Jr., and Sears, Richard I., "Pressure Distribution Investigation of an N.A.C.A. 0009 Airfoil with an 80 - Percent - Chord Plain Flap and Three Tabs," T.N. No. 761, NACA, 1940.

11. Harris, Thomas A., "Reduction of Hinge Moments of Airplane Control Surfaces by Tabs," Rep. No. 528, NACA, 1935.

12. Anderson, Raymond F., "Determination of the Characteristics of Tapered Wings," Rep. No. 572, NACA, 1936.

13. Silverstein, Abe, and Katzoff, S., "Design Charts for Predicting Downwash Angles and Wake Characteristics behind Plain and Flapped Wings," Rep. No. 648, NACA, 1939.

14. Ames, Milton B., Jr., and Sears, Richard I., "Determination of Control-Surface Characteristics from NACA Plain Flap and Tab Data," T.N. No. 796, NACA, 1941.

15. Sears, Richard I., "Wind Tunnel Data on the Aerodynamic Characteristics of Airplane Control Surfaces," Wartime Report (Originally issued December 1943), NACA, 1943.

16. Crandall, Stewart M., and Murray, Harry E., "Analysis of Available Data on the Effects of Tabs on Control Surface Hinge Moments," T.N. No. 1049, NACA, 1946.

Thesis 15490
G14 Gallagher
Investigation of a yaw
damper for aircraft.